Studying the behavior of Dhahran dune sand using the 3rd invariant stress dependent combined hardening cap model

Isa Mahmoud Al-Buraim

Civil Engineering

May 1990

Abstract

A three stress-invariant dependent combined hardening cap model is considered in this work to study the behavior of Dhahran dune sand. The model differs from the original cap model, primarily, in its capability to simulate the response of soil when subjected to cyclic loading. In order to assess the applicability of this model, the local sand is tested using a modified triaxial device. Using this device, it is possible to conduct ycclic triaxial tests at a constant confining pressure. Different types of triaxial tests are conducted by using this device; namely; conventional triaxial compression test, triaxial compression test (J_1 = constant) triaxial extension test (J_1 = constant) and cyclic triaxial test. The results of those tests are used to determine the model parameter. The model is shown to realistically predict the soil responses under cyclic triaxial loading. The model is implemented into a two-dimensional finite element code to study the behavior of a rigid model footing resting on sand. Results indicate that the combined hardening cap model predictions agree well with the experimental observations.

Studying the Behavior of Dhahran Dune Sand using the 3rd Invariant Stress Dependent Combined Hardening Cap Model

by

Isa Mahmoud Al-Buraim

A Thesis Presented to the

FACULTY OF THE COLLEGE OF GRADUATE STUDIES

KING FAHD UNIVERSITY OF PETROLEUM & MINERALS

DHAHRAN, SAUDI ARABIA

In Partial Fulfillment of the
Requirements for the Degree of

MASTER OF SCIENCE

In

CIVIL ENGINEERING

May, 1990

Studying the Behavior of Dhahran Dune Sand Using the 3rd Invariant Stress Dependent Combined Hardening Cap Model

BY

Isa Mahmoud Al-Buraim

A Thesis Presented to the

FACULTY OF THE COLLEGE OF GRADUATE STUDIES

KING FAHD UNIVERSITY OF PETROLEUM & MINERALS

DHAHRAN, SAUDI ARABIA

In Partial Fulfillment of the
Requirements for the Degree of

MASTER OF SCIENCE

In

CIVIL ENGINEERING

MAY 1990

KING FAHD UNIVERSITY OF PETROLEUM & MINERALS

DHAHRAN, SAUDI ARABIA

This thesis, written by

ALBURAIM, ISA MAHMOOD MOHAMMED

under the direction of his Thesis Advisor, and approved by his Thesis Committee, has been presented to and accepted by the Dean of the College of Graduate Studies, in partial fulfillment of the requirements for the degree of

MASTER OF SCIENCE IN CIVIL ENGINEERING

Thesis Committee

June/20/1990
Chairman (Dr. Sahel Abduljauwad)

Member (Dr. Ramdan Al Ghamdi)

Member (Dr. Mahmoud Safar)

14-7-90
Dr. Ghazi J. Al-Sulaimani
Department Chairman

Dr. Ala H. Al-Rabeh
Dean College of Graduate Studies

Date : 14 - 7 - 90

Dedicated

To

MOHAMMED The Massenger of ALLAH

ACKNOWLEDGEMENT

First of all, I thank "ALLAH" for all the knowledge and science HE had given to mankind including myself. Thanks are also to our Prophet MOHAMMED,PEACE BE UPON HIM, who encouraged us as Moslems to seek science wherever it can be found.

Acknowledgement is to the KING FAHD UNIVERSITY OF PETROLEUM and MINERALS for supporting this work and for giving me the honour to be one of its high studies students in the Civil Engineering Department.

I do not find appropriate words to express my deep appreciation, respect and gratefullness to my Main Advisor : Dr. SAHEL ABDUL JAWUAD for all the help, support, encouragement he had given me all the way. Also I thank deeply both of : Dr. Safar, M. and Dr. Ghamdi, H. for their guidance and valuable suggestion they made to complete this work.

Acknowledgement is also due to Dr. AL-SULAIMANI, G. who during his tenure as chairman of Civil Engineering Department lent considerable help and encouragement.

I wish to acknowledge the assistance given by Mr. Hassan Zakaria, supervisor of the Soil Mechanics Laboratory at KFUPM, during the course of laboratory work. Also, i wish to tank my friends for their ecouragement, cooperation and help. Special thanks are for Nedhal Al-Dhahabi, Ahmad and Mohammed Al-Twabini, Yousef Al-Haj, and Bassam Zemmo.

I wish also to express my deep gratitude to MY PARENTS for all what they had given me including their love, encouragement, and support.

I shouldn't forget to thank MY WIFE and OUR CHILDERN : SARA and YOUSEF, for being extremely patient and I don't forget their suffering all the way until I had accomplished this work.

TABLE OF CONTENTS

Page

LIST OF TABLES

Page

LIST OF FIGURES

Page

Page

Page

Page

ABSTRACT

Name Of Student : Isa Mahmood Al Buraim.

Title Of Study : Studying The Behavior of Dhahran Dune Sand Using Combined Hardening 3rd invarient dependent Cap Model.

Major Field : Geotechincal Engineering.

A three stress-invariant dependent combined hardening cap model is considered in this work to study the behavior of Dhahran dune sand. The model differes from the original cap model, primarily, in its capability to simulate the response of soil when subjected to cyclic loading. In order to assess the applicability of this model, the local sand is tested using a modified triaxial device. Using this device, it is possible to conduct cyclic triaxial tests at a constant confining pressure. Different types of triaxial tests are conducted by using this device; namely; conventional triaxial compression test, triaxial compression test (J_1 = constant), triaxial extension test J_1 = constant) and cyclic triaxial test. The results of those tests are used to determine the model prameter. The model is shown to realistically predict the soil responses under cyclic triaxial loading. The model is implemented into a two-dimensional finite element code to study the behavior of a rigid model footing resting on sand. Results indicate that the combined hardening cap model predictions agree well with the experimental observations.

خلاصة الرسالة

اسم الطالب الكامـــل : عيسى محمود محمد البريم
عنوان البحـــــــث : إستخدام نموذج القلنسوه المعتمد على ثابت الإجهاد الثالث والصلادة المشتركة لدراسة تصرف رمال الكثبان .
مجـــــال التخصص : هندسة التربة .
تاريخ الدرجة العلمية : ١٠ شوال ١٤١٠هـ .

لقد أستخدم في هذا البحث نموذج قلنسوي الشكل يعتمد على ثابت الإجهاد الثالث والصلادة المشتركة لدراسة تصرف رمال الكثبان الموجودة في الظهران . ويتميز هذا النموذج عن النموذج القلنسوي التقليدي المعروف بقدرته على محاكاة مقاومة التربة للقوى المترددة. ولكي نعين مدى إستخدامية هذا النموذج فقد إختبرت عينات من الرمال المحلية بإستخدام جهاز ثلاثي المحاور معدل لهذا الغرض . ويمكن باستخدام هذا الجهاز اجراء اختبار الثلاثي المحاور المتردد تحت ضغط حصر ثابت . ولقد اجريت اختبارات ثلاثية المحاور عديدة باستخدام هذا الجهاز وتتضمن الاختبارالتقليدي ، الاختبار الانضغاطي والاختبار التمددي وكذلك الاختبار الترددي تحت ضغط حصر ثابت . ولقد أستخدمت هذه الإختبارات لإيجاد ثوابت النموذج . ولقد لوحظ قدرة هذا النموذج على تمثيل تصرف التربة تحت تأثير القوة المترددة ذات الثلاث محاور . ولقد أدمج هذا النموذج في برنامج تجزءة محدودة ذو إتجاهين لدراسة تصرف نموذج قاعدة صلبة أنشئت على سطح رمال الكثبان . ولقد قورنت أيضاً هذه النتائج مع النتائج التجريبية ولوحظ توافق جيد بينهم .

CHAPTER 1

INTORDUCTION

1.1 GENERAL

Sand is an elasto-plastic material that undergoes both recovered (elastic) and unrecovered (plastic) deformations upon loading. The stress-strain behavior of such material is complex and dependent on many vraiables. Simulation of such behavior does not need the govering field equations only, but also the internal constitution of the material. A constitutive law is a mathematical model that describes the behavior of a material. In other words, a constitutive law simulates physical behavior that has been perceived mentally.

A solution to a boundary value problem in continuum mechanics requires constitutive equations in addition to assumptions to the nature or expected behavior of the material. In case of soils, the classical methods treat the soil as (Chen and Baladi, 1985):

1. a perfectly 'elastic' material under working load condition;
2. a perfectly 'plastic' material under ultimate load condition

and

3. a perfectly 'visco-elastic' material under long-term load condition.

With such assumptions made, it is possible to solve the problem using the well-defined mathematical theories of elasticity, plasticity and viscosity.

For a long time, soil mechanics has been based on linear elasticity (Hooke's law) for stress and deformation analysis of a soil mass under a footing, or behind a retaining wall, when no failure of soil is involved (working load condition). This is known as 'elasticity' problem in soil mechanics. On the other extreme, the teory of perfect plasticity is used to treat the conditions of 'ultimate failure' or 'limit analysis' of a soil mass, such as problems of earth pressure and retaining wall, bearing capacity of foundations and stability of slopes. Long term settlement problems and consolidation problems are dealt essentially as visco-elastic problems.

Partly due to the historical development of mechanics of sloids and partly for simplicity in practice, the elasticity and the stability problems in soil mechanics are treated separately and in unrelated ways. The essential bridge between them is the progressive failure problems. The progressive failure problems deal with the elasto-plastic transition from the initial linear elastic state to the ulimate state of the soil by plastic flow. The essential set of equations for the solution of progressive failure problems is the

constitutuve equation of soils (Chen and Baladi, 1985).

Constitutive laws vary from very simple laws such as linear Hooke's law to very complex laws. For soils such constitutive laws are complex because of the nature of material itself. Soil as a naturally occuring material, is heterogeneous, anisotropic and discontinous; it's response to loading is dependent on the rate and magnitude of loading, state of stress, stress history or stress paths, volume changes under shear, fluid in the pores, etc.

Depending upon the conditions to which a soil mass is subjected, different models can be used to predict its behavoir. Under short-term loading, soil behavior may be idealized as time-independent. This time independent idealization can be further sub-divided into elastic time-independent idealization and plastic time-independent idealization. For an elastic material there exists a one to one relation between stress and strain, which is not so in the case of plastic material.

Although these idealizations have enabled many useful solutions to be developed for the two extremes (elastic and plastic), neither is adequate for analyzing the stress-strain response of soils within the intermediate range (working stress or progressive problems).

Past research into the stress-strain response study of soils under working stress range, due to limited availability of computational techniques and relatively unsophisticated testing equipment, was confined to the

influence of such compositional parameters as confining pressure, density, drainage condition, strain rate, void ratio and water content. Few attempts have been made to actually develop and implement realistic constitutive models. Several groups of constitutive models are currently available, but only those based on the theory of plasticity are relevant to us. Among all the available plasticity models for geologic materials, the model developed by DiMaggio and Sandler (1971) is very popular and commonly known as "cap model".

1.2 OBJECTIVES

The main objective of this study is to check the validity of extending of the three invariant-dependent isotropic cap model into a combined hardening form to predict the cyclic stress-strain response and to solve a boundary value problem. This can be achieved by :

1. Determining the material parameters associated with the combined hardening cap model.
2. Back-predicting cyclic triaxial tests using the combined hardening cap model.
3. Solving a boundary value problem of a model rigid strip footing rests on the surface of sand, by implementing the model into a finite element programm.
4. Comparing predicted results with the experimental ones.

CHAPTER 2

THEORY OF INCREMENTAL FLOW PLASTICITY AND ITS APPLICATION TO CAP MODELS

2.1 INTRODUCTION

This chapter presents a brief history about the origin of cap models, and the concept behind the constitutive relation between stress and strain at any stage of loading and unloading sequences. The componenets of the flow theory of incremental plasticity and its application on the cap model are also discussed here.

2.2 GENERAL

From a general point of view, cap models fall within the framework of the classical incremental theory of work-hardening plasticity for materials

that have time and temperature-independent properties and which are capable of undergoing small plastic (permenant) as well as elastic (recoverable) strain at each loading increment. The aim in the incremental plasticity is to esatblish an elasto-plastic constitutive operator $C_{ij}^{e\text{-}p}$, which relates increments of stress to increments of strain at any arbitrary stage of loading or unloading sequences

$$\{d\sigma\} = [C^{e\text{-}p}]\{d\varepsilon\} \qquad 2.1$$

Qualitatively typical stress versus strain response curves often take the shape of Fig.2.1. In small range of deformation total strain can be decomposed into an elastic and plastic parts

$$\{\varepsilon\} = \{\varepsilon^e\} + \{\varepsilon^p\} \qquad 2.2$$

Where $\{\varepsilon^e\}$ is the elastic part and is attributed to the recoverable deformations between grain groups and indivisual grains or particles that constitute the soil skeleton. And $\{\varepsilon^p\}$ is the plastic strain part, which is due to the rearrangements, expansion, contraction, and translation between the soil particles.

Assuming small deformations, Eq.2.2 can be rewritten incrementally as follows

$$\{d\varepsilon\} = \{d\varepsilon^e\} + \{d\varepsilon^p\} \qquad 2.3$$

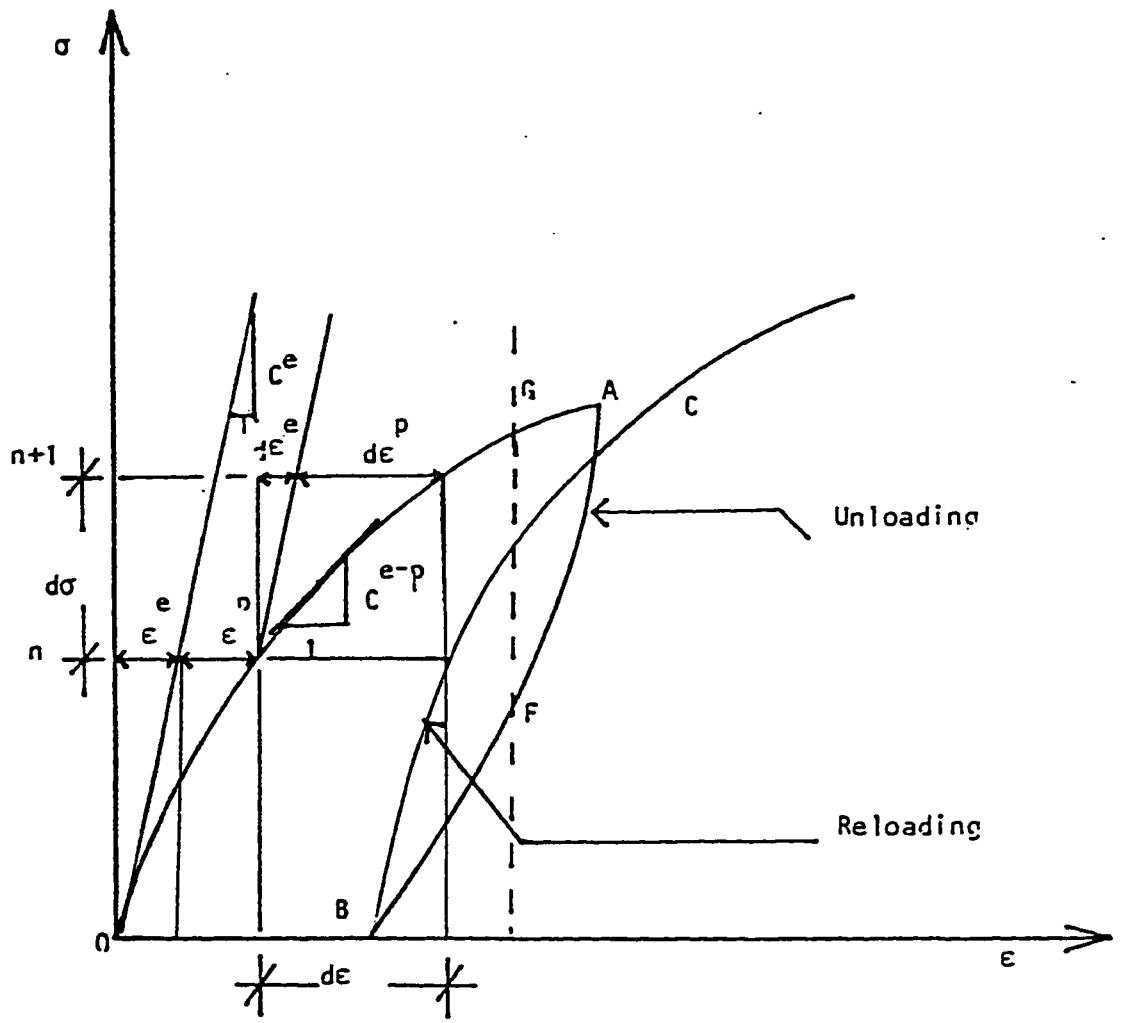

Fig.2.1 Stress-Strain Relationship

The following sections will discuss the concept behind the formulation of the incremental stress-strain relation (Eq.2.1).

2.3 FLOW THEORY OF WORK-HARDENING PLASTICITY:

In the flow theory of plasticity for strain or work- hardening materials, the developement of the incremental stress-strain relation is based on the following three fundamental requirements (Chen, 1975, 1982, Chen and Saleeb,1986):

1. The existence of initial and subsequent yeild(loading) surfaces.
2. The formulation of an apropriate hardening (softening) rule that describes the evolution of subsequent loading surface.
3. A flow rule which specifies the general form of the stress-strain relationship.

These requirements will be discussed in detail in the following sections.

2.3.1 *Yield Surfaces:*

As load is applied to a material it deforms elastically untill it reaches the yield point, then it deforms both elastically and plastically (elasto-plastically). In order to determine where the material yields, a yield criterion is needed. The yield criterion can be defined as the limit of elastic deformations expressed by a combination of states of stress. For a one-dimensional state of stress, the yield criterion can be easily visulaized. However, under multiaxial states of stress, this becomes complicated, and a mathematical expression is required to include all stresses. Formulation of the yield

criterion should be based on experimental observations. Different material parameters are involved in the formulation and are to be determined experimentally. A yield criterion can be defined as a a scalar function, F, that contains all the states of stress in a three-dimensional problem:

$$F = F(\sigma_{11}, \sigma_{22}, \sigma_{33}, \sigma_{12}, \sigma_{23}, \sigma_{13}) \qquad 2.4$$

In the most general case, F will be a function of all six components of the stress tensor. If the material is homogeneous, this function is valid every where in the material. The yield criterion can be expressed in terms of principal stresses and their directions as follow (Malvern, 1969) :

$$F = F(\sigma_1, \sigma_2, \sigma_3, n_1, n_2, n_3) \qquad 2.5$$

where σ_1, σ_2, and σ_3 are the principal stresses, and n_1, n_2, and n_3 are their direction cosines. Assuming the material is isotropic (no preferred directions), Eq. 2.5 can be written in terms of principal stresses only:

$$F = F(\sigma_1, \sigma_2, \sigma_3) \qquad 2.6$$

This can also b expressed in terms of the invariants of the stress tensor as follows:

$$F = F(J_1, J_{2D}, J_{3D}) \qquad 2.7$$

where :

J_1 : first invariant of stress tensor $= \sigma_{ll} = \sigma_{11} + \sigma_{22} + \sigma_{33}$

J_{2D}: second invariant of deviatoric stress tensor $= \frac{1}{2}S_{ij}S_{ij}$

S_{ij}: deviatoric stress tensor $= \sigma_{ij} - \frac{1}{3}\sigma_{nn}\delta$

J_{3D}: third invariant of deviatoric stress tensor $= \frac{1}{3}S_{ij}S_{jk}S_{ki}$

An alternative representation for the third stress invariant is the angle, 0, which is defined as follows

$$\cos 3\theta = \frac{3\sqrt{3}}{2}\frac{J_{3D}}{J_{2D}^{\frac{3}{2}}} \qquad 0 \le 0 \le \frac{\pi}{3} \qquad 2.8$$

A yield criterion is usually used to model the perfomance of a material in such a way that the material behaves elastically when F ≤ 0, and elasto-plastically when F = 0. It defines a closed convex surface in the stress space, and separates the states of stress that may exist ($F \le 0$) from those that may not be allowed ($F > 0$). If F > 0 a new yield surface is established for hardening materials according to the assumed hardening rule .

2.3.2 Hardening Rule :

Drucker, Gebson and Henkel (1957) were the first to suggest that soil might be modeled as elasto-plastic work-hardening material. Consequently, the concept of the fixed yield surface in stress space can be generalized to the concept of changing loading surfaces. A hardening rule describes the post yielding response, which specifies rule for the evolution

of the loading or yielding surfaces during the coarse of plastic deformations.

The choice of a hardening rule, among the available hardening rules, depends primarily on the ease which can be applied and its ability to represent the hardening behavior of a particular material. Three types of hardening rules have been commonly used (Chen, 1982), namely, isotropic hardening, kinematic hardening, and combined hardening. Isotropic hardening applies to proportional monotonic loading. On the other hand, kinematic hardening rule applies to cyclic or reverse types of loading for materials with pronouced Bauschinger effect. For most geological materials such as soil, combined hardening rule is suitable.

Isotropic Hardening

The simplest work hardening rule is to assume that the yield surface expands uniformly without distortion as plastic flow occurs as shown in (Fig. 2.2). The size of the yield surface is governed by the value of k^2, which depends on plastic strain history. The equation for subsequent loading surfaces is :

$$F(\sigma_{ij}) = k^2(\bar{\varepsilon}_p) \qquad 2.9$$

where :

k^2 : a scalar and is a measure of isotropic hardening.

$\bar{\varepsilon}_p$: effective plastic strain which is an integrated increasing function

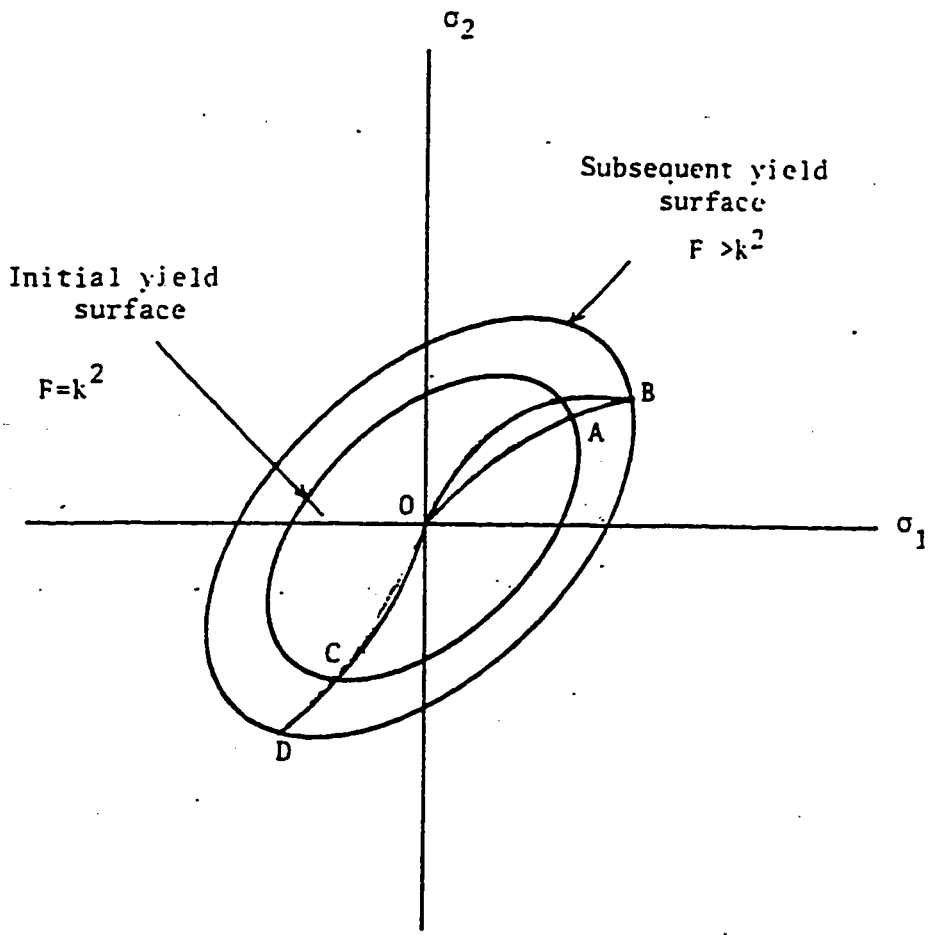

Fig. 2.2 Schematics of subsequent yield surfaces for isotropic hardening.

of the plastic strain increments.

Due to the uniform expansion of the yield surface, isotropic hardening can not account for Baushinger effect exhibited by most structural materials. The Bauschinger effect refers to a particular kind of directional anisotropy, induced by plastic deformation. Which implies that initial plastic deformation in one sign reduces the material resistence to subsequent plastic deformation of the opposite sign, see (Fig. 2.3). Actually, isotropic rule implies that the material will exhibit an increase in the compressive yield stress equal to an increase in the tensile yield stress, which is contrary to experimental evidances (Fig. 2.4).

Kinematic Hardening :

The kinematic hardening rule assumes that during plastic deformation the loading surface translates as a rigid body in stress space, maintaining its shape, size and orientation of the initial yield surface. This hardening rule due to Prager (1955, 1956), provides a means of accounting for the Bauschinger effect. The concept of kinematic hardening is illustrated in (Fig. 2.5). As the stress point moves along its loading path from point A to point B, the yield surface translates (no rotation) as a rigid body in the direction normal to the surface at the contact or yield point. If the stress is unloaded from state B through the path BAO, it will behave elastically untill it reaches point C then the material flows plastically before the stress is completely released. This is a realistic representation of Bauschinger

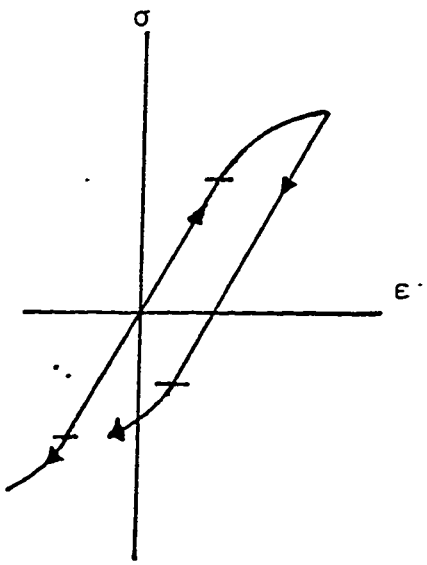

Fig.2.3 Schematic of Bauschinger effect

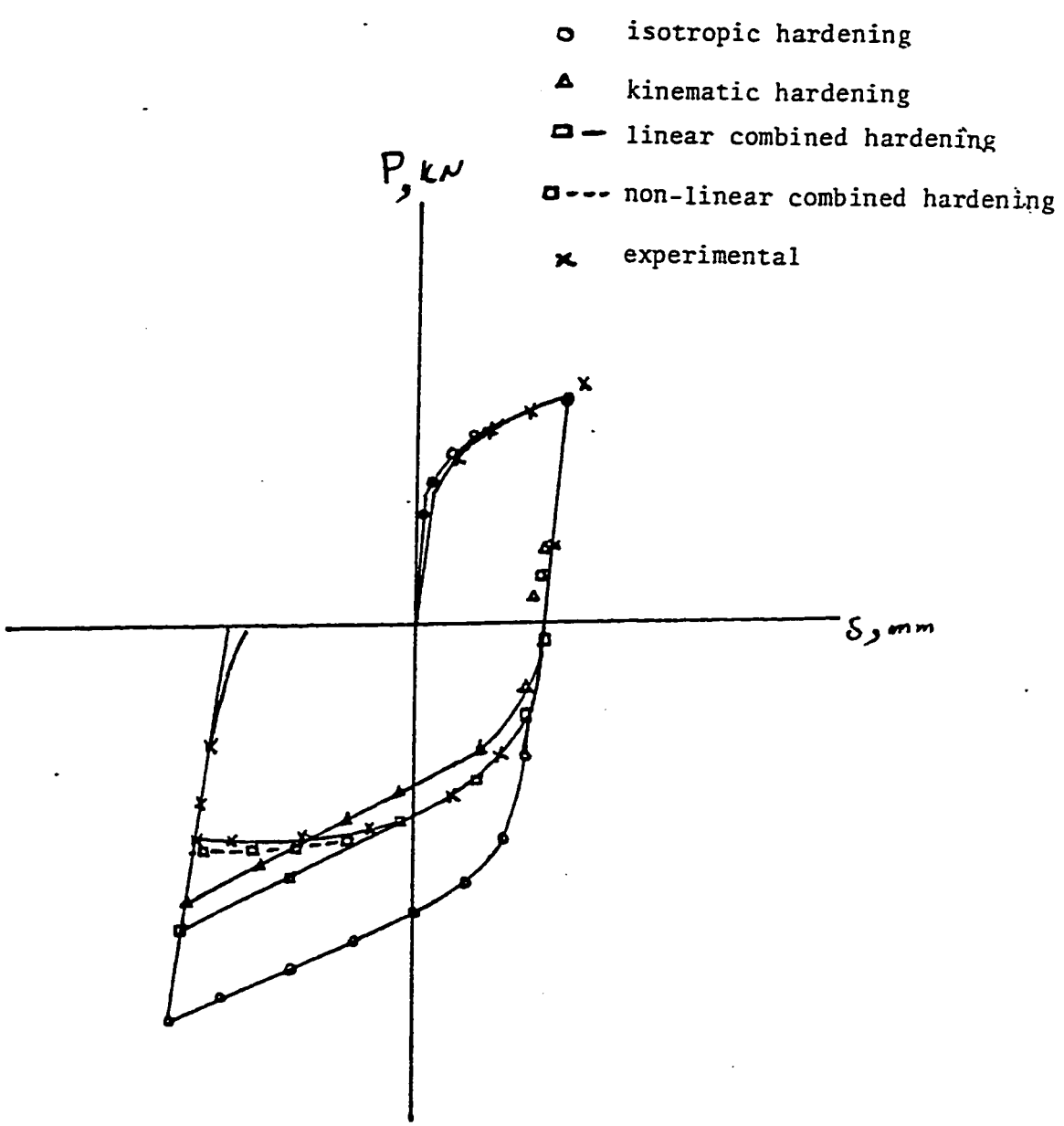

Fig.2.4 Load-Displacement curves. (chen)

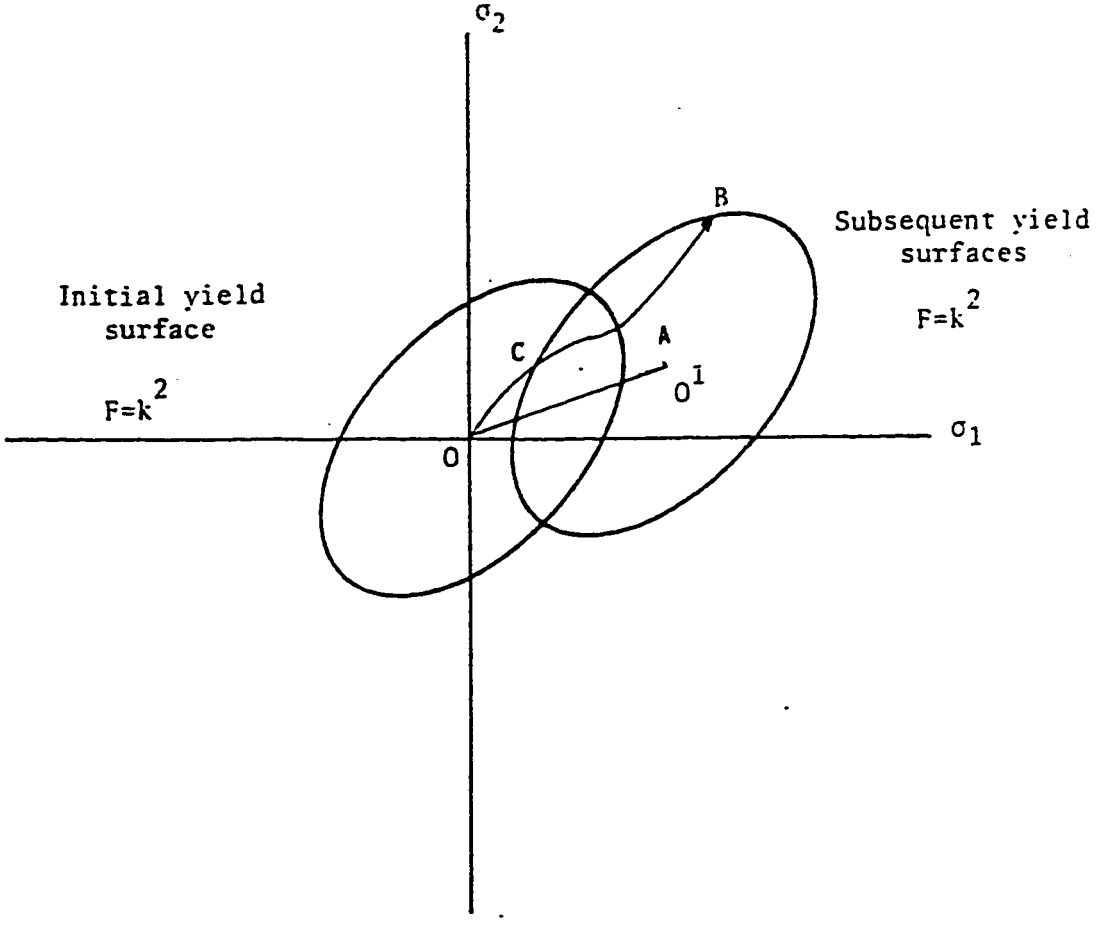

Fig.2.5 Schematic of subsequent yield surfaces for kinematic hardening.

effect for completely reversed loading conditions.

The governing equation for the loading surfaces is :

$$f(\sigma_{ij},\varepsilon^p_{ij}) = F(\sigma_{ij} - \alpha_{ij}) - k^2 = 0 \qquad 2.10$$

where :

α_{ij} : coordinates of the center of the loading surface (or the vector OO', Fig. 2.5), which change with plastic deformation.

Combined Hardening :

A combination of the two previously mentioned hardening rules leads to a more general hardening rule. In this case, the yield surface undergoes both uniform expansion and translation (no rotation, no distortion) in all directions. With this model different degrees of Bauschinger effect can be produced (Fig. 2.6).

The loading surface equation is :

$$f(\sigma_{ij},\varepsilon^p_{ij},k) = F(\sigma_{ij} - \alpha_{ij}) - k^2(\varepsilon_p) = 0 \qquad 2.11$$

In reversed loading it has been obsereved that the kinematic hardening rule sometimes, overpredicts the Baushinger effect, while combined hardening gives closer results to experimental data (Fig. 2.4).

2.3.3 The Flow Rule

When the state of stress reaches the yield surface,F, the material

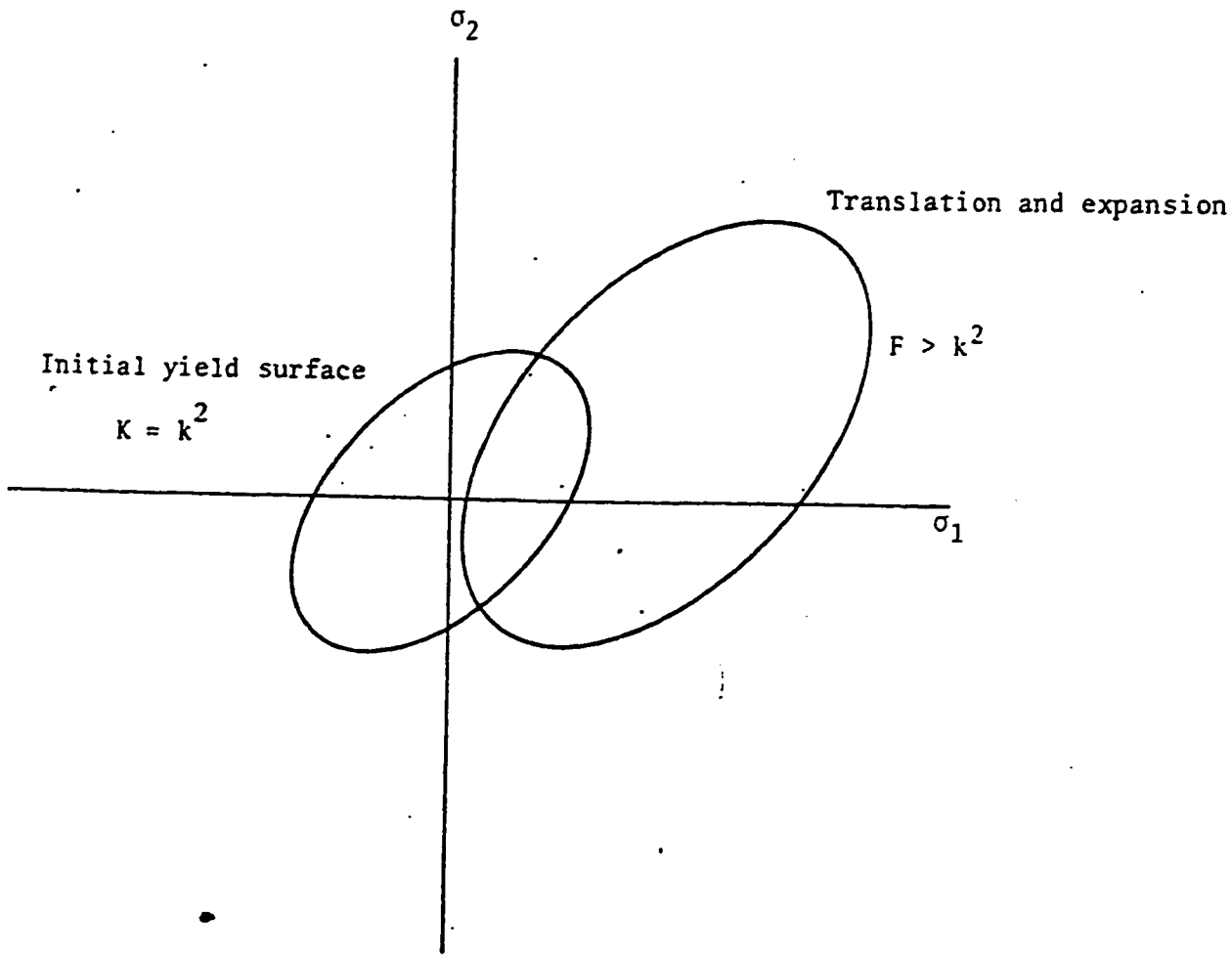

Fig.2.6 Schematic of loading surfaces for combined hardening rule.

undergoes plastic deformation; this is called plastic flow. For work hardening material a flow rule is used to relate the plastic strain increment with stress increments. In the mathematical theory of plasticity, it is common to assume the existence of a plastic potential whose gradient with respect to the stress tensor yields the direction of incremental plastic strain tensor. In other words, incremental plastic strain tensor is normal to the so-called plastic potential; Mathematically, this can be written in the form (Hill, 1950):

$$d\varepsilon_{ij}^{p} = d\lambda \frac{\partial Q}{\partial \sigma_{ij}} \qquad 2.12$$

where :

$d\lambda$ is a positive scalar factor of proportionality,

Q is the plastic potential function.

The quantity $\partial Q/\partial \sigma_{ij}$ determines the dirction of the incremental plastic strain vector. In general Q is an arbitrary function of σ_{ij} and can be defined independently of the yield function, F. The resulting constitutive laws should, however, satisfy certain quasi-thermodynamic restrictions. Invoking such principles, D. C. Drucker (1950) has shown that the yield function could be the plastic potential and the yield surface should be a convex surface in the stress spaces. The resulting flow rule is termed as "associated flow rule". On the contrary, if $Q \neq F$, the flow rule is termed as "non-associated flow rule" (Maroz, 1963; Davis, 1968).

Although soils have been found to exhibit both associated and non-associated flow responses, there are problems that arise with the use of non-associated flow rule. Firstly, no uniqueness proofs are available for the solution obtained by using non-associated flow rule. Secondly, the elasto-plastic constitutive relation tensor, $C^{e\text{-}p}_{ijkl}$ (in the equation relating increments of stress with those of strain, $d\sigma_{ij} = C^{e\text{-}p}_{ijkl} d\varepsilon_{kl}$) becomes non-symmetric which poses additional problems in numerical applications.

Derivation of the Incremental Stress-Strain Relationship

When a state of stress reaches the yield surface plastic strains strart to accumulate. For continuous loading, the stress point moves smoothly from one yield surface to the next, which never leaves the evolving yield surface. This is known as the consistency condition (Prager, 1949), which can be stated mathematically as

$$dF = 0 \qquad 2.13$$

which means $\{\frac{\partial F}{\partial \{\sigma\}}\}^T \{d\sigma\} + \{\frac{\partial F}{\partial \{\alpha\}}\}^T \{d\alpha\} + A_h d\lambda = 0$ 2.14

where

A_h : a scalar of proportionality, termed the plastic modulus.

$$d\lambda = \frac{1}{A_h} \{\frac{\partial F}{\partial \{\sigma\}}\}^T \{d\sigma\} \qquad 2.15$$

Using generalized linear Hooke's law

$$\{d\sigma\} = [C^e]\{d\varepsilon^e\} \qquad 2.16$$

substituting Eq.2.3 into Eq. 2.16

$$\{d\sigma\} = [C^e][\{d\varepsilon\} - \{d\varepsilon^p\}] \qquad 2.17$$

substituting Eq.2.12 into Eq. 2.17 gives

$$\{d\sigma\} = [C^e][\{d\varepsilon\} - d\lambda\{\frac{\partial Q}{\partial \sigma_{ij}}\}] \qquad 2.18$$

where $[C^e]$ is the elastic matrix. The number of independent constants needed to define it is controlled by the degree of anisotropy exhibited by the material (Boresi and Lynn, 1974). In the simplest case where complete isotropy is assumed, only two independent elastic moduli fully define the elastic matrix (reffer to Appendix A), which can be written now in the indecial form :

$$C^e_{ijkl} = (K - \frac{2}{3}G)\delta_{ij}\delta_{kl} + G(\delta_{ik}\delta_{jl} + \delta_{il}\delta_{jk}) \qquad 2.19$$

Incorporating Eq.2.15 into Eq.2.18 and solving for $d\lambda$

$$d\lambda = \frac{\{\frac{\partial F}{\partial\{\sigma\}}\}^T [C]\{d\varepsilon\}}{\{\frac{\partial F}{\partial\{\sigma\}}\}^T [C^e]\{\frac{\partial Q}{\partial\{\sigma\}}\} - A_h} \qquad 2.20$$

substituting $d\lambda$ into Eq.2.18, equation 2.1 can be obtained.

where

$$[C^{e\text{-}p}] = [C^e] - \frac{[C^e]\{\frac{\partial Q}{\partial\{\sigma\}}\}\{\frac{\partial F}{\partial\{\sigma\}}\}^T[C^e]}{\{\frac{\partial F}{\partial\{\sigma\}}\}^T[C^e]\{\frac{\partial Q}{\partial\{\sigma\}}\} - A_h} \qquad 2.21$$

As indicated earlier, A_h is a plastic modulus that depends on the type of hardening rule that is assumed (i.e. isotropic, kinematic, or combined hardening). For the present work the combined hardening rule is assumed here and full description of the elastoplastic matrix will be shown in chapter 3.

2.4 GENERALIZED CAP MODEL :

As stated eralier a cap model falls within the framework of the classical incremental theory of work-hardening plasticity for materials which have time and temperature-independent properties and which are capable of undergoing small plastic (permenant) as well as elastic (recoverable) strain at each loading increment.

The classical theory of plasticity allows for abroad range of material behavior, and the cap model falls within this range. Many previous applications of the plasticity theory for metals involved the assumption that volumetric strains are purely elastic. However, the cap model is predicted on the fact that the volumetric hysteresis exhibited by many geological materials can also be described by a plasticity model, if the model is based

on a hardening yield surface which includes conditions of hydrostatic stress. Drucker has provided a mechanism, through which, a cap model can be applied. This mechanism is called Drucker's postulates of stability (1950,1951,1954) which is sufficient, although not necessary, to satisfy all thermodynamic and continuity requirements for continuum models. Drucker's postulates can be stated as follows

1. Yield surface(loading function) should be convex in stress space.
2. Yield surface and plastic potential should coincide (which results in an "associated" flow rule), i.e., the plastic strain increment is a vector normal to the yield surface.
3. Work"softening" should not occur, i.e., the material must not collapse during yielding or its strength must not decrease during failure under increasing loads.

Drucker's stability criteria can be summarized mathematically by the following:

$$d\sigma_{ij}d\varepsilon_{ij} > 0 \qquad 2.22$$

$$d\sigma_{ij}d\varepsilon^{p}_{ij} \geq 0 \qquad 2.23$$

The first inequality implies that during the application of stress, the work done by the external agency will be possitive (Fig.2.7). The second inequality implies that over a cycle of application and removal of stresses, the work done by the external agency will be zero or positive (Drucker, D.

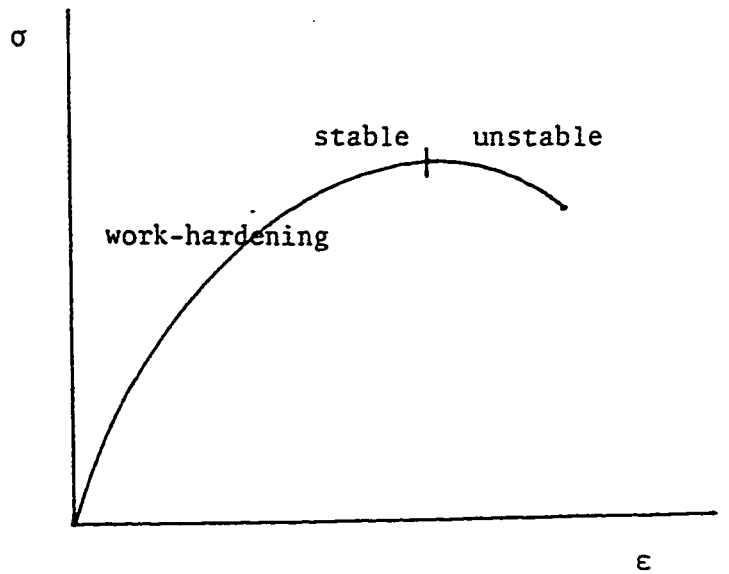

Fig.2.7 Stress-Strain behavior

C., 1950). This is due to the irreversible nature of plastic deformations (Prager, W., 1949).

2.4.1 Mathematical Formulation of Cap Model

Cap model, which is originally proposed by DiMaggio, 1971, Baron, 1973, and Sandler, 1976, and subsequently modified by Baron, 1971, and Sandler, 1979, is based on the concept of continuous yielding of soils, establishing new caps whenever state of stress reaches yielding according to the assumed hardening rule (Fig. 2.8). Caps are expressed in terms of three-dimensional states of stress and are formulated on the basis of critical state soil mechanics.

The cap model is defined by a non-softening convex yield surface and a plastic strain rate vector that is normal to the yield surface in stress space. The yield surface is defined by means of a failure envelope and a hardening cap. The name cap model is derived from the shape of the elliptical yield surfaces which look like "Caps"(Fig. 2.8).

Failure Surface

DiMaggio and Sandler (1971) propsed a generalized cap model, in which, the failure surface was assumed to be composed of an initial portion of the Drucker-Prager envelope joined smoothely to the subsequent von Mises surface (Fig. 2.8). The reason for using the von Mises surface at higher stress was based on the observation that the material flows like a

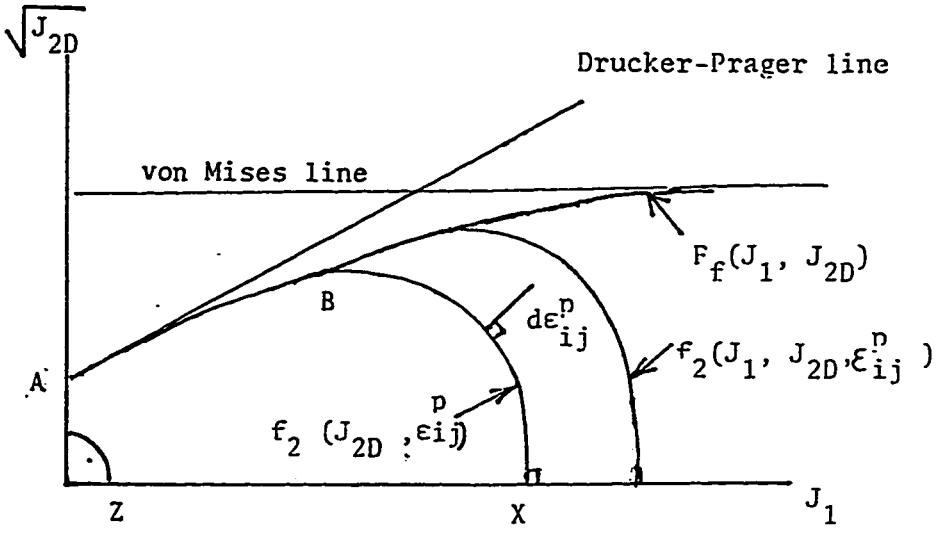

Fig.2.8 Cap Model

liquid at high stresses. The equation of the failure surface is (see Fig. 2.9):

$$F_f = \sqrt{J_{2D}} - A + Ce^{-BJ_1} = 0 \qquad 2.24$$

where A, B, and C are the failure constants.

Note that the failure surface defined by Eq. 2.24 is independent of θ and thus plots circular on the octahedral plane (Fig. 2.10). Since experimental evidence supports the use of all three invariants (J_1, J_{2D}, θ), Faruque modified the failure equation as follows (M. O. Faruque, 1987) :

$$F_f = g(\theta,J_1).\sqrt{J_{2D}} - A - MJ_1 + Ce^{-BJ_1} = 0 \qquad 2.25$$

where $g(\theta,J_1)$ is a dimensionless scaling function, which, appropriately changes the shape of the failure surface on the octahedral plane. M is an additional constant introduced by Desai et al (1979). The assumed form of $g(\theta,J_1)$ should be such that the failure surface is convex in the stress space. Two different forms of $g(\theta,J_1)$ were proposed by some researchers , and they are : a one- parameter form (Lade & Duncane (1975), Matsuoka (1976), and Ottosen (1977)) and a two-parameter form (Podgorski (1985)). In general a two parameter form is more appropriate than a one-parameter form. However, based on experimental evidence presented by Lade and Duncane (1975), Matsuoka(1976), and Ottosen (1977), a one- parameter form of $g(\theta,J_1)$ can be said to be adequate for most geological materials. Explicit form of $g(\theta,J_1)$ can now be written as :

$$g(\theta,J_1) = \frac{2}{\sqrt{3}}\cos[\frac{1}{3}\cos^{-1}(-A_f\cos 3\theta)] \qquad 2.26$$

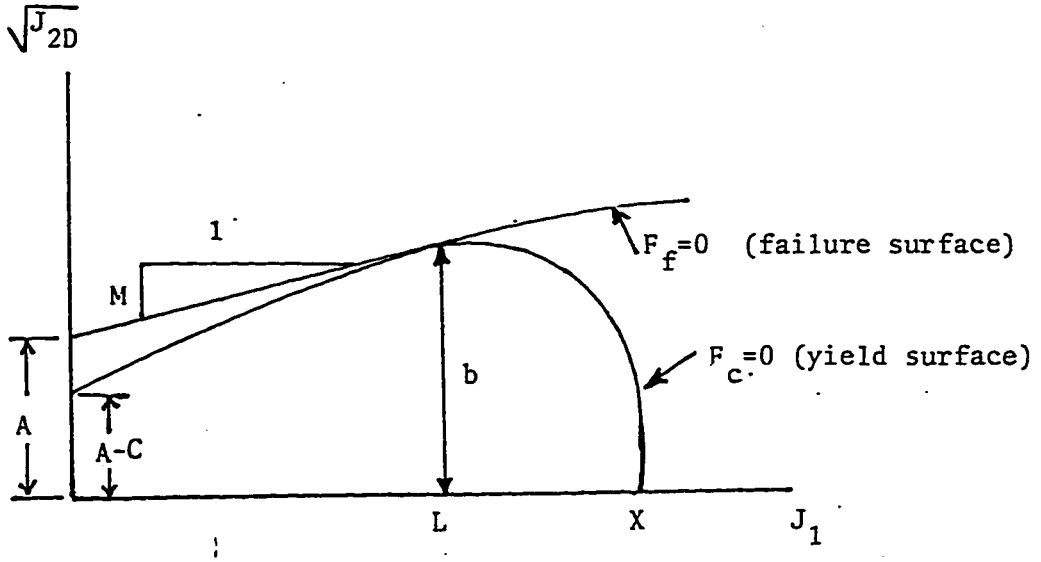

Fig.2.9 Schematic illustration of the yield and failure surfaces.

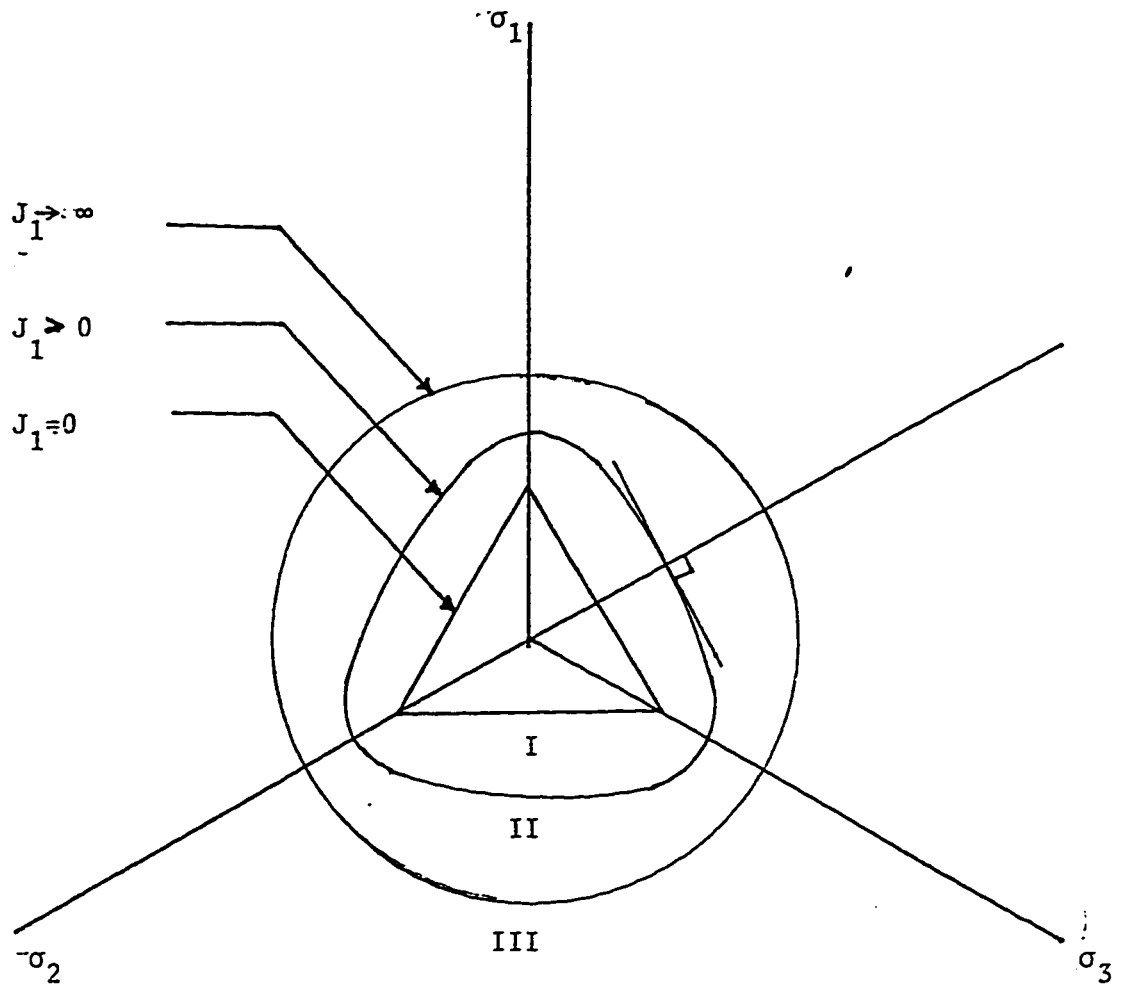

Fig.2.10 Schematic illustration of the failure surface on the octahedral plane.

where A_f is defined as follow :

$$A_f = A_0 e^{-\gamma \frac{J_1}{P_a}} \qquad 2.27$$

The parameter A_0 is not a material constant but should be properly chosen to satisfy the limiting shapes of the failure surface on the octahedral plane. It is also dectated by the convexity requirement of the failure surface on the octahedral plane. To satisfy convexity, A_0 should be between 0 and 1 (Podgorski, 1985). when $A_0 = 0$, the failure surface presented by Eq. 2.25 becomes independent of 0 and plots circular. On the extreme, when $A_0 = 1$, the cross-section of the failure surface on the octahedral plane approaches a triangle as $J_1 \rightarrow 0$ (Fig. 2.10). However, A_0 can be correctly choosen to be unity for frictional materials . The parameter γ is a material constant to be determined experimentally. P_a is the atmospheric pressure. Typical plots of Eq. 2.25 on the octahedral plane is shown in Fig. 2.10. Eq. 2.25 may also be plotted on $\sqrt{J_{2D}} - J_1$ space for constant values of 0, as shown in Fig. 2.11.

Yield Surfaces

DiMaggio and Sandler (1979) express the yield surfaces in the following form

$$F_c(J_1, \sqrt{J_{2D}}, k_1) = 0 \qquad 2.28$$

where k_1 defines the deformation history, and is usually taken as the

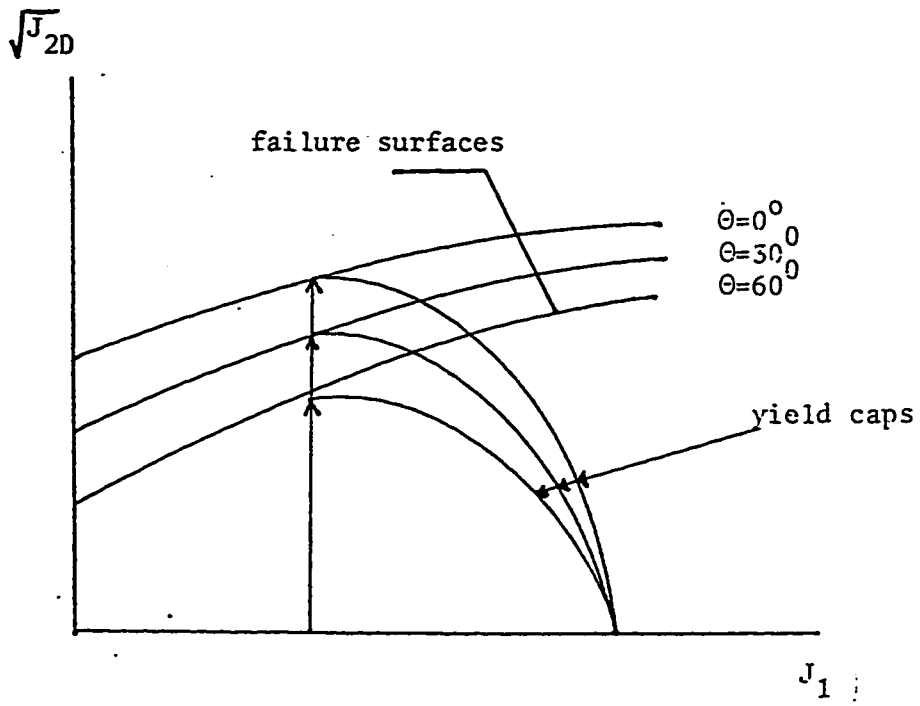

Fig.2.11 Failure surfaces and yield caps for different values of θ.

volumetric plastic strain, $\varepsilon_v^p = \varepsilon_{ii}^p$. Consequently, a yield surface represents the locus of the points with the same volumetric plastic strain. The failure and yield surfaces are assumed to intersect such that the tangents to the yield surfaces at the intersection are parallel to the $J_1 -$ axis. As a result, with the associated plasticity, the increment of plastic strain vector is parallel to the $\sqrt{J_{2D}}$ axis implying no volume change once the failure surface is reached, which is similar to the critical state concept in which the material does not change in volume at the critical state. Another feature of the yield surfaces is that they intersect the $J_1 -$ axis at right angles, which indicates that under hydrostatic compression there is no shear deformation (Desai & Siriwardane, 1984).

The cap model has been applied successfully to simulate behavior of various geological materials such as McCormick Ranch Sand ((Baron, 1973), (Sandler, 1976), (Baron, 1971)), Dhahran beach sand (Azeemuddin, 1988). DiMaggio and Sandler (DiMaggio, 1971) adopted an elliptic cap for representing yield surfaces for cohesionless materials. The expression for the yield surface is as follows:

$$F_c = \sqrt{J_{2D}} - \sqrt{b^2 - \frac{(J_1 - L)^2}{R^2}} = 0 \qquad 2.29$$

where L is the value of J_1 where the elliptic cap intersects the failure surface, and b is usually the minor axis of the ellips as shown in (Fig. 2.9). R is a material constant called shape factor, and it is the ratio of the major

to the minor axis of the ellipse (to be determined expermintally).

$$Rb = (\chi - L) \qquad 2.30$$

Since the failure surface has been modified by including the variable θ, for compatibility the yield cap should also be modified (Faruque, 1987). The modified form of the yield cap proposed is :

$$F_c = g(\theta,L)\sqrt{J_{2D}} - \sqrt{b^2 - \frac{(J_1 - L)^2}{R^2}} = 0 \qquad 2.31$$

where, $g(\theta,L) = g(\theta,J_1)$ at $J_1 = L$.

$$b = A + ML - Ce^{-BL} \qquad 2.33$$

Thus the cross-section of the failure surface and the yield cap are compatible on the octahedral plane. Plots of Eq.2.8 for different values of θ are shown in (Fig. 2.11).

CHAPTER 3

THE COMBINED HARDENING THREE-INVARIANT CAP MODEL

3.1 INTRODUCTION

This chapter represents the theoritical formulation of the combined hardening cap model along with the derivation of the stress-strain relation. Techniques used to determine the model parameters are also presented here.

3.2 GENERAL

The cap model presented in Eq.2.24 assumed isotropic hardening rule, as plastic flow occurs the yield surface expands uniformly without distortion, as shown schematically in Fig.2.2. This does not account for the Bauschinger effect exhibited by most geological materials. Actually, con-

trary to experimental observations, isotropic hardening rule implies that material exhibits an increase in the tensile yield stress equal to the increase in the yield compressive stress. This was shown in Fig.2.2 where the yield limits in the (OAB)and inverse loading (OCD) directions are equal in magnitude. Since plastic deformations is anisotropic process, it is not expected to have realistic results when the isotropic hardening rule is used with complex paths involving significant changes in the direction of stress vectors in stress space (not necessarily completely reversed).

Bauschinger effect can be simulated by assuming kinematic hardening rule. Here the yield surface moves as a rigid body in the stress space (no change in size or in shape) as shown in Fig.2.5. Kinematic hardening predicts an ideal Bauschinger effect for completely reversed loadings. But it can not produce different degrees of Bauschinger effect, and it overpredicts the real cyclic response.

A combination of the two preceding cases leads to the more general combined hardening rule (Hodge, 1957). In this case, the yield surface experiences translation and uniform expansion in all directions (i.e. no change in the original shape). With this rule different degrees of Bauschinger effect can be simulated (Fig.2.6).

In this work, the kinematic hardening rule is used along with the three-invariant stress dependent isotropic cap model proposed by Faruque (1988). The behavior of soil in cyclic triaxial tests will be predicted by

using this model. Furthermore, the model will be implemented into a finite element program to solve a boundary value problem of a rigid model footing placed on the surface of dry sand.

3.3 FORMULATION OF THE MODEL

In order to extend the isotropic cap model into a combined hardening form, the kinematic parameter α_{ij} is invoked into the isotropic model [(Drucker and palgen, 1981) , (Sandler and Baron, 1979)]. This will lead to the translation of the expanding yield surface (Fig.3.1). Now, translation of the yield surface is formulated by replacing J_{2D} in Eq.'s 2.25 and 2.31 by

$$\frac{1}{2}(S_{ij} - \alpha_{ij})^2 \qquad 3.1$$

where α_{ij} is a tensor defines the center of the translated yield surface (Fig.3.2). This results in changing the center of the yield surface in the stress space. α_{ij} is updated at the end of each load increment if the material yields due to that increment, otherwise it remainse unchanged in the elastic zone.

$$\alpha_{ij}^{n+1} = \alpha_{ij}^{n} + d\alpha_{ij} \qquad 3.2$$

where

$$d\alpha_{ij} = C_{\alpha} de_{ij}^{P} \qquad 3.3$$

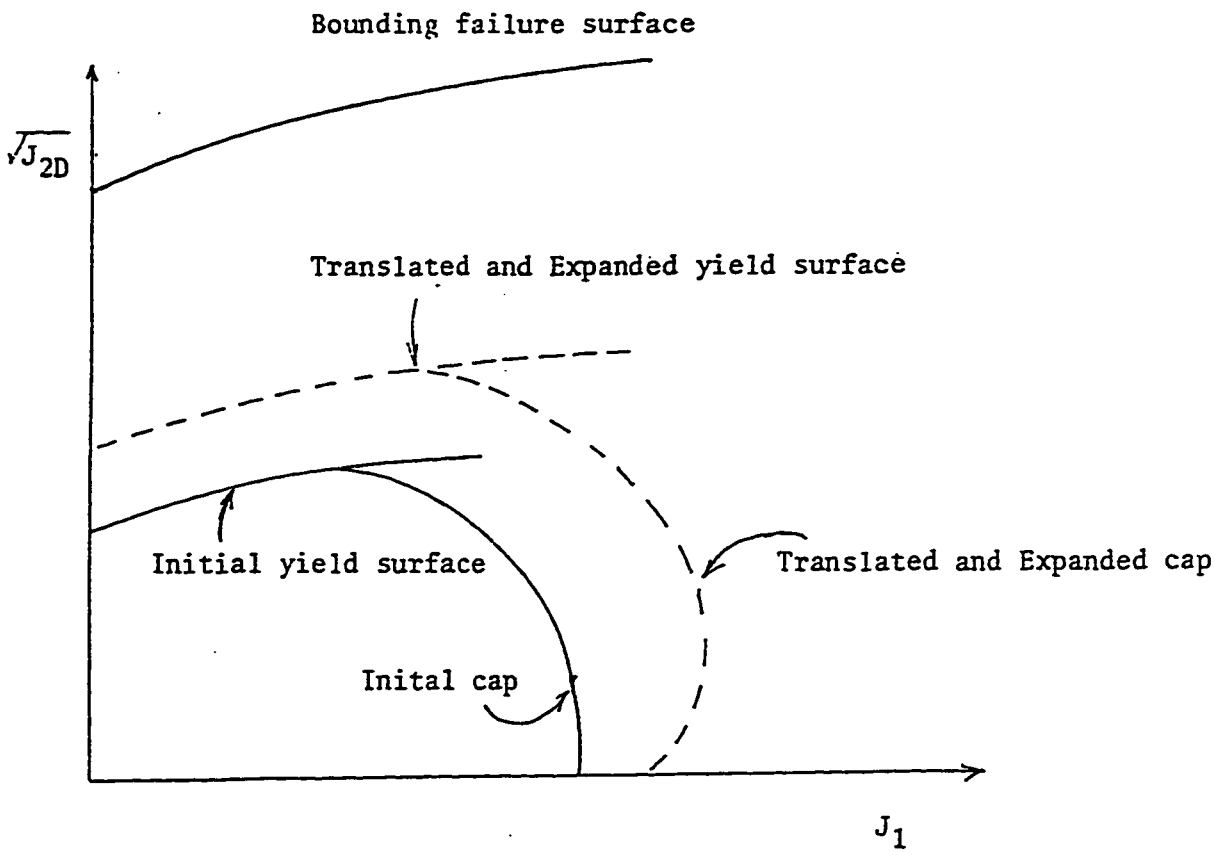

Fig.3.1 Translation and expansion of yield surface.

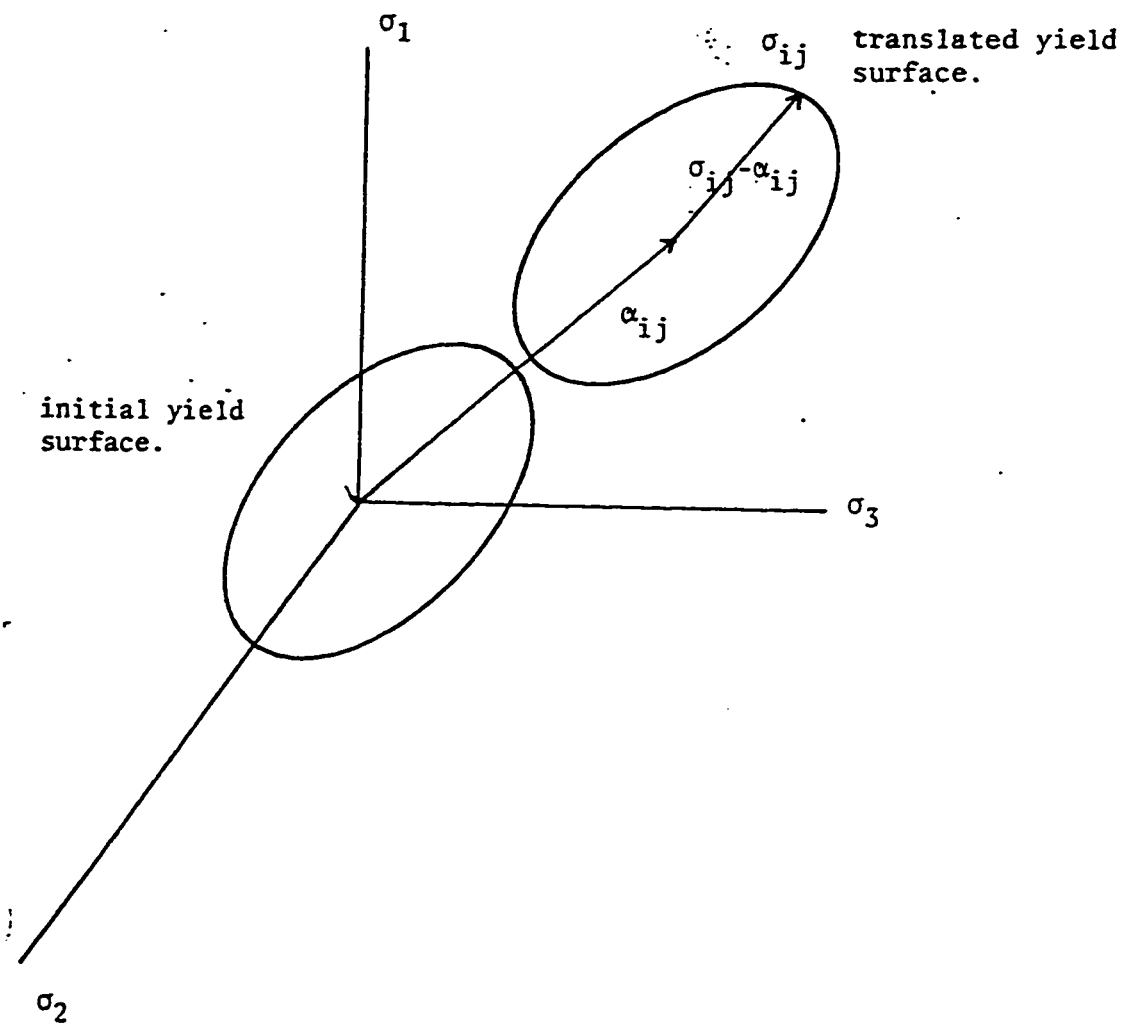

Fig. 3.2. Translating yield surface in the stress space for kinematic hardening.

where

C_α : a material constant to be determined experimentally.

de_{ij}^p : The incremental deviatoric plastic strain vector.

$$de_{ij}^p = d\varepsilon_{ij} - \frac{1}{3} d\varepsilon_{kk}^p \delta_{ij} \qquad 3.4$$

$$d\varepsilon_{kk}^p = \frac{(d\varepsilon_{11}^p + d\varepsilon_{22}^p + d\varepsilon_{33}^p)}{3} \qquad 3.5$$

where

$d\varepsilon_{ij}^p$: plastic strain increment.

δ_{ij} : kronecker delta (unity matrix).

The yield and failure functions of the new model will be as follows :

$$F_f = g(\theta, J_1)[\frac{1}{\sqrt{2}}(S_{ij} - \alpha_{ij})] - A - MJ_1 + C\exp(-\beta J_1) = 0 \qquad 3.6$$

$$F_c = g(0, L)[\frac{1}{\sqrt{2}}(S_{ij} - \alpha_{ij})] - \sqrt{b^2 - \frac{(J_1 - L)^2}{R^2}} = 0 \qquad 3.7$$

The hardening parameter that is responsible for expantion of the yield surface is χ, that is defined as follows :

$$\chi = -\frac{1}{D}\ln(1 - \frac{\varepsilon_v^p}{W}) + Z \qquad 3.8$$

Where D, w, and Z are material constants, w is the maximum plastic volumetric strain, D denotes the total volumetric plastic strain rate (which con-

trols the initial loading moduli), and Z determines the initiation of plastic deformation under hydrostatic loading conditions. The accumulation of plastic volumetric plastic strain ε_v^p leads to the expansion of the cap isotropically and hence combining this effect by the effect of α_{ij} (kinematic translation), so the cap presented here hardens according to the combined hardening rule.

The general form of the relationship that governs the stress-strain response of elastic-isotropic material will be derived using the combined-hardening rule. From that constitutive relation the elasto-plastic matrix will also be derived. Formulation of the elasto-plastic matrix will contain the elastic matrix, which is not going to be derived here. Many references, like Chen and Saleeb 1982, contains full derivation of the linearly elastic isotropic matrices. Derivations of the elasto-plastic matrix will be done for both a general 3-D case and a specialized 2-D case (plane strain case).

The consistency condition indicates that every time the material yields the state of stress does not lie outside the yield surface, but it lies on a new yield surface. This can be defined as follows :

$$dF = 0 \qquad 3.9$$

Since the yield and failure surfaces are functions of σ, α, and$\kappa(\varepsilon_v^p)$, Eq.3.9 gives

$$\{\frac{\partial F}{\partial\{\sigma\}}\}^T\{d\sigma\} + \{\frac{\partial F}{\partial\{\alpha\}}\}^T\{d\alpha\} + \frac{\partial F}{\partial\kappa}d\kappa = 0 \qquad 3.10$$

since

$$\{\frac{\partial F}{\partial\{\alpha\}}\}^T = -\{\frac{\partial F}{\partial\{\sigma\}}\}^T \qquad 3.11$$

The derivaction of Eq.3.11 is shown in appendix B.

$$\{\frac{\partial F}{\partial\{\sigma\}}\}^T\{d\sigma\} - \{\frac{\partial F}{\partial\{\sigma\}}\}^T\{d\alpha\} + \frac{\partial F}{\partial\kappa}d\kappa = 0 \qquad 3.12$$

where

$$\{d\sigma\}^T = \{d\sigma_x, d\sigma_y, d\sigma_z, d\tau_{xy}, d\tau_{yz}, d\tau_{zx}\} \qquad 3.13$$

and

$$\{\frac{\partial F}{\partial\{\sigma\}}\}^T = \{\frac{\partial F}{\partial\sigma_x}, \frac{\partial F}{\partial\sigma_y}, \frac{\partial F}{\partial\sigma_z}, \frac{\partial F}{\partial\tau_{xy}}, \frac{\partial F}{\partial\tau_{yz}}, \frac{\partial F}{\partial\tau_{zx}}\} \qquad 3.14$$

The total incremental strain can be written as in Eq.2.3.

substituting Eq.'s 2.12 and 2.16 into Eq. 2.3

$$\{d\varepsilon\} = [C^e]^{-1}\{d\sigma\} + d\lambda\frac{\partial Q}{\partial\{\sigma\}} \qquad 3.15$$

The isotropic hardening parameter κ is related to plastic strain in one way or the other and a correlation between $d\kappa$ of Eq. 3.12 and $d\lambda$ of Eq. 3.15 may be assumed. Thus Eq. 3.12 can be written as :

$$\{\frac{\partial F}{\partial\{\sigma\}}\}^T\{d\sigma\} - \{\frac{\partial F}{\partial\{\sigma\}}\}^T\{d\alpha\} + \frac{\partial F}{\partial\kappa}\frac{d\kappa}{d\lambda}d\lambda = 0 \qquad 3.16$$

$$\{\frac{\partial F}{\partial\{\sigma\}}\}^T\{d\sigma\} - \{\frac{\partial F}{\partial\{\sigma\}}\}^T\{d\alpha\} + A_h d\lambda = 0 \qquad 3.17$$

where

$$A_h = \frac{\partial F}{\partial \kappa}\frac{d\kappa}{d\lambda} \qquad 3.18$$

The incremental deviatoric plastic strain vector can be expressed as follow

$$\{de^p\} = \begin{bmatrix} d\varepsilon_1^p \\ d\varepsilon_2^p \\ d\varepsilon_3^p \\ d\varepsilon_4^p \\ d\varepsilon_5^p \\ d\varepsilon_6^p \end{bmatrix} - \frac{1}{3}\begin{bmatrix} (d\varepsilon_1^p + d\varepsilon_2^p + d\varepsilon_3^p) \\ (d\varepsilon_1^p + d\varepsilon_2^p + d\varepsilon_3^p) \\ (d\varepsilon_1^p + d\varepsilon_2^p + d\varepsilon_3^p) \\ 0 \\ 0 \\ 0 \end{bmatrix} \qquad 3.19$$

Using Eq.2.12 $\{e^p\}$ can be expressed as follows

$$\{e^p\} = d\lambda\{\frac{\partial Q}{\partial\{\sigma\}}\} - \frac{d\lambda}{3}\{Y\} \qquad 3.20$$

where

$$\{Y\} = \begin{bmatrix} (\frac{\partial Q}{\partial \sigma_{11}} + \frac{\partial Q}{\partial \sigma_{22}} + \frac{\partial Q}{\partial \sigma_{33}}) \\ (\frac{\partial Q}{\partial \sigma_{11}} + \frac{\partial Q}{\partial \sigma_{22}} + \frac{\partial Q}{\partial \sigma_{33}}) \\ (\frac{\partial Q}{\partial \sigma_{11}} + \frac{\partial Q}{\partial \sigma_{22}} + \frac{\partial Q}{\partial \sigma_{33}}) \\ 0 \\ 0 \\ 0 \end{bmatrix} \qquad 3.21$$

$$\{e^p\} = d\lambda[\{\frac{\partial Q}{\partial\{\sigma\}}\} - \frac{1}{3}\{Y\}] \qquad 3.22$$

substituting Eq. 3.22 into Eq. 3.3

$$\{d\alpha\} = C_\alpha d\lambda |\{\frac{\partial Q}{\partial\{\sigma\}}\} - \frac{1}{3}\{Y\}| \qquad 3.23$$

replacing $\{d\alpha\}$ in Eq. 3.17 by Eq. 3.23

$$\{\frac{\partial F}{\partial\{\sigma\}}\}^T \{d\sigma\} - C_\alpha \{\frac{\partial F}{\partial\{\sigma\}}\}^T |\{\frac{\partial Q}{\partial\{\sigma\}}\} - \frac{1}{3}\{Y\}| d\lambda + A_h d\lambda = 0 \qquad 3.24$$

or

$$\{\frac{\partial F}{\partial\{\sigma\}}\}^T \{d\sigma\} - |C_\alpha \{\frac{\partial F}{\partial\{\sigma\}}\}^T \{\frac{\partial Q}{\partial\{\sigma\}}\} - \frac{C_\alpha}{3}\{\frac{\partial F}{\partial\{\sigma\}}\}^T \{Y\} + A_h| d\lambda = 0 \qquad 3.25$$

Eq.'s 2.12 and 3.25 can be written as :

$$\begin{bmatrix} \{d\varepsilon\} \\ \text{----} \\ 0 \end{bmatrix} = \begin{bmatrix} [C^e]^{-1} & \vdots & \{\frac{\partial Q}{\partial\{\sigma\}}\} \\ \text{----------} & \vdots & \text{-------} \\ \{\frac{\partial F}{\partial\{\sigma\}}\}^T & \vdots & -A_h^* \end{bmatrix} \begin{bmatrix} \{d\sigma\} \\ \text{----} \\ d\lambda \end{bmatrix} \qquad 3.26$$

Following the procedure developed by Yamada et. al., (1968), (see also Zienkiewiez, et. al., (1969); Steinar Nordal, (1983)) to derive an explicit expression for the elasto-plastic matrix $[C]^{e-p}$.

Multiplying eq 3.15 by $\{\frac{\partial F}{\partial\{\sigma\}}\}^T [C^e]$ produces :

$$\{\frac{\partial F}{\partial\{\sigma\}}\}^T [C^e]\{d\varepsilon\} = \{\frac{\partial F}{\partial\{\sigma\}}\}^T [C^e][C^e]^{-1}\{d\sigma\} + \{\frac{\partial F}{\partial\{\sigma\}}\}^T [C^e]\{\frac{\partial Q}{\partial\{\sigma\}}\} d\lambda \qquad 3.27$$

so

$$\{\frac{\partial F}{\partial\{\sigma\}}\}^T\{d\sigma\} = \{\frac{\partial F}{\partial\{\sigma\}}\}^T[C^e]\{d\varepsilon\} - \{\frac{\partial F}{\partial\{\sigma\}}\}^T[C^e]\{\frac{\partial Q}{\partial\{\sigma\}}\}d\lambda \qquad 3.28$$

substituting Eq. 3.28 into 3.24

$$\{\frac{\partial F}{\partial\{\sigma\}}\}^T[C^e]\{d\varepsilon\} - \{\frac{\partial F}{\partial\{\sigma\}}\}^T[C^e]\{\frac{\partial Q}{\partial\{\sigma\}}\}d\lambda - C_\alpha\{\frac{\partial F}{\partial\{\sigma\}}\}^T[\{\frac{\partial Q}{\partial\{\sigma\}}\} - \frac{1}{3}\{Y\}]d\lambda + A_h d\lambda = 0 \qquad 3.29$$

solving Eq.3.29 for $d\lambda$

$$d\lambda = \frac{\{\frac{\partial F}{\partial\{\sigma\}}\}^T[C^e]\{d\varepsilon\}}{\{\frac{\partial F}{\partial\{\sigma\}}\}^T[C^e]\{\frac{\partial Q}{\partial\{\sigma\}}\} + C_\alpha\{\frac{\partial F}{\partial\{\sigma\}}\}^T[\{\frac{\partial Q}{\partial\{\sigma\}}\} - \frac{1}{3}\{Y\}] - A_h} \qquad 3.30$$

substituting Eq. 3.30 into Eq. 3.15

$$\{d\sigma\} = [C]\{d\varepsilon\} - \frac{[C^e]\{\frac{\partial Q}{\partial\{\sigma\}}\}\{\frac{\partial F}{\partial\{\sigma\}}\}^T[C^e]\{d\varepsilon\}}{\{\frac{\partial F}{\partial\{\sigma\}}\}^T[C^e]\{\frac{\partial Q}{\partial\{\sigma\}}\} + C_\alpha\{\frac{\partial F}{\partial\{\sigma\}}\}^T[\{\frac{\partial Q}{\partial\{\sigma\}}\} - \frac{1}{3}\{Y\}] - A_h} \qquad 3.31$$

Eq.3.31 can be written in the form of Eq.2.22, where the the elasto-plastic matrix will be as follow

$$[C^{e-p}] = [C] - \frac{[C]\{\frac{\partial Q}{\partial\{\sigma\}}\}\{\frac{\partial F}{\partial\{\sigma\}}\}^T[C]}{\{\frac{\partial F}{\partial\{\sigma\}}\}^T[C]\{\frac{\partial Q}{\partial\{\sigma\}}\} + C_\alpha\{\frac{\partial F}{\partial\{\sigma\}}\}^T[\{\frac{\partial Q}{\partial\{\sigma\}}\} - \frac{1}{3}\{Y\}] - A_h} \qquad 3.32$$

for associated plasticity, $[C^{e-p}]$ can be written as :

$$[C^{ep}] = [C] - \frac{[C]\{\frac{\partial F}{\partial\{\sigma\}}\}\{\frac{\partial F}{\partial\{\sigma\}}\}^T[C]}{\{\frac{\partial F}{\partial\{\sigma\}}\}^T[C]\{\frac{\partial F}{\partial\{\sigma\}}\} + C_a\{\frac{\partial F}{\partial\{\sigma\}}\}^T[\{\frac{\partial F}{\partial\{\sigma\}}\} - \frac{1}{3}\{Y\}] - A_h} \qquad 3.33$$

If F is expressed in terms of stress invariants, $\{\frac{\partial F}{\partial\{\sigma\}}\}^T$ can be found from the chain rule of derivations as follows :

$$\{\frac{\partial F(J_1,J_{2D},J_{3D})}{\partial\{\sigma\}}\} = \frac{\partial F}{\partial J_1}\{\frac{\partial J_1}{\partial\{\sigma\}}\} + \frac{\partial F}{\partial J_2}\{\frac{\partial J_2}{\partial\{\sigma\}}\} + \frac{\partial F}{\partial J_3}\{\frac{\partial J_3}{\partial\{\sigma\}}\} \qquad 3.34$$

$$\{\frac{\partial}{\partial\{\sigma\}}\} = \{\frac{\partial}{\partial\sigma_x},\frac{\partial}{\partial\sigma_y},\frac{\partial}{\partial\sigma_z},\frac{\partial}{\partial\tau_{xy}},\frac{\partial}{\partial\tau_{yz}},\frac{\partial}{\partial\tau_{zx}}\} \qquad 3.35$$

where

J_1,J_{2D},J_{3D} are stress invariants defined in chapter 2.

A_h can be found by defrentiating the yield function with respect to χ (appendix B). Detailed description of Eq.3.34 and Eq.3.35 is found in apendix B.

The plane strain condition, which is commom for many field problems, can be expressed as follows :

$$d\varepsilon_z = d\gamma_{xz} = d\gamma_{yz} = 0 \qquad 3.36$$

so

$$\{d\varepsilon\}^T = \{d\varepsilon_x,d\varepsilon_y,d\gamma_{xy}\} \qquad 3.37$$

Writing Eq.3.26 in an expanded form and introducing Eq.3.36 into it :

$$\begin{bmatrix} d\varepsilon_x \\ d\varepsilon_y \\ 0 \\ d\gamma_{xy} \\ 0 \\ 0 \\ \text{-----} \\ 0 \end{bmatrix} = \left[\begin{array}{cccccc:c} -\frac{\nu}{E} & -\frac{\nu}{E} & -\frac{\nu}{E} & 0 & 0 & 0 & \frac{\partial Q}{\partial \sigma_x} \\ -\frac{\nu}{E} & \frac{1}{E} & -\frac{\nu}{E} & 0 & 0 & 0 & \frac{\partial Q}{\partial \sigma_y} \\ 0 & -\frac{\nu}{E} & \frac{1}{E} & 0 & 0 & 0 & \frac{\partial Q}{\partial \sigma_z} \\ 0 & 0 & 0 & \frac{2(1+\nu)}{E} & 0 & 0 & \frac{\partial Q}{\partial \tau_{xy}} \\ 0 & 0 & 0 & 0 & \frac{2(1+\nu)}{E} & 0 & \frac{\partial Q}{\partial \tau_{yz}} \\ 0 & 0 & 0 & 0 & 0 & \frac{2(1+\nu)}{E} & \frac{\partial Q}{\partial \tau_{zx}} \\ \hdashline \frac{\partial F}{\partial \sigma_x} & \frac{\partial F}{\partial \sigma_y} & \frac{\partial F}{\partial \sigma_z} & \frac{\partial F}{\partial \tau_{xy}} & \frac{\partial F}{\partial \tau_{yz}} & \frac{\partial F}{\partial \tau_{zx}} & -A_h^* \end{array}\right] \begin{bmatrix} d\sigma_x \\ d\sigma_y \\ d\sigma_z \\ d\tau_{xy} \\ d\tau_{yz} \\ d\tau_{zx} \\ \text{--------} \\ d\lambda \end{bmatrix} \qquad 3.38$$

solving for $d\sigma_z$

$$d\sigma_z = \nu(d\sigma_x + d\sigma_y) - Ed\lambda\frac{\partial Q}{\partial \sigma_z} \qquad 3.39$$

substituting back the value of $d\sigma_z$ into Eq.3.38 and eleminating 3, 5, and 6 lines will give :

$$\begin{bmatrix} d\varepsilon_x \\ d\varepsilon_y \\ d\gamma_{xy} \\ \text{----} \\ 0 \end{bmatrix} = \left[\begin{array}{ccc:c} 1-\frac{\nu^2}{E} & \frac{-nu(1+\nu)}{E} & 0 & \frac{\partial Q}{\partial \sigma_x}+\nu\frac{\partial F}{\partial \sigma_z} \\ \frac{-\nu(1+\nu)}{E} & \frac{1-\nu^2}{E} & 0 & \frac{\partial Q}{\partial \sigma_y}+\nu\frac{\partial F}{\partial \sigma_z} \\ 0 & 0 & \frac{1-\nu^2}{E} & \frac{\partial Q}{\partial \tau_{xy}} \\ \hdashline \frac{\partial F}{\partial \sigma_x}+\nu\frac{\partial F}{\partial \sigma_z} & \frac{\partial F}{\partial \sigma_y}+\nu\frac{\partial F}{\partial \sigma_z} & \frac{\partial F}{\partial \tau_{xy}} & -A_h^*-E\frac{\partial F}{\partial \sigma_z}\frac{\partial Q}{\partial \sigma_z} \end{array}\right] \begin{bmatrix} d\sigma_x \\ d\sigma_y \\ d\tau_{xy} \\ \text{--------} \\ d\lambda \end{bmatrix} \qquad 3.40$$

Eq.3.40 can be represented in a condesed form as follows :

$$\begin{bmatrix} \{d\varepsilon\} \\ \hline 0 \end{bmatrix} = \begin{bmatrix} [C^e]^{-1} & \{b\} \\ \hline \{a\}^T & -A_h^{**} \end{bmatrix} \begin{bmatrix} \{d\sigma\} \\ \hline d\lambda \end{bmatrix} \qquad 3.41$$

where

$$\{d\varepsilon\}^T = \{d\varepsilon_x, d\varepsilon_y, d\gamma_{xy}\} \qquad 3.42a$$

$$\{d\sigma\}^T = \{d\sigma_x, d\sigma_y, d\tau_{xy}\} \qquad 3.42b$$

$$\{a\}^T = \{(\frac{\partial F}{\partial \sigma_x} + \nu\frac{\partial F}{\partial \sigma_z}),(\frac{\partial F}{\partial \sigma_y} + \nu\frac{\partial F}{\partial \sigma_z}),(\frac{\partial F}{\partial \tau_{xy}})\} \qquad 3.42c$$

$$\{b\}^T = \{(\frac{\partial Q}{\partial \sigma_x} + \nu\frac{\partial Q}{\partial \sigma_z}),(\frac{\partial Q}{\partial \sigma_y} + \nu\frac{\partial Q}{\partial \sigma_z}),(\frac{\partial Q}{\partial \tau_{xy}})\} \qquad 3.42d$$

$$A_h^{**} = C_a\{\frac{\partial F}{\partial \{\sigma\}}\}^T\{d\sigma\}[\{\frac{\partial Q}{\partial \{\sigma\}}\} - \frac{1}{3}\{I\}] + A_h + E\frac{\partial F}{\partial \sigma_z}\frac{\partial Q}{\partial \sigma_z} \qquad 3.42e$$

Now, the elasto-plastic matrix for the plane strain condition is derived from the original elasto-plastic matrix by replacing :

a) $\{a\}$ for $\{\frac{\partial F}{\partial \{\sigma\}}\}^T$

b) $\{b\}$ for $\{\frac{\partial Q}{\partial \{\sigma\}}\}^T$

c) The plane stress elastic matrix for the 3D one.

d) A_h^{**} for A_h^*.

3.4 PARAMETERS DETERMINTAIONS

The combined hardening three-invariant cap model has now 12 parameters that are to be determined experimentally. They are

Elastic parameters

E, and ν

Failure surface parameters

γ , A, B, C, and M

The hardening parameters

D, W, Z, R, and C_α

3.4.1 Determination of Elastic Constants E and ν

The Young's modulus, E and the Poisson's ratio, ν can be determined from the results of CTC tests directly, or from those of HC and CTC tests indirectly. The indirect method, which consists of HC test data is plotted as mean preassure p vs. volumetric strain ε_v. The slope of unloading-realoading portion of such a curve gives the bulk modulus, K. The bulk modulus is related to E and ν through the following relationship

$$K = \frac{E}{3(1-2\nu)} \qquad 3.43$$

A second relation is required to determine E and ν explicitly. For this purpose, results from CTC tests are utilized. A plot of $(\sigma_1 - \sigma_3)$ vs. $2*(\varepsilon_1 - \varepsilon_3)$ is obtained. The average slope of the unloading-reloading curve gives the shear modulus G (Fig.3.3), which is related to E and ν as follows

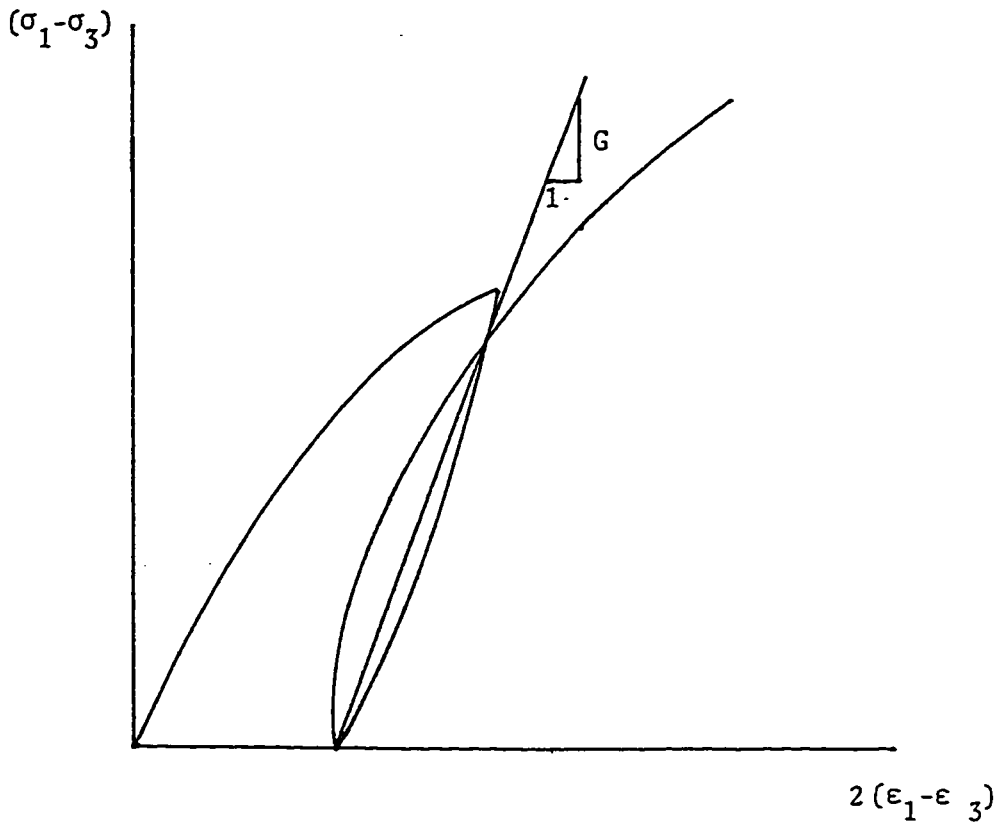

Fig.3.3 Evaluation of shear modulus from CTC test.

$$G = \frac{E}{2(1+\nu)} \qquad 3.44$$

Using Eq.'s 3.43 and 3.44, E and ν can be obtained explicitly.

3.4.2 Determination of Failure Surface Parameters γ, A, B, C, and M

The following tests can be utilized in the determination of the parameters for the failure surface F_f

(i) TC and TE Test at different confining pressures.

(ii) CTC Test at a wide range of confining pressures

γ will be determined firstly, since it will be utilized in the determination of other parameters later. γ can be determined easily from the following equation using an iterative procedure

$$s = \frac{g(60,J_1)}{g(0,J_1)} = \frac{\cos[\frac{1}{3}\cos^{-1}(A_f)]}{\cos[\frac{1}{3}\cos^{-1}(-A_f)]} \qquad 3.45$$

Once γ is determined, the rest of the failure surface parameters can be determined based on the procedure suggested by Desai and Siriwardane (1984). This procedure suggests to obtain the failure values of various tests (CTC, TC and TE) and plot the result on $J_1 - \sqrt{J_2 D}$ space as shown in Fig.3.4. The failure surface equation which is given by Eq.2.25 is reduced to the following form for $J_1 = 0$

$$\sqrt{J_{2D}} = \frac{A - C}{g(0)} \qquad 3.46$$

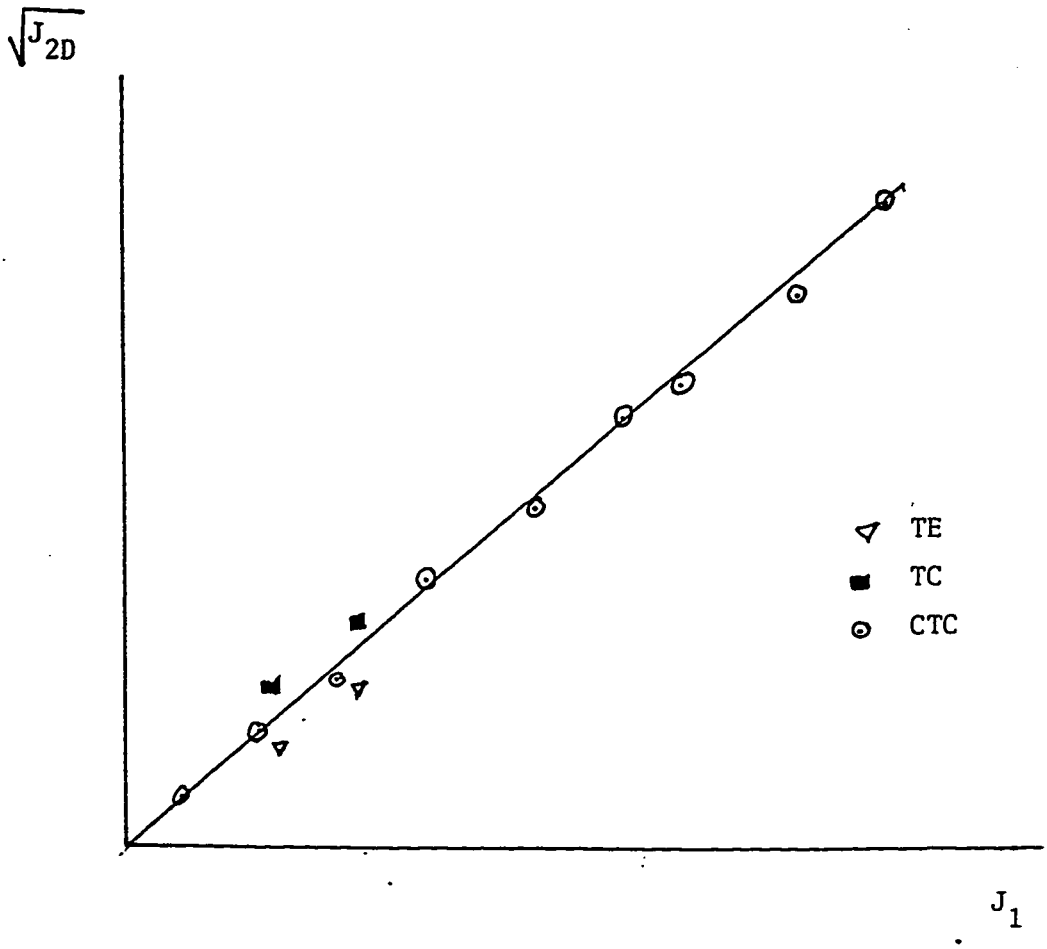

Fig.3.4. Exp. failure surface on J_1- J_{2D} space.

At large values of J_1, Eq. 2.25 becomes

$$\sqrt{J_{2D}} = A + MJ_1 \qquad 3.47$$

This equation is reffered to as "Drucker-Prager II" surface (Fig.3.5). The intercept of this surface with the $\sqrt{J_{2D}}$ axis gives $\frac{A}{g(0)}$, and its slope is $\frac{M}{g(\theta)}$, where $g(0)$ can be evaluated since γ is known. So, A and M can be evaluated. Knowing A, C can be determined using Eq. 3.46. In order to determine B, the following equation will be used

$$B = \frac{-1}{J_1}\ln\left(\frac{A + MJ_1 - \sqrt{J_{2D}}g(0,J_1)}{C}\right) \qquad 3.48$$

3.4.3 Determination of Hardening Parameters :

HC test data is required for the determination of the hardening parameters. Mean pressure, p, vs. volumetric strain, ε_v, curve is drawn for the HC test. The bulk modulus is evaluated as mentioned erlier.

The values of Z, D and w can be computed by using the hardening rule

$$\chi = \frac{-1}{D}\ln\left(1 - \frac{\varepsilon_v^p}{w}\right) + Z \qquad 3.49$$

For soil Z is assumed to be zero (Fig.2.8). So, Eq.3.49 becomes

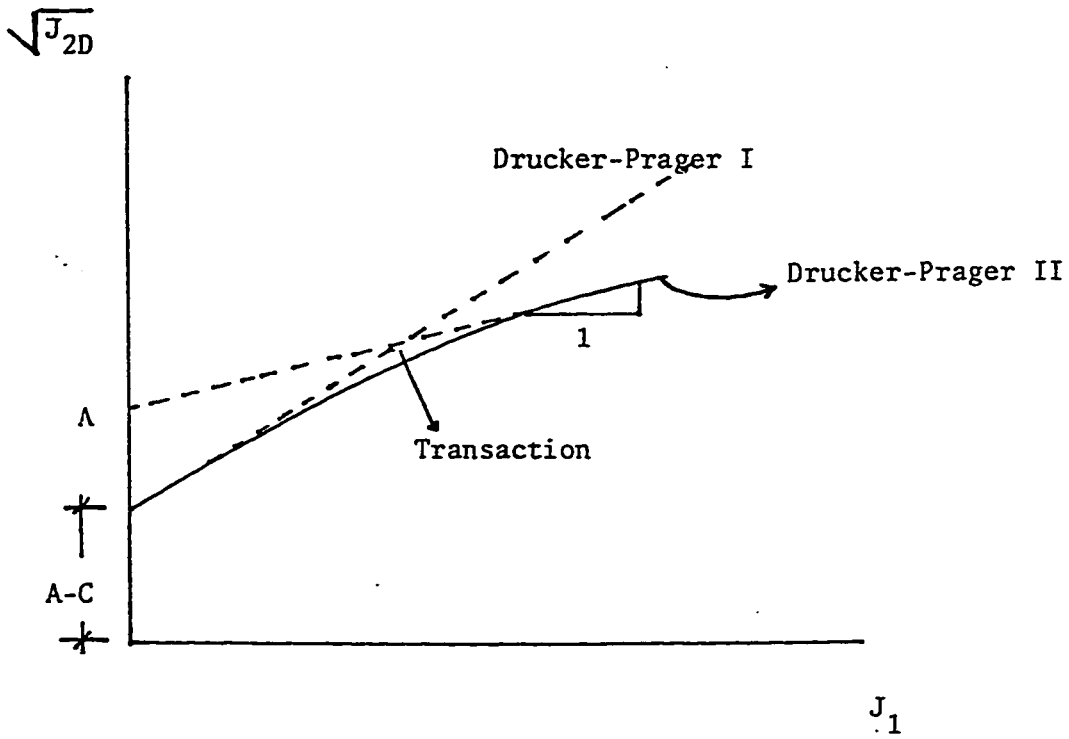

Fig.3.5 Interpretation of failure surface parameters.

$$\chi = \frac{-1}{D}\ln(1-\frac{\varepsilon_v^p}{w}) \qquad 3.50$$

Here $\chi = 3p$, where p is the mean pressure. Substituting and rearranging, we have,

$$\varepsilon_v^p = W(1\text{-}e^{-3pD}) \qquad 3.51$$

However, the plastic volumetric strain can be expressed as

$$\varepsilon_v^p = \varepsilon_v - \varepsilon_v^e \qquad 3.52$$

The elastic volumetric strains ε_v^e can be computed since the bulk modulus is known. Therefore,

$$\varepsilon_v = W(1 - e^{-3pD}) + \frac{p}{K} \qquad 3.53$$

Considering different sets of two points on the loading portion and substituting them into Eq.3.53, two expressions in W and D can be solved by trial and error to get D and W.

To Determine R, the shape factor, the yield caps (contours of equal volumetric plastic strains) are to be plotted. To do so, incremental plastic strain vectors have to be determined using the following equation

$$d\varepsilon_v^p = d\varepsilon_v - d\varepsilon_v^e \qquad 3.54$$

By plotting the values of $d\varepsilon_v^p$ (Fig.3.6), R can be determined. For detailed

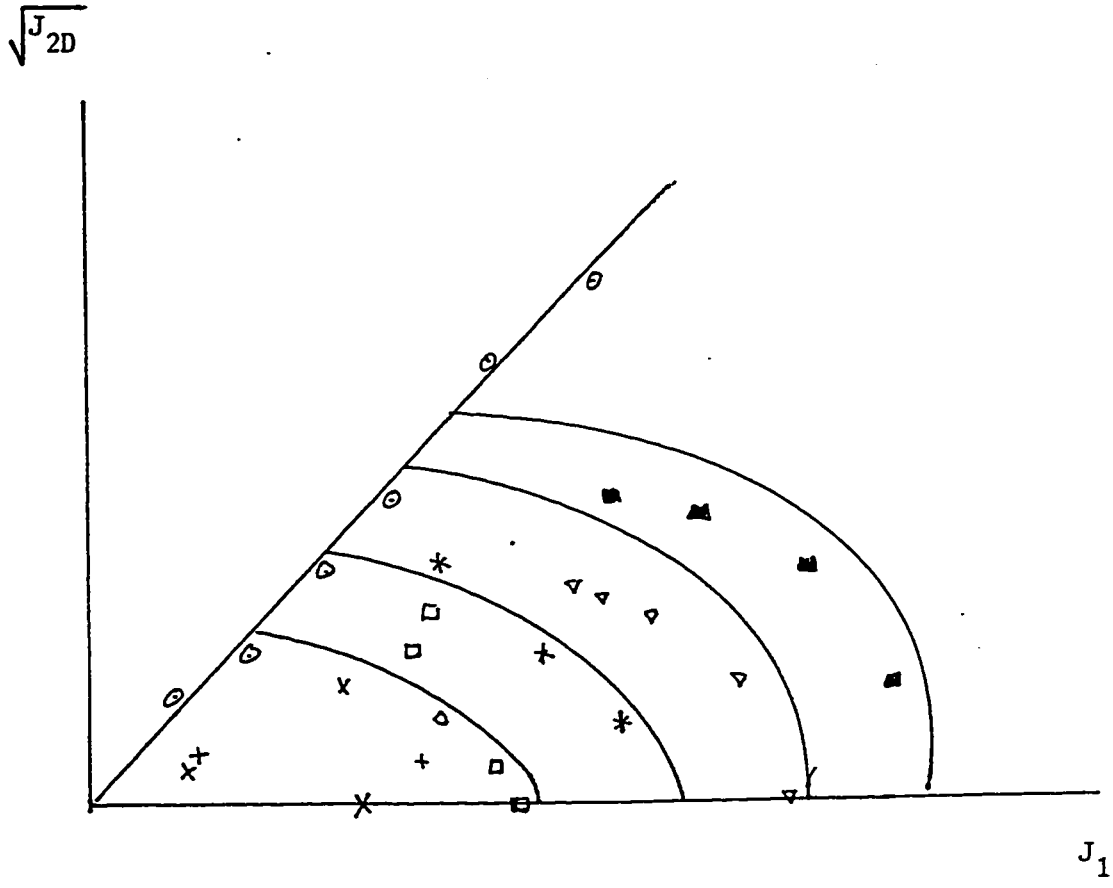

Fig.3.6 Determination of shape factor R.

description of the determination of the previous parameters see Azeemuddin, 1988.

In order to include the effect of of kinematic hardening, one additional parameter, C_α must be found. A good estimate of C_α can be found by plotting the octahedral shear stress versus the plastic octahedral shear strain at low amplitude cycles of shear stress. C_α is approximated by taking the average slope of the stress- strain cycles. Ploting the octahedral shear stress τ_{oct} versus plastic octahedral shear strain γ^p_{oct}, C_α can be determined as the average slope of the cycles of unloading and reloading. This will be discussed in detail in chapter 4.

CHAPTER 4

EXPIREMENTAL PROGRAM AND ANALYSIS OF DATA

4.1 INTRODUCTION

This chapter describes the material which will be used in this study including dune sand and the model rigid footing. Also it describes the testing devices used in the cyclic triaxial tests and in the experimental model footing problem. Discussion of the results will be presented at the end of this chapter.

4.2 MATERIAL

Dune sand is very common geological formation in the Kingdom of Saudi Arabia. Very large area is covered by dune sand. Dune sand was brought from the sand dunes located at the KFUPM beach and subjected to seive analysis test using standard procedure. Sand was dry and uni-

formly-graded with nearly 80% of it in the size range of 0.149 mm to 0.420mm (Fig.4.1). Direct shear test was used to detrmine the values of shear strength parameters as shown in table 4.1.

The modell strip footing is simulated in the lab by cutting a 50 mm thick steel plate to achieve length/width ratio of 12.

4.3 TEST PROGRAM

Dhahran dune sand is subjected to different types of tests icluding cyclic triaxial tests and is used as a foundation material for the model strip footing. The test program can be summerized as follow:

1. Convential triaxial (CTC) tests are conducted at confining pressures of 69 and 138 KPa.
2. Cyclic triaxial tests are conducted at a confining pressure of 69 KPa with :

    a. 4 complete cycles of loading, unloading, and reverse loading with maximum stress of 30% of the ultimate stress, then continued to failur.

    b. 3 complete cycles of different sizes were used up to 30%, 50% and 70% of the ultimate condition.

3. Cyclic triaxial tests at a confining pressure of 138 KPa with 4 complete cycles of loading, unloading and reverse loading to a maximum stress of 30% of the ultimate, then continued to failure.
4. A model footing is loaded axially till failure. Furthermore, the model

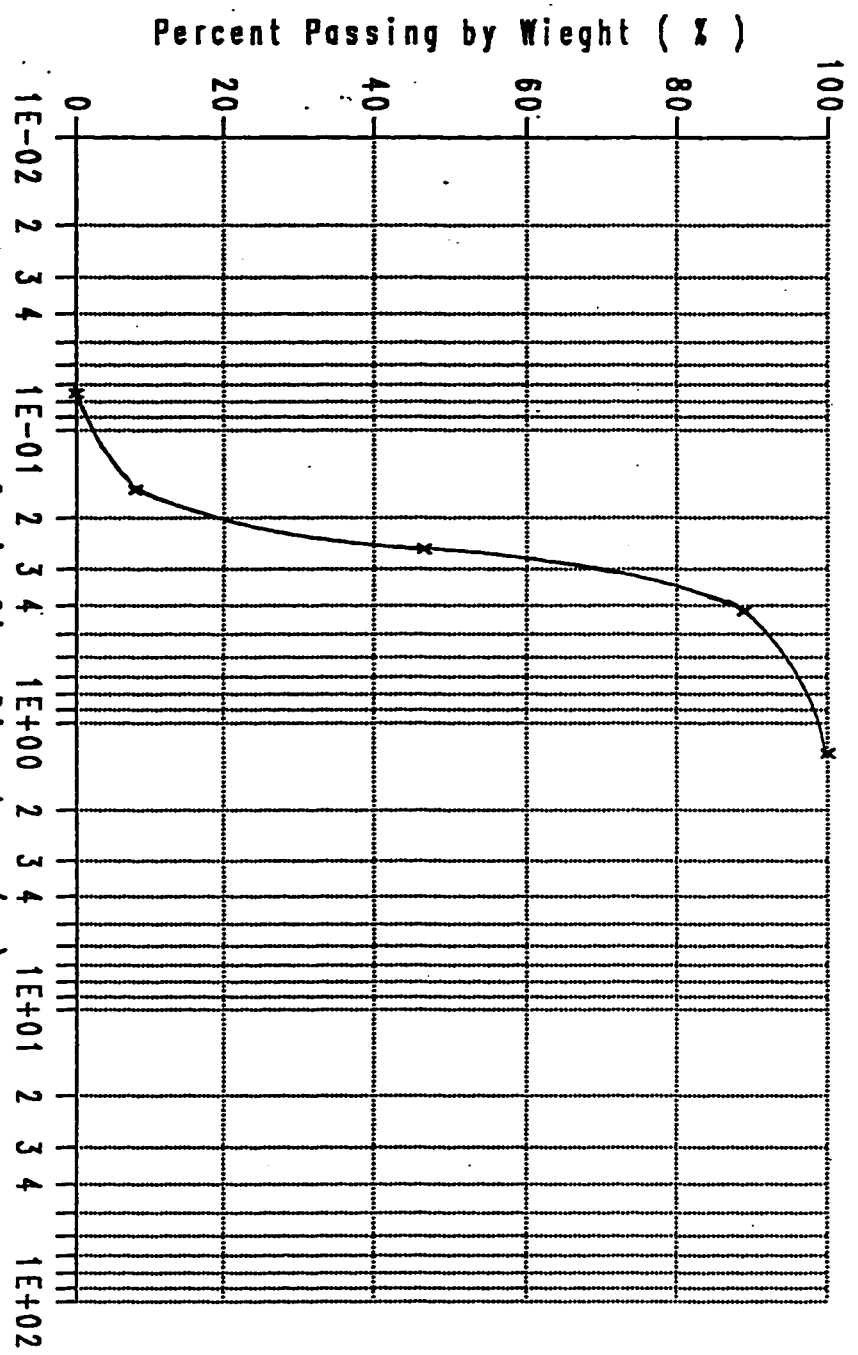

Fig.4.1 Sieve analysis of Dhahran Dune sand.

Table 4.1 Dhahran Dune Sand Properties

Max. Density (KN/m**3) Min. Density (KN/m**3) Measured Density (KN/m**3) Avg. Relative Density (%)	17.71 14.73 16.40 81.0
D_{10} (mm)	0.15
Uniformity Cofficient $C_u = \frac{D_{60}}{D_{10}}$	1.84
Cofficient of Curvature $C_c = \frac{D_{30}^2}{D_{10} * D_{60}}$	0.998
Angle of Internal Friction φ° Cohesion (c) (KN/mm**2)	33.0 0.0

footing is subjected to cyclic loads up to 30%, 50% and 70% of the ultimate axial load. In every cycle footing will be unloaded down to very small level of load and then reload to the next cycle.

4.3.1 Triaxial Test :

Geological materials are path-dependent. So, to simulate field conditions, certain stress-paths should be followed. Fig.4.2 shows the possible stress paths that could be followed in the laboratory. It is clear that any testing device should give the required stress-path in order to simulate field conditions more closely.

A stress-control triaxial apparatus was manufactured at KFUPM at the Research Workshop to performe tests under a wide variety of stress paths. Almost all stress paths shown in Fig. 4.2 could be followed using the developed device except the simple shear test that requites a truly triaxial device. Using this device elastic parameters E, and ν can be determined from CTC tests. Failure surface parameters γ, A, B, C, and M can be determined using TC, TE and CTC tests at different confining pressures. Hardening parameters can also be determined from HC tests. Finally, the additional parameter C_α is determined from cyclic triaxial tests conducted at cycles of low amplitudes.

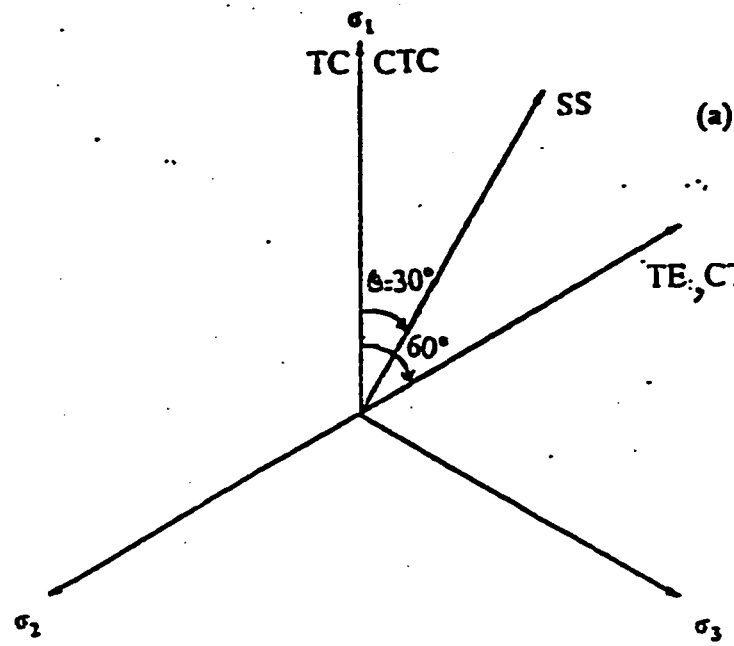

(a) On the Octahedral Plane.

(b) On the Triaxial Plane.

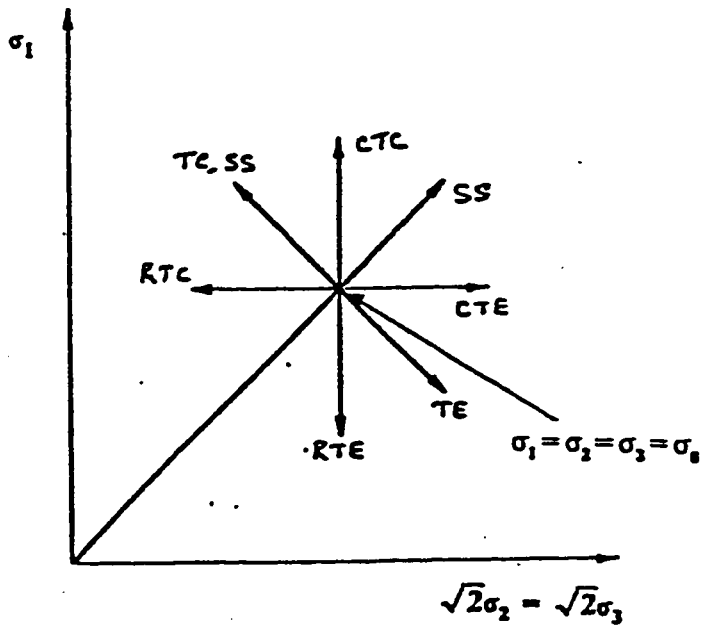

Fig. 4.2: Stress Paths for Some of the Tests Performed in the Laboratory

Testing Device

Many factors can affect manufacturing any device. Among them is the stress path, which has a great influence on test results. Following different stress paths will lead to different test results for the same soil and test conditions. Taking this into account, a new testing device has been manufactured at the University of King Fahd for Petroleum and Minerals workshop. This device can produce many stress paths such as (CTC, TC, TE, ...), (Fig.4.3). Moreover, the device used here is a stress-controlled device that provides an independent control on σ_v and σ_h. This is achieved by isolating σ_v chamber from the triaxial cell(where σ_h is applied to the sample). In order to do so, σ_v is not applied directly to top of the sample, but, through a hollow stainless steel piston that has the same diameter as the sample's diameter. To have a complete separation between the two chambers, an 'O' ring is fixed on the inner surface of σ_v chamber (Fig.4.3). Another feature of the device is that it has a valve-system that enables the user to follow any desired stress path. Here, there are three main valves. Two of them are for σ_v and σ_h respectively, that separately control the pressures that come from the pressure generating machines. So, to apply either σ_v or σ_h on the sample the corresponding valve is open. The third valve is used when a hydrostatic condition is required.

A balancing system has been introduced to nullify the weight of piston, and hence preventing its extra weight from exerting pressure on the sample

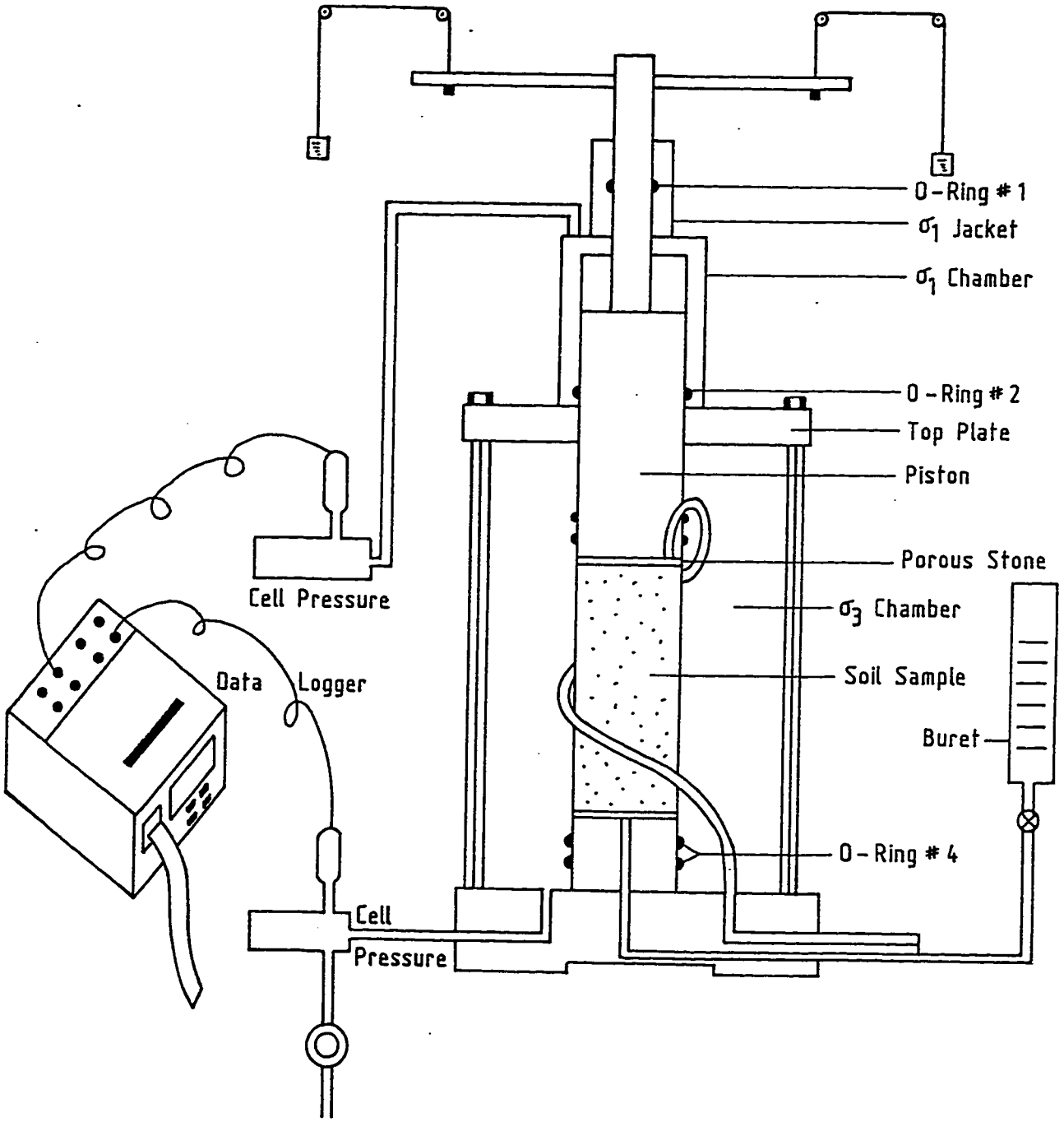

Fig. 4.3 Schematic Diagram of the triaxial apparatus.

before applying the confinig pressure σ_h. This can be done by attatching the piston to weigts that equal the weight of the piston, as shown in (Fig.4.3).

σ_v and σ_h are measured through pressure trasducers that are connected to a portable data logger (Fig.4.3). The amount of water drains out or into the sample is used to measure the sample volumetric change by means of a glass buret that has a least count of 0.05.. Assuming small deformation, ε_3 (radial strain) can be calculated by the following equation :

$$\varepsilon_3 = \frac{(\varepsilon_v - \varepsilon_1)}{2} \qquad 4.1$$

where

ε_v : volumetric strain.

ε_1 : axial strain.

The axial deformation is measured through an LVDT (linear variable differential transformer) connected to the data logger.

Sample Preparation

Samples needed for the triaxial tests have to be prepared carefully. Any small disturbance, even little vibration caused by movement of sand mold, can affect the sample density. Cylindrical samples of 2.8" are prepared of the dry sand with hight to diameter ratio of approximately 2, and of an average density of $1.67 g/cm^3$. In order to get this density, sand is poured from different heights untill the desired hieght is reached. Vaccum

pressure is applied to the container in order to make the rubber membrane stick to the container wall to get a uniform sample's diameter. A special set up has been manufactured to suspend the triaxial set parts including the piston that has some weight to be eliminated. The weight of the piston is eliminated by equivalent weights which are pulled over a pulley with the other end of the cable pulling the piston up (Fig.4.4). In this way, the extra weight of the piston is eliminated and it no longer has an effect on the sample. Having fixed the piston on top of the sample, σ_v chamber and triaxial cell are fixed around the sample. The piston is clambed in position, so that it will not rest on the sample while transfering the cell to the triaxial machine. Data logger is connected to an LVDT to measure the axial deformation, and two pressure gages to measure σ_v and σ_h values. A hydrostatic pressure is applied to the sample. Then, carbon dioxide is passed through the sample in order to replace air in the sample for about 10 minutes. Then, the sample is saturated with water and a pressure of 55.2 KPa is applied inside the sample (along with the hydrostatic pressure that is bieng applied around the sample) for about 1 hour, to insure full saturation of the sample. At the beginning of the test the draining valve is opened to allow for water drainage, and hence to measure volumetric change.

4.3.2 Laboratory Model of Rigid Strip Footing Resting on Sand .

The model strip footing is made of a thick steel plate to simulate

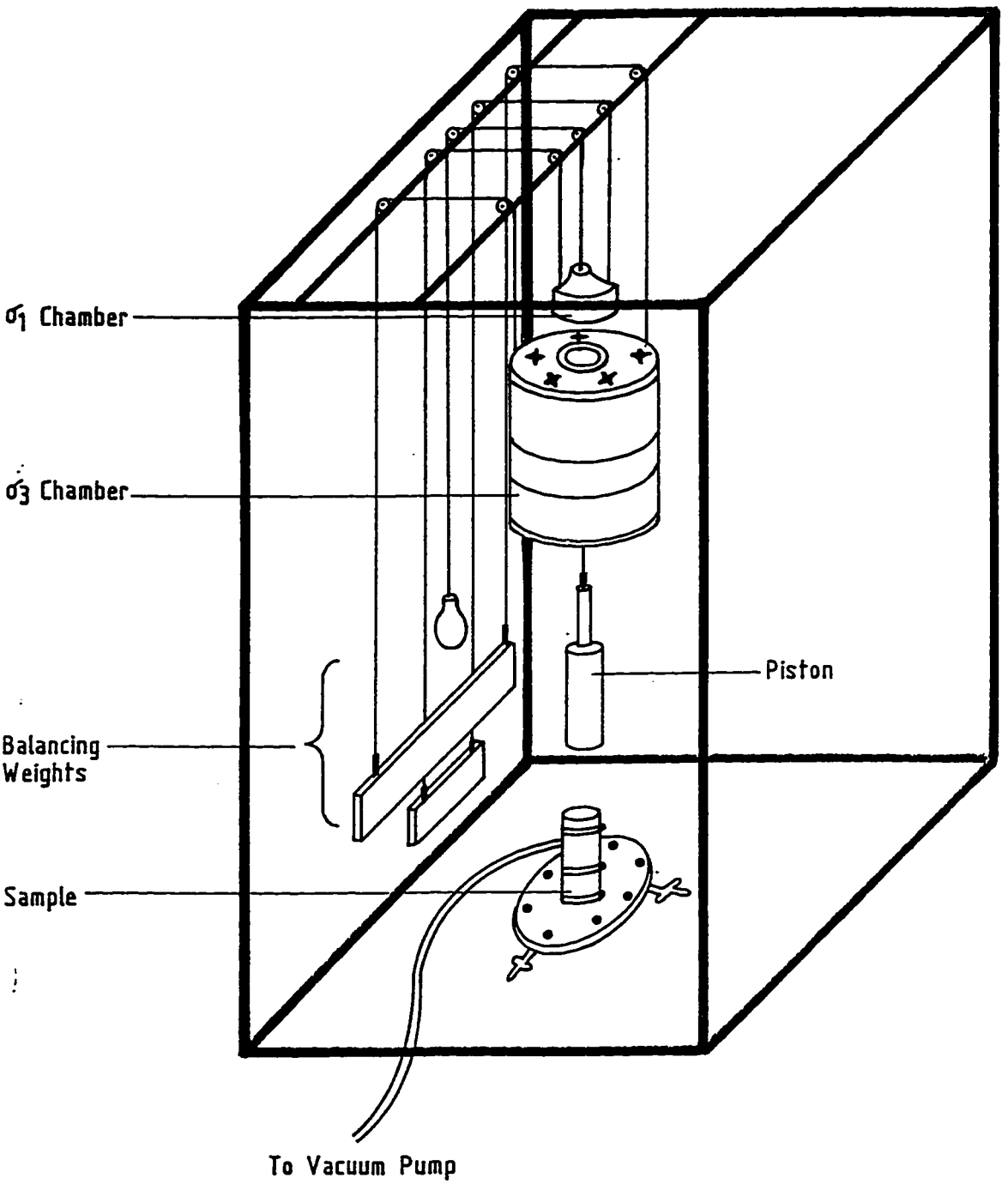

Fig. 4.4 Sample Preparation

a rigid footing. Sand is distributed into the test tank by means of a sand laying machine to achieve a uniform density by controlling the height of fall of sand and the speed of the receptacle. Load cell is fixed on top of the footing so as to measure the amount of load applied. A lever is used in order to apply load. One end of the lever is connected to a load cell, and the other end has a hook on which weights are added. Load is transmitted to the footing through 4 points to simulate uniformly distributed load. The settlement of the footing is measured at 6 points along its length by means of LVDTs. The load cell and LVDTs are connected to portable data logger (Fig.4.5). Detailed description of the test set up will be discussed in the following :

Test Tank

The test tank is made from plexiglass sheets. The plan dimension of the box are 120 cm x 80 cm with a height of 60 cm. This tank is stiffened with vertical and horizontal stiffeners to prevent it from bulging under the load when filled up with sand (Fig.4.5)

Sand Laying Machine

An automatically traversing sand laying machine similar to the machine used previously by the Danish Geotechnical Institute (Stteenfelt, 1973) was constructed at Central Research Workshop at KFUPM. It consists of two parts as shown in Fig.4.5. The upper part consists of two vertical screw spindles from which the receptacle is suspended. The rotation of

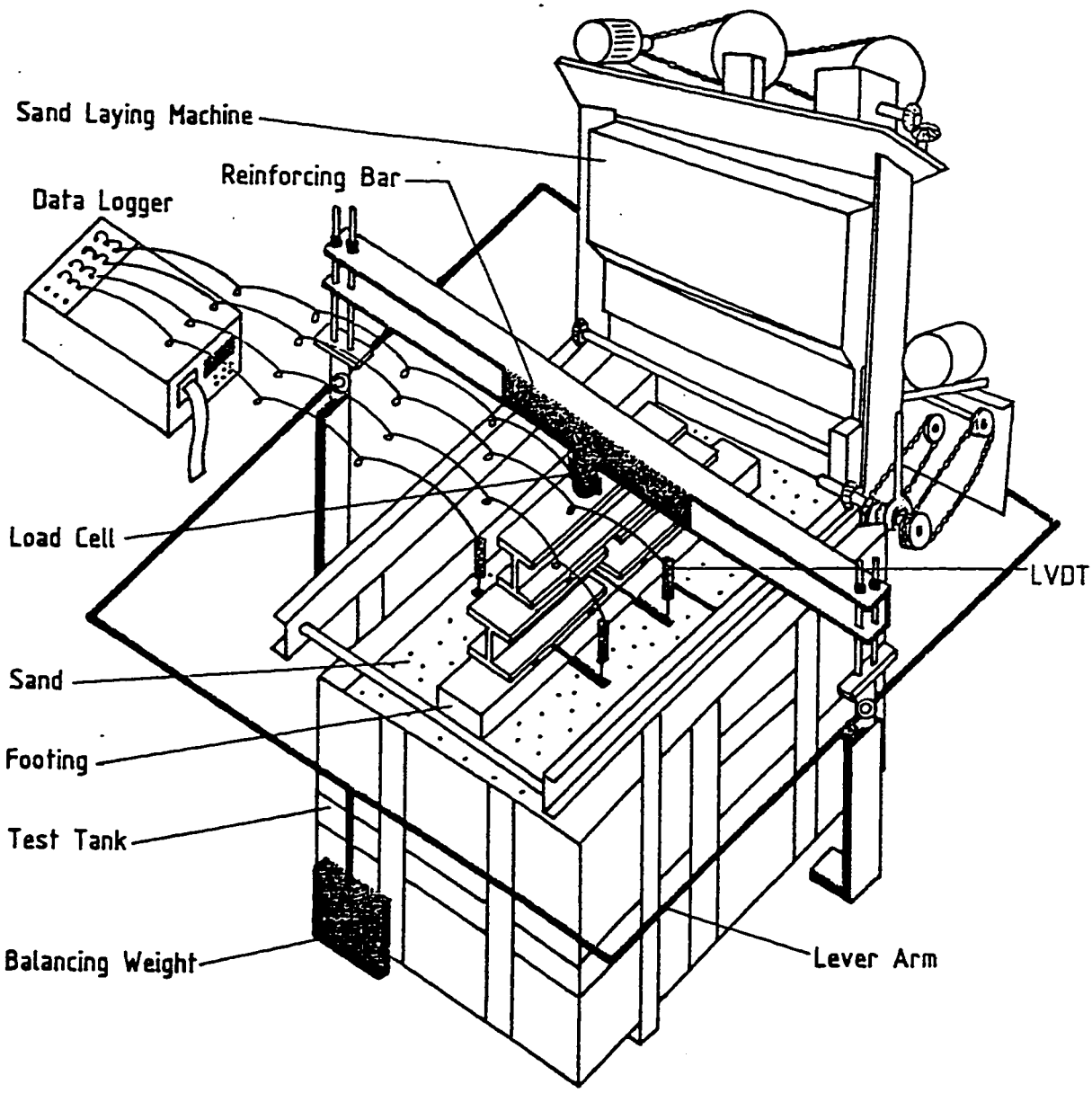

Fig. 4.5. Test Setup for Model Footing.

the screw spindles is produced by an electric motor combined with a gear. The spindle's function is to raise the receptacle automatically as the sand surface raises. The receptacle traverses forwards and backwards on two rails placed along the sides of the test box. It is driven by an electric motor and a gear box. The direction of the traversing is shifted automatically when receptacle reaches the end of the test box. the horizontal traversing speed of the receptacle is about 40 mm/sec, and it is raised at a vertical speed of 0.175 mm/sec. The type of opening used at the receptacle's bottom is a continuous horizontal slot of a 3 mm width at the two ends, and a 2 mm width in the middle. This configuration is adopted in order to minimize the sand heap produced along the middle part of the test box.

Loading Device

Load is applied to the strip footing in a way to simulate uniformly distributed load. A 4-point loading system is used to transmit the load to the top of the footing. A steel arm carries at one end a hook on which the weights are placed, and it rests on the other end on a load cell that transmits the load to the footing. The ratio between the load at the end of the hook and the actual load transmitted to the footing is 1:10. The load is rigestered by the load cell as shown in Fig.4.6.

Strip Model Footing

Model footing was prepared by cutting 50 mm thick steel plate to achieve length/width ration of about 12.

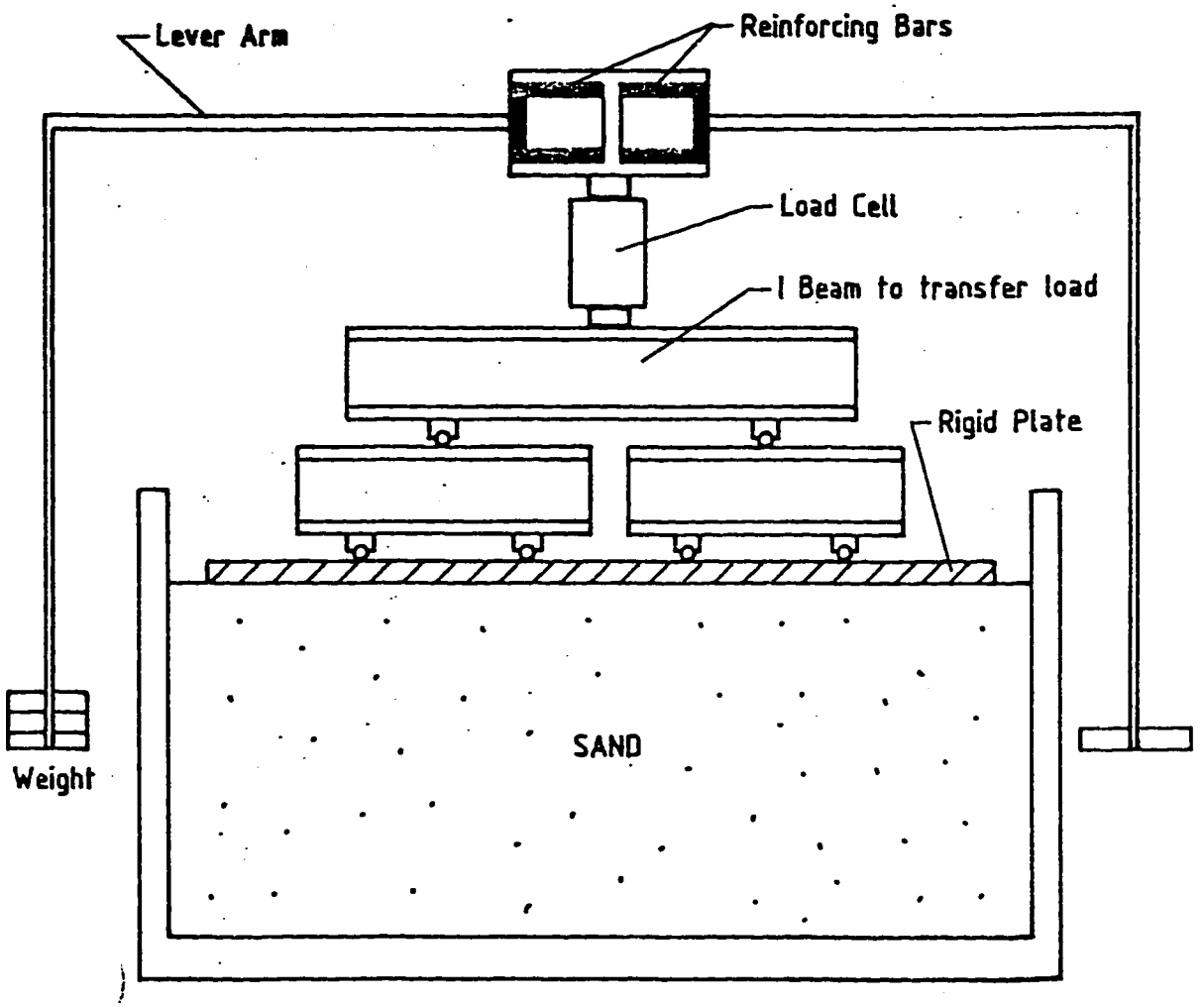

Fig. 4.6.a Side View of the Test Setup.

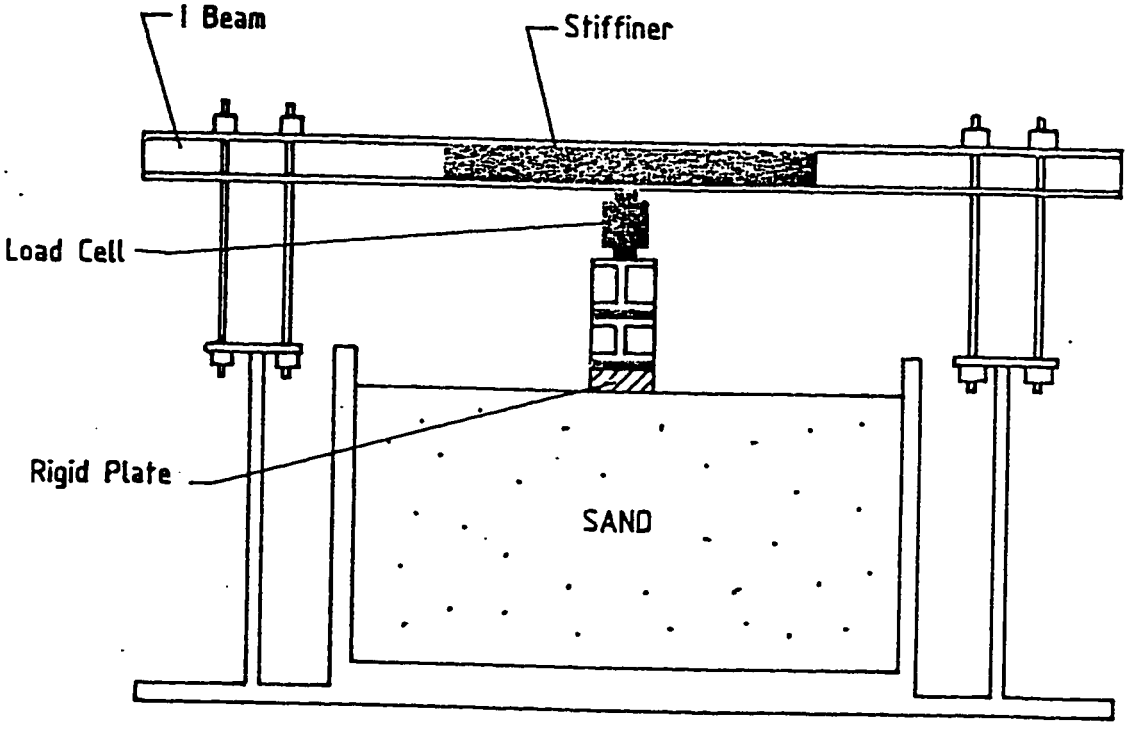

Fig. 4.6.b Front View of Test Setup.

4.4 Test Results :

The following figures represent the triaxial tests conducted on cyclindrical samples. Both stress-strain responses and volumeric change and axial strain responses are shown in the figure (4.7 to 4.22).

Fig's 4.7 and 4.8 represent CTC tests conducted at confining pressures of 69 and 138 KPa respectively. It is clear that sand behaves elastoplastically from the beginning of loading of the two tests. This is a typical behavior of sand, which does not have a well defined elastic region. Furthermore, the figure shows that an icrease in the confining pressure will cause an icrease in the deviatoric stress at failure.

Fig.4.9 represents the first cycle of a cyclic triaxial test at a confining pressure of 69 KPa. When the material is unloaded, it behaves almost elastically untill the axial stress is released. When the direction of loading is reversed plastic deformations accumulate quickly as depicted in the Fig.4.9, which represents the Bauschinger effect. Here the material yielded at a stress level lower than the loading stage. Fig.4.10 represents the full experiment conducted to failure.

Fig.4.10 is replotted with τ_{oct} versus γ^{p}_{oct} (Fig.4.11) C_{α} is the average slope of the initial cycles of unloading and reloading. The list of complete material prameters is shown in table 4.2.

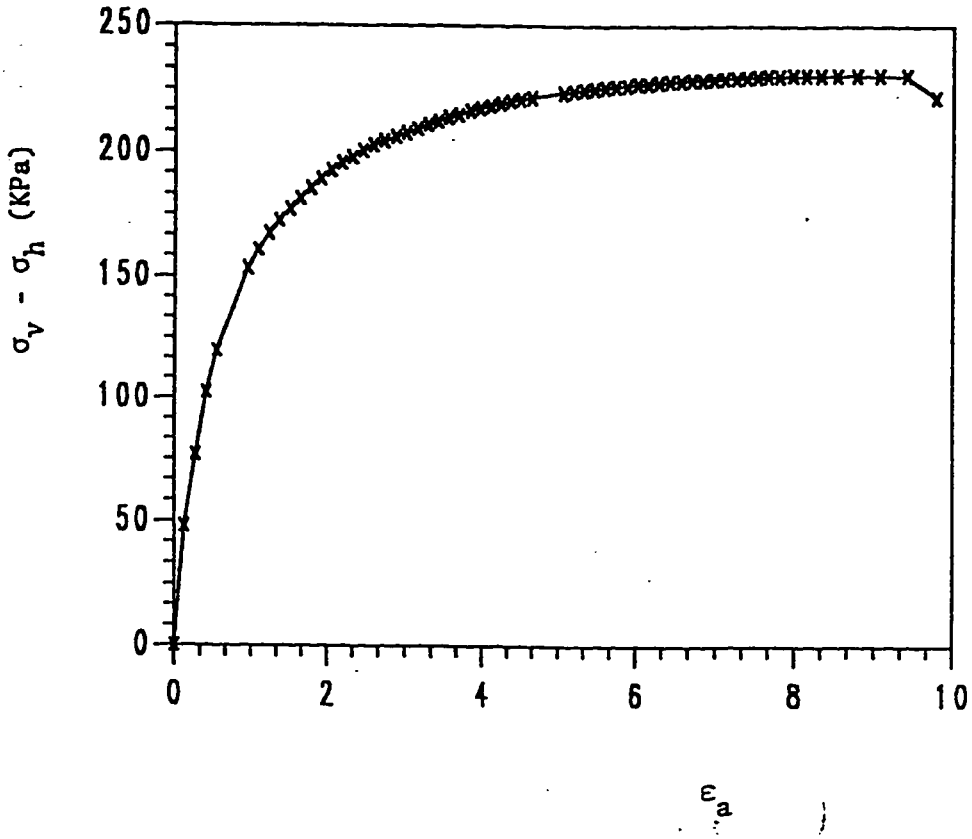

Fig.4.7 CTC test result conducted at confining pressure of 69 KPa (10 psi).

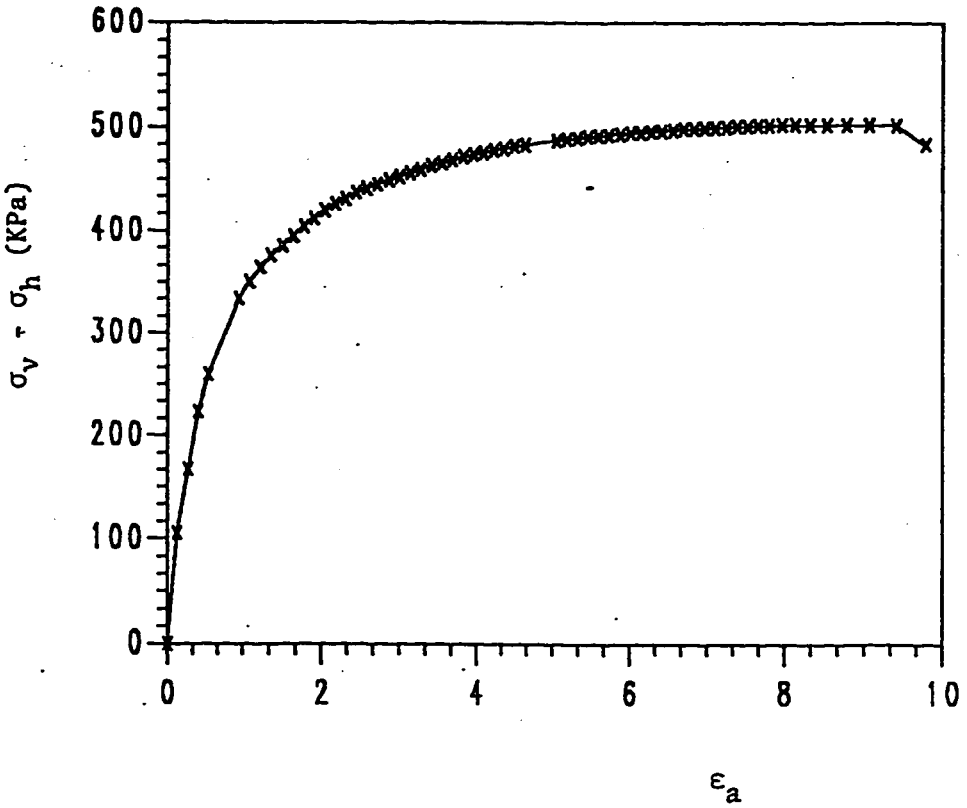

Fig. 4.8 CTC test result conducted at confining pressure of 139 KPa (20 psi).

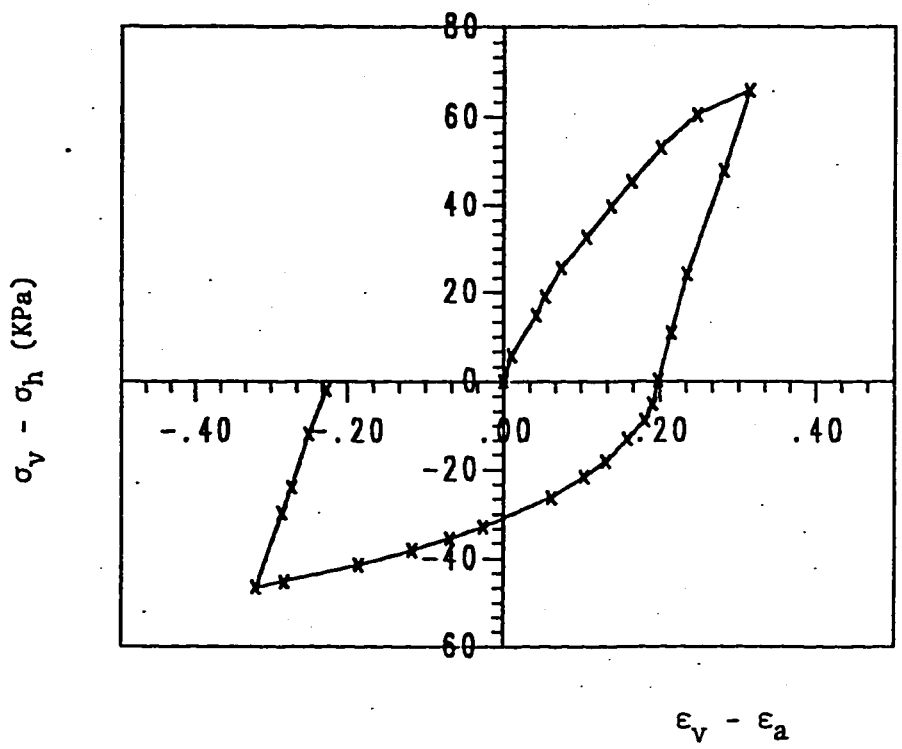

Fig. 4.9 A complete one cycle under one cyclic range, 30% of ultimate (confining pressure = 69 KPa)

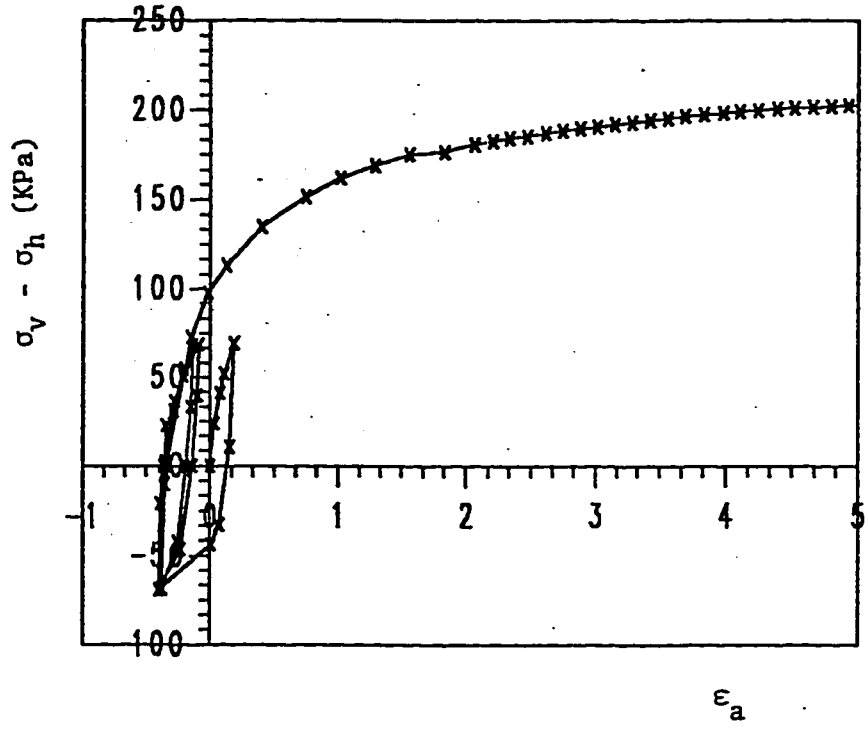

Fig. 4.10 Cyclic triaxial test with 30% cyclic load (confining pressure = 69 KPa)

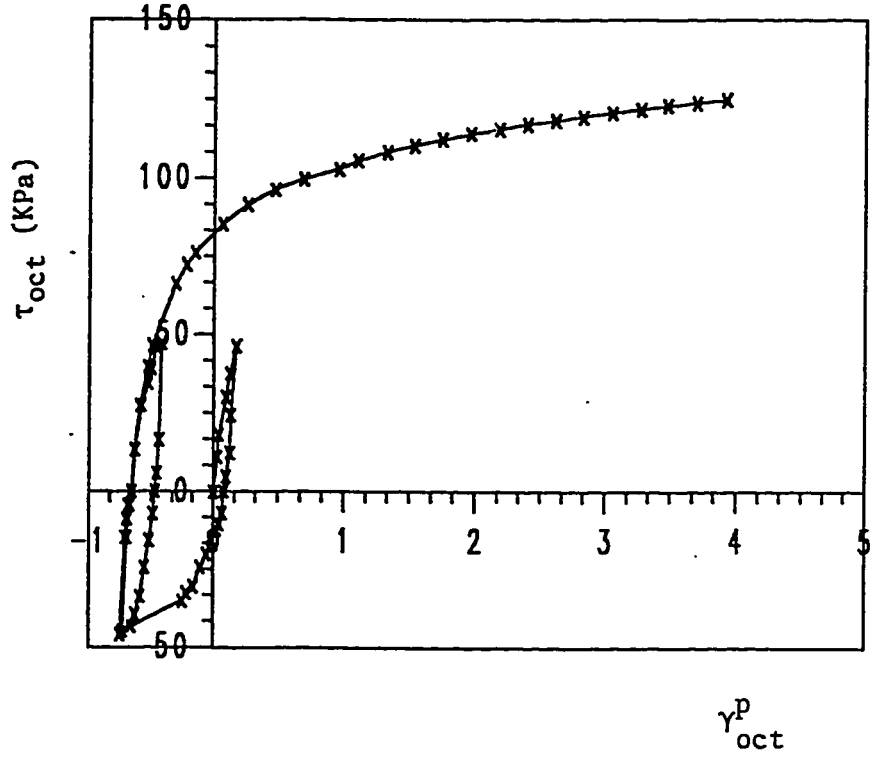

Fig. 4.11 Octahedral shear stress versus plastic octahedral shear strain.

Table 4.2 Material Parameters

Elastic Parameters	E = 3739 + 756.4P (psi) = 25780.4 + 756.4P (KPA)
Failure Surface Parameters	A = 2.5 psi (17.24 KPA) B = 0.004/psi ($5.8x10^{-04}$ *KPA*) M = 0.18 C = 2.5 psi (17.24 KPA) γ = 0.008
Hardening Surface Parameters	D = 0.006/psi ($8.7x10^{-04}$ *KPA*) w = 0.0085 R = 7.00 Z = 0.0
Kinematic Parameter	C_α = 2500(*psi*) (15000 KPA)

In the second type of test,where three different sizes of cycles are considered two phenomena were observed. First, in the second cycle (50%), and while the sample was loaded in the radial direction and before unloading, it failed by necking. This phenomenon, as was described before, is called the bauschinger effect where the sample strength in extension is less than in compression (Fig.4.12). The second phenomenon which was obsereved also, was that the sample can not be loaded to the same level of stress in the two directions. In other words, when the sample is loaded in the axial direction up to a certain value, it should be loaded to a smaller value when loaded in the radial direction. Otherwise, the sample will approach failure if it is loaded to the same level in the radial direction (Fig.4.12). So, in the second test sample during extension will not be loaded up to 50% of ultimate strength, but instead, it is loaded up to about 40% of the ultimate (Fig.4.13).

Finally, a test at a confining pressure of 138 KPa is conducted only for one cyclic load range, which is 30% of the ultimate strength (Fig.'s 4.14,4.15). Similar trend of the stress-strain response is obsereved here.

Fig's 4.16 to 4.20 represent volumetric strain versus axial strain responses of the triaxial tests. Fig.4.16 represents the volumetric behavior of the soil under CTC test. The material first contracts up to some value, then it expands untill the material failes. Fig.4.17 represents the initial portion of the cyclic triaxial test conducted with 30% cycles. A close view of the cycles is shown in Fig.4.18. Here, the voumetric behavior of the

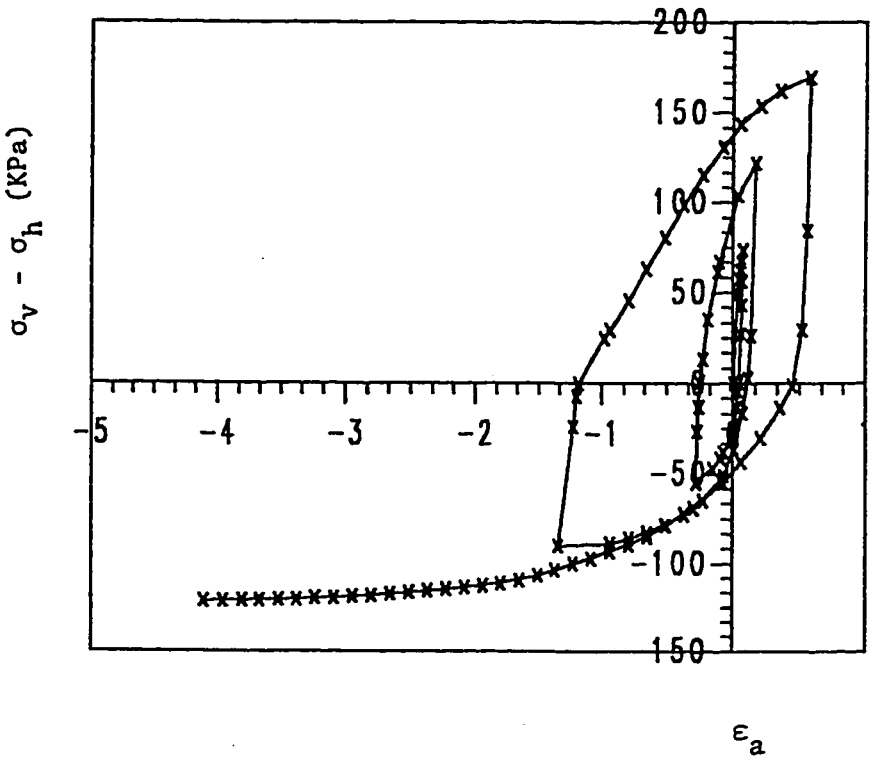

Fig. 4.12 Cyclic triaxial test results with 30, 50 and 70% of ultimate cyclic range. (confining pressure = 69 KPa)

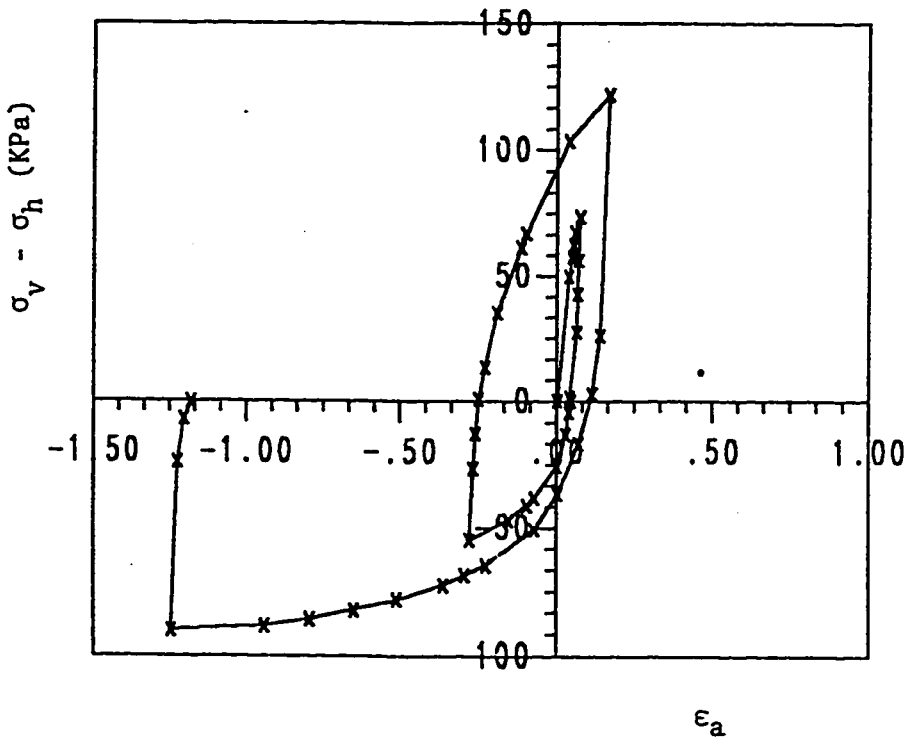

Fig. 4.13 Loading the sample with 30% and 50% cyclic loads in compression; and 30% and 40% cyclic loads in extension (confining pressure = 10 psi)

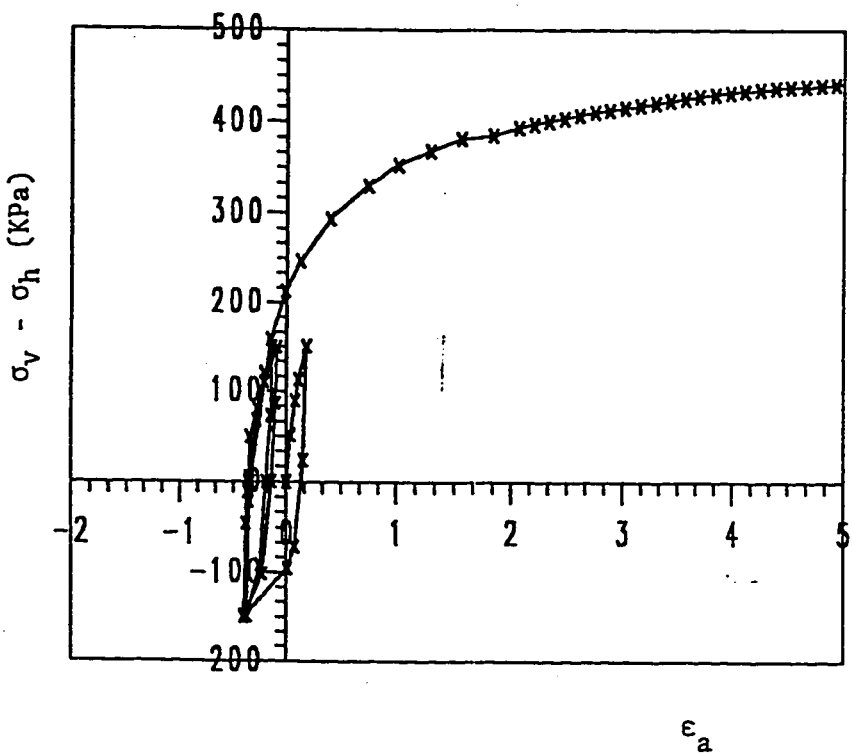

Fig. 4.14 Cyclic triaxial test conducted with 30% cyclic load (confining pressure 139 KPa).

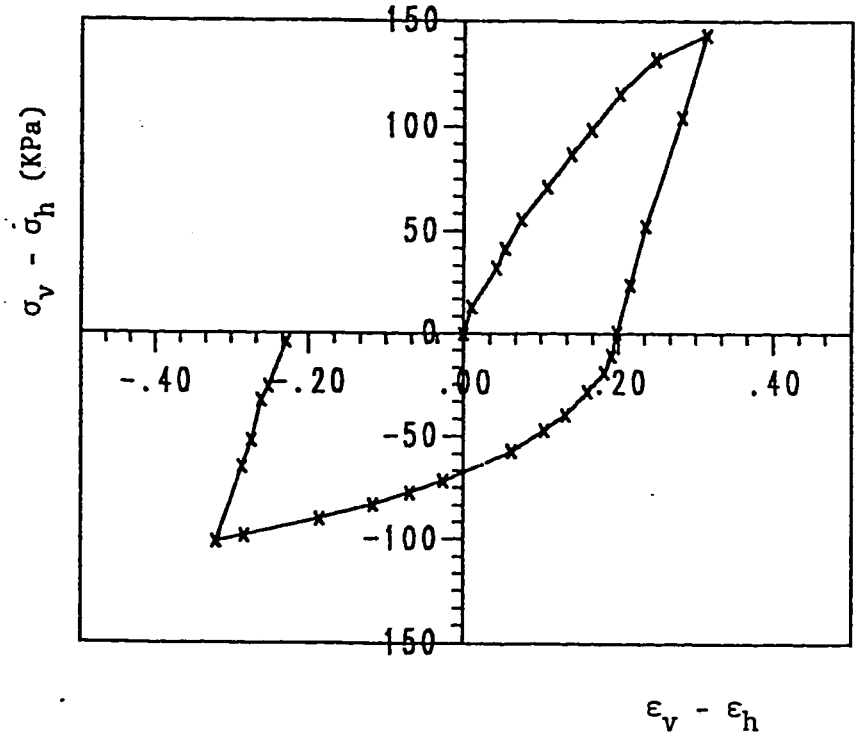

Fig. 4.15 The first cycle of the cyclic triaxial test conducted with 30% cyclic load (confining pressure = 139 (KPa).

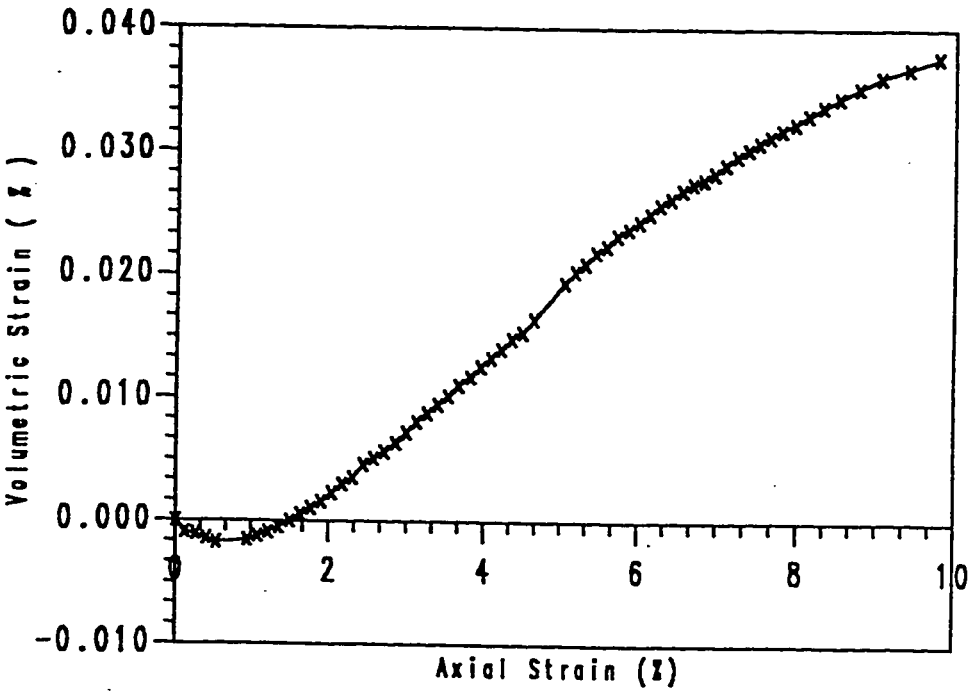

Fig. 4.16 Volumetric behavior of CTC test at a confining pressure of 10 psi (69 KPa).

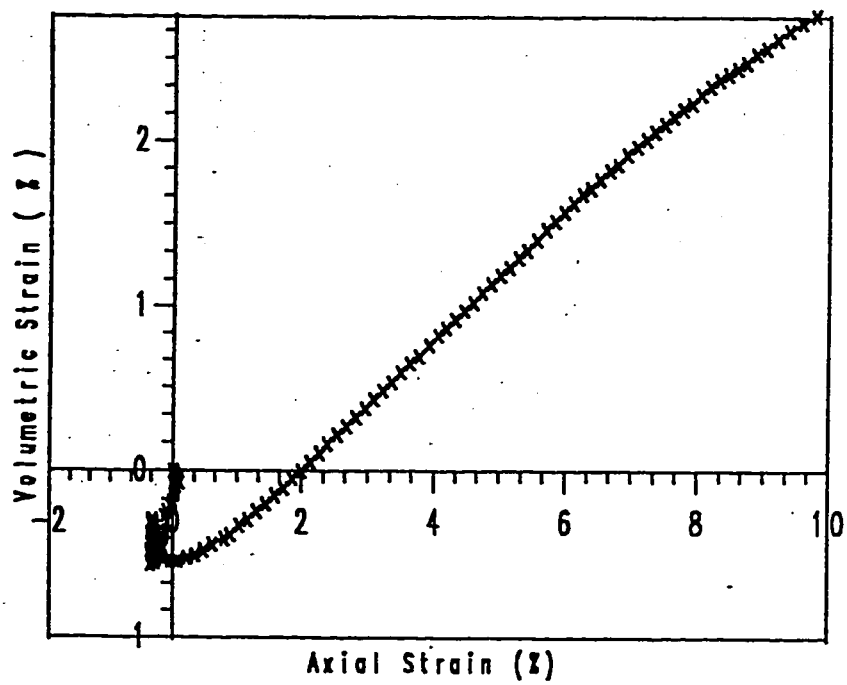

Fig.4. 17 volumetric behavior of cyclic triaxial test conducted with 30% cyclic load.

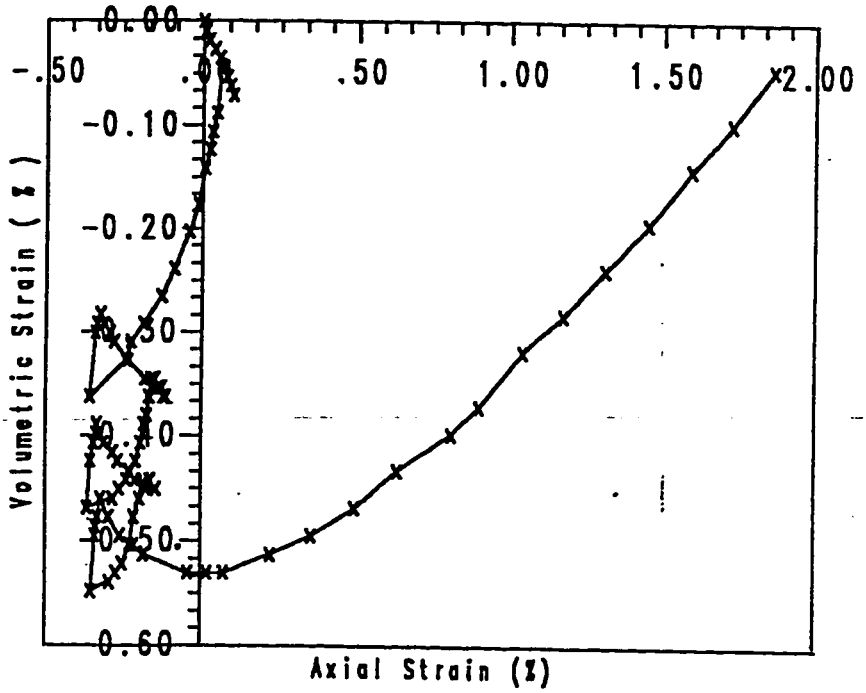

Fig.4.18 A close view of the volumetric behavior of the first 4 cycles of the 30% cyclic load.

material alters between contraction (upon loaded axially or radially) and recovering part of the strain (upon unloading). This process is repeated in the four cycles. Fig.4.19 represents the volumetric behavior of the cyclic triaxial test with 30%, 50% and 70% cycles (in compression). A close study of the curve is presented in Fig.4.20. The behavior of the material in the 30% cycle is similar to what presented earlier. However, when the material is loaded in the radial direction it recovers some of the volumetric strain, then, it expands untill it is unloaded again where it conctracts. Similar behavior is depicted in the next cycle. Finally, the material expands untill it fails.

Fig.4.21 represents the static load-deformation curve of the model footing. Fig.4.22 represents the cyclic loading of the footing. It is observed that the material deforms elasto-plastically at the beginning of loading. As a result, the sand does not return to its origingal possition when the model footing is unloaded. Upon reloading sand again behaves elasto-plastically and this is clear in the open loops. Three cycles of unloading and reloading are conducted to see the effect of kinematic hardening on the behavior of sand.

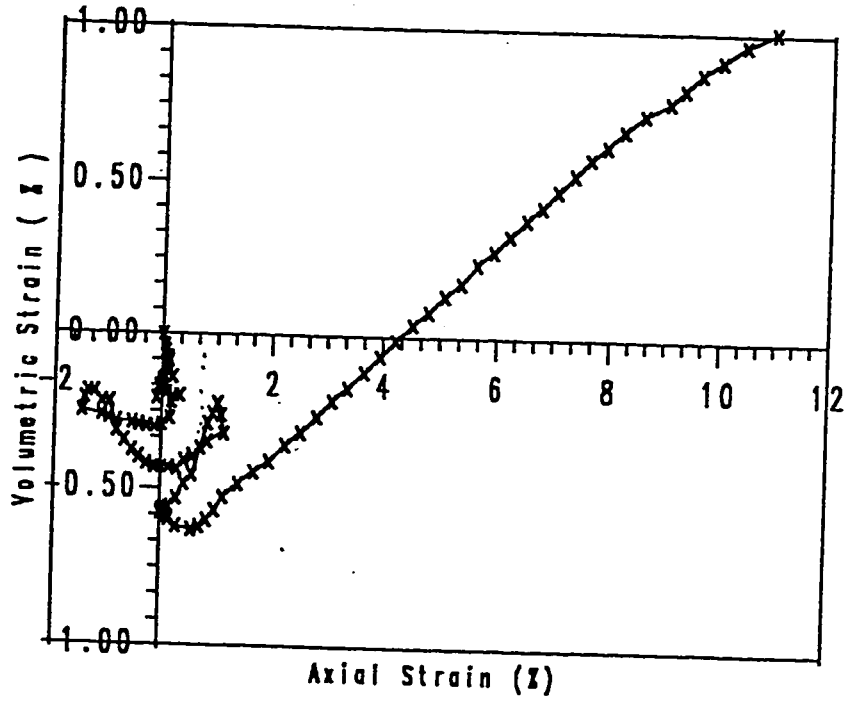

Fig. 4. 19 Volumetric behavior of the cyclic triaxial test conducted with 30%, 50% and 70% cyclic loads (in compression).

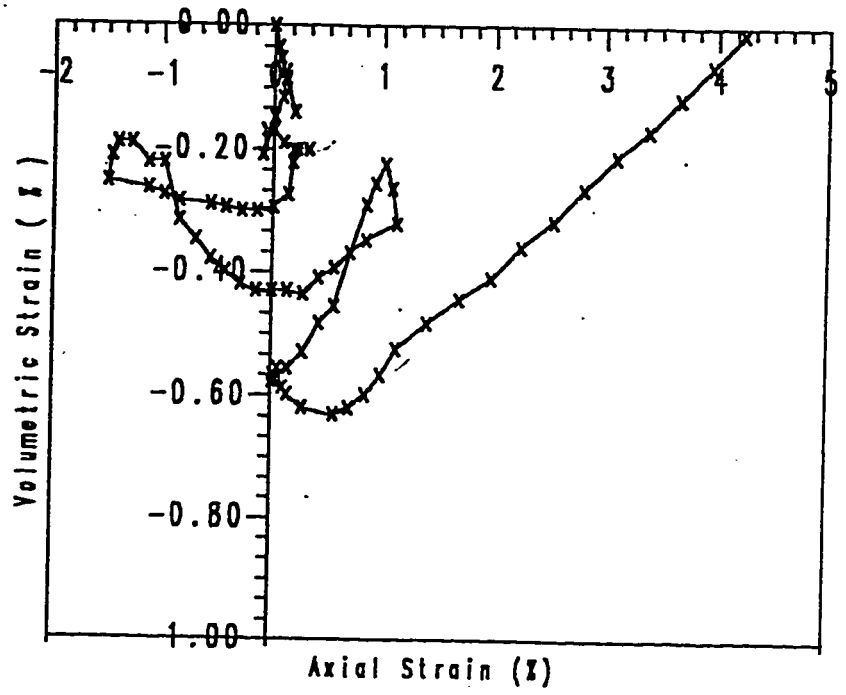

Fig.4.20 A close view of the three cycles (30%, 50% and 70%) (confining pressure = 69 KPa)

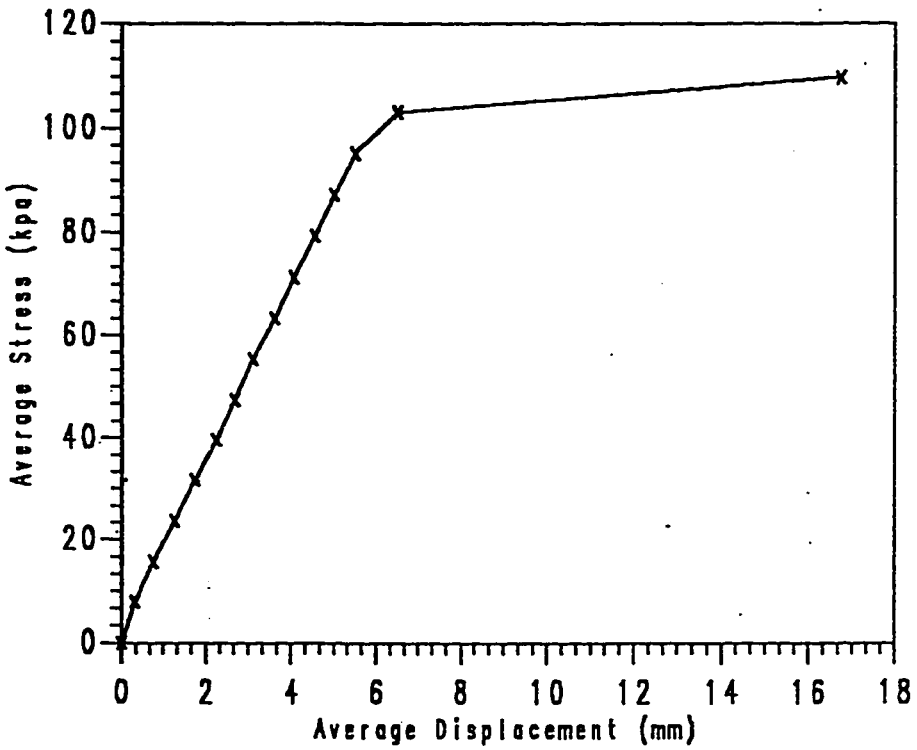

Fig.4.21 static load-displacement curve of the model footing.

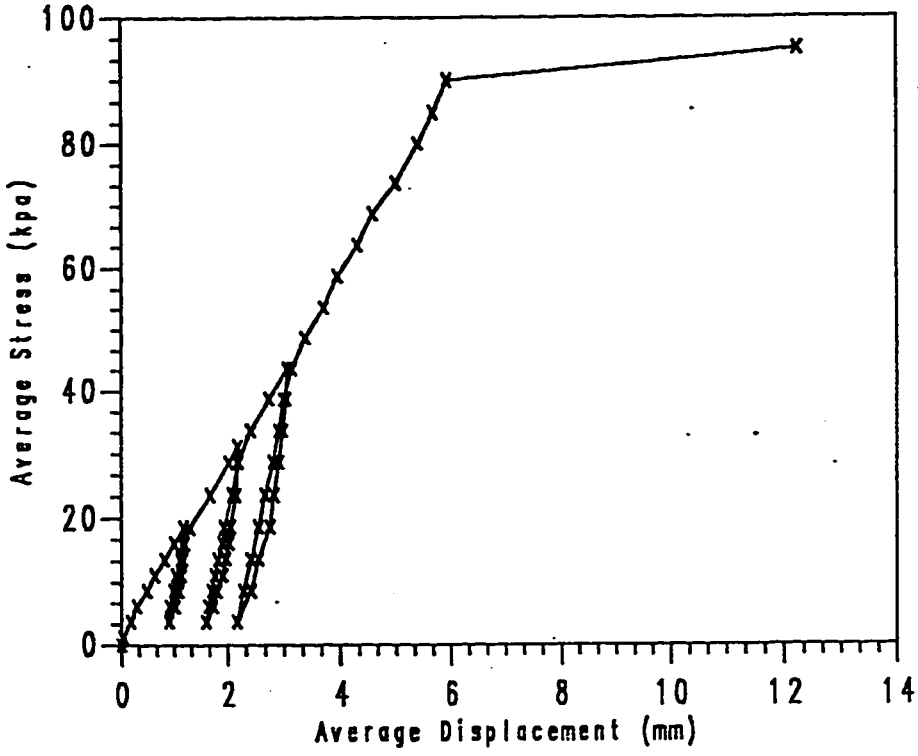

Fig.4..22 Cyclic load-displacement curve of the model footing.

CHAPTER 5

BACKPREDICTION OF THE CYCLIC TRIAXIAL TEST RESULTS AND NUMERICAL IMPLEMENTATION OF THE COMBINED HARDENING CAP MODEL

5.1 INTRODUCTION

This chapter discusses two parts : a) using the combined hardening cap model in a computer code to backpredicts the cyclic triaxial tests; b) implementing the model into a finite element code to solve the boundary value problem of the model strip footing which rests on the surface of dry sand. The same parameters that are used in the backprediction part will be used in the finite element code. Finally, discussion of the results in both parts will be considered and comparison between the theoritical and experimental results will be made.

5.2 BACK PREDICTION

The exteded three invariant-dependent cap model is used to backpredict the expremintal results of cyclic triaxial tests, discussed in chapter 4. A comparison between the experimental and the predicted results will be done to verify the validity of the model and the accuracy of its parameters. Total strain is divided into a number of increments. Accuracy of the model depends on the size of the increments. The smaller the increments are, the better the results will be. Stress increments can be determined by using Eq.2.1. Stress state is updated using the following equation :

$$\{\sigma\} = \int\{d\sigma\} \qquad 5.1$$

The integration in Eq.5.1 can be converted into summation as followed

$$\{\sigma\} = \{\sigma_o\} + \sum_{i=1}^{N}[C]_{i-1}^{e-p}\{d\varepsilon_i\} \qquad 5.2$$

where

$\{\sigma_o\}$: initial state of stress.

$[D]_{i-1}^{e-p}$: the (i-1) constitutive elasto-plastic matrix.

This procedure will develope a stress-strain response as shown in Fig.5.1. It is clear that there is a big difference between the experimental and predicted results due to the large size of the increments. The difference between the simulated and actual curves can be minimized by dividing each increment into smaller sub-increments over which the

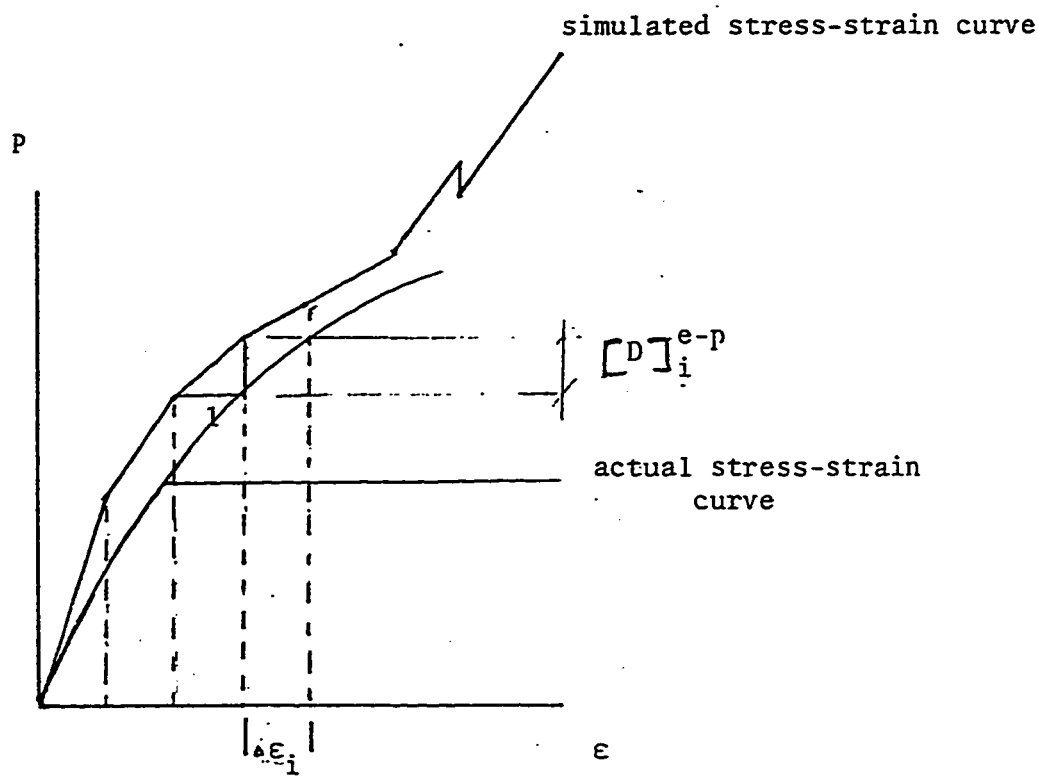

Fig.5.1 Simulated Stress-Strain Curve Using Incremental Technique.

elasto-plastic matrix is assumed constant (Faruque and Desai, 1985). Here, strain increment is divided into a number of sub-increments (N_s), with the size of the sub-increment $\{\Delta(\Delta\varepsilon)\}$ is $\{\Delta\varepsilon\}/N_s$. The error encountered by this approximation is a direct function of the subincrement and can be made negligible by using the following prescribed small number

$$\max|\{\Delta(\Delta\varepsilon)\}| \leq 0.0005 \qquad 5.3$$

Using that criterion, the elasto-plastic matrix $[C]^{e\text{-}p}$ can now be assumed to be constant over the subincrement, and it is updated at the end of each subincrement. Equation 5.2 can be rewritten as :

$$\{\sigma\} = \{\sigma_o\} + \sum_{i=1}^{N} \{\Delta\sigma_i\} = \{\sigma_o\} + \sum_{i=1}^{N} \sum_{j=1}^{N_s} [C^{e\text{-}p}]_{j-1}^{i} \{\Delta(\Delta\varepsilon)\}_j \qquad 5.4$$

As shown in Fig.5.2, the results obtained using this technique are better and closer to the experimental data.

Equation 5.4 is used for a strain control test, but, it can be rewritten to determine strain increments when stress increments are given as follows :

$$\{\varepsilon\} = \sum_{i=1}^{N} \{\Delta\varepsilon_i\} = \sum_{i=1}^{N} \sum_{j=1}^{N_s} ([C^{e\text{-}p}]_{j-1}^{i})^{-1} \{\Delta(\Delta\sigma)\}_j \qquad 5.5$$

5.2.1 Discussion of Model Predictions

The combined hardening cap model is used to backpredict th experimental results discussed in chapetr 4. Figures 5.3 through 5.6 show a comparison between the experimental and theoritical results. Good agreements

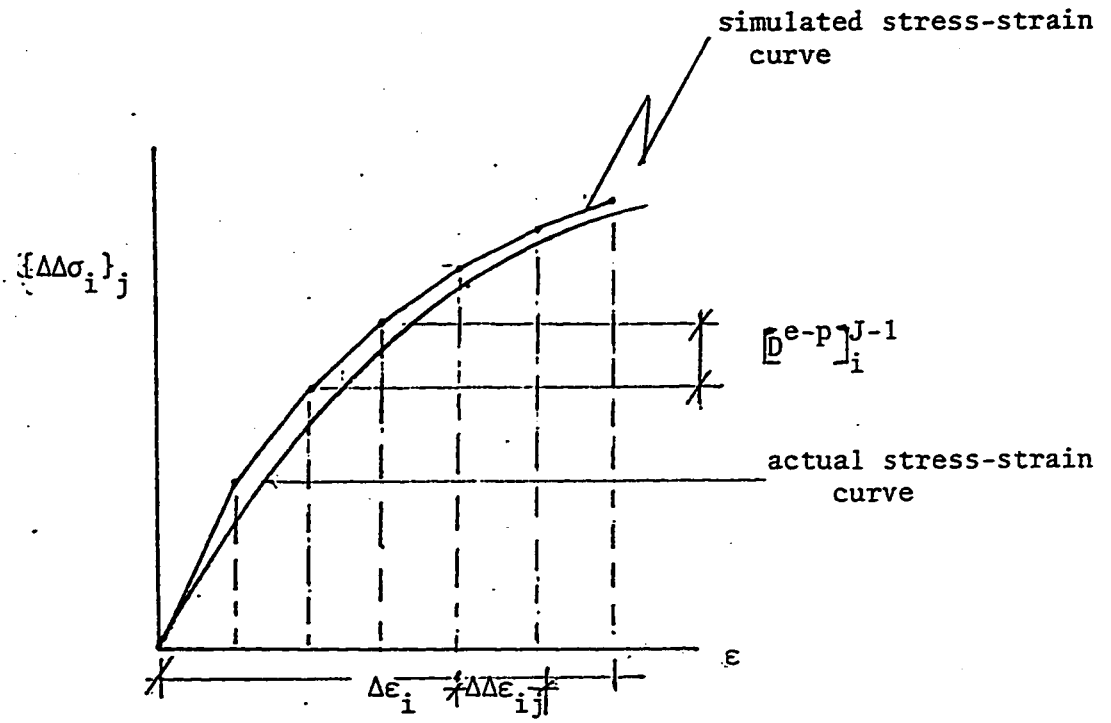

Fig.5.2 Subincrementation Technique.

are observed between the experimental and theoritical results in the first half cycle (loading). In addition, the model shows good simulation in the second half of the cycle (reverse loading), with small diversion from the experimental curve after the material yields. This diversion may be related to using a linear kinematic hardening rule which is an approximation of the real behavior of soil. Actual behavior can be obtained by using a non-linear kinematic hardening rule (Chen, 1982). The results of the model are still comparable with the experimental results. To see the effect of kinematic hardening on the material, more cycles have been applied through the model and the difference between the output of the model and the experimental results is still small, and so, the model predicts the experimental results successfully. The effect of the introduced kinematic parameter α is clear in the stress-strain response when the material yields, which is better than the isotropic cap model when it is used to backpredict reverse loadings, since the isotropic models overpredicts the stress-strain behavior (Fig.5.7)

Fig.5.8 represents a comparison between the predicted volumetric change behavior and experimental one for the cyclic loading. As seen the combined hardening model could predict the cyclic behavior of the volumetric change in a good manner. The differences here might be due to the way of measuring the volumetric change in the lab. However the difference as seen is small.

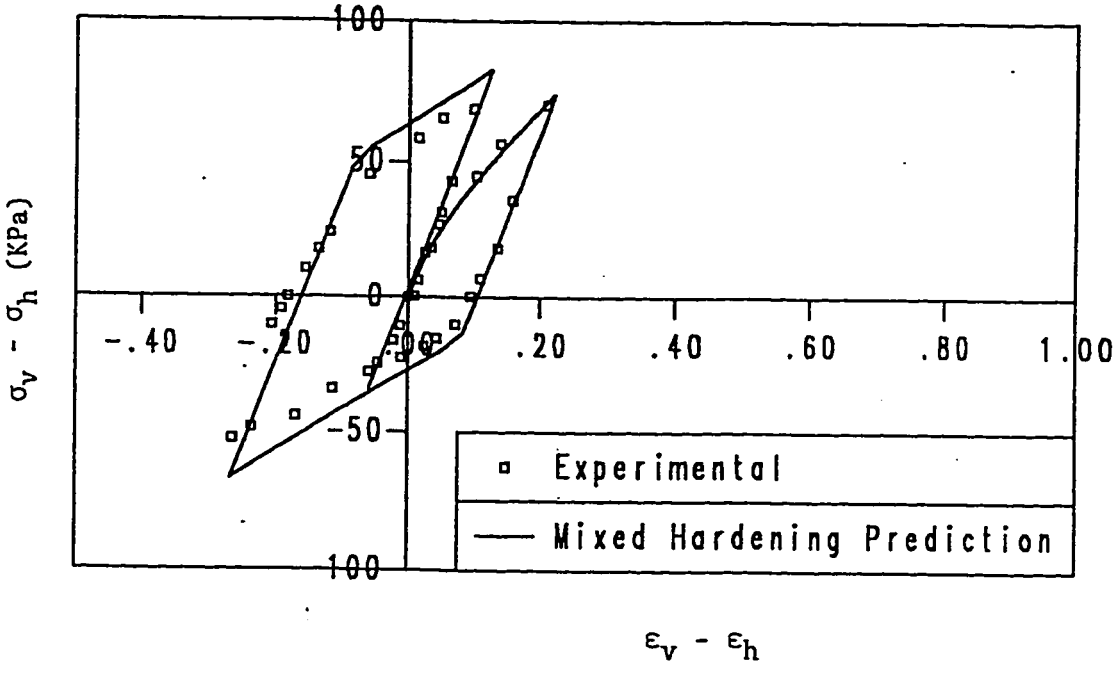

Fig. 5.3 Prediction of two cycles with 30% cyclic load (confining pressure = 69 KPa)

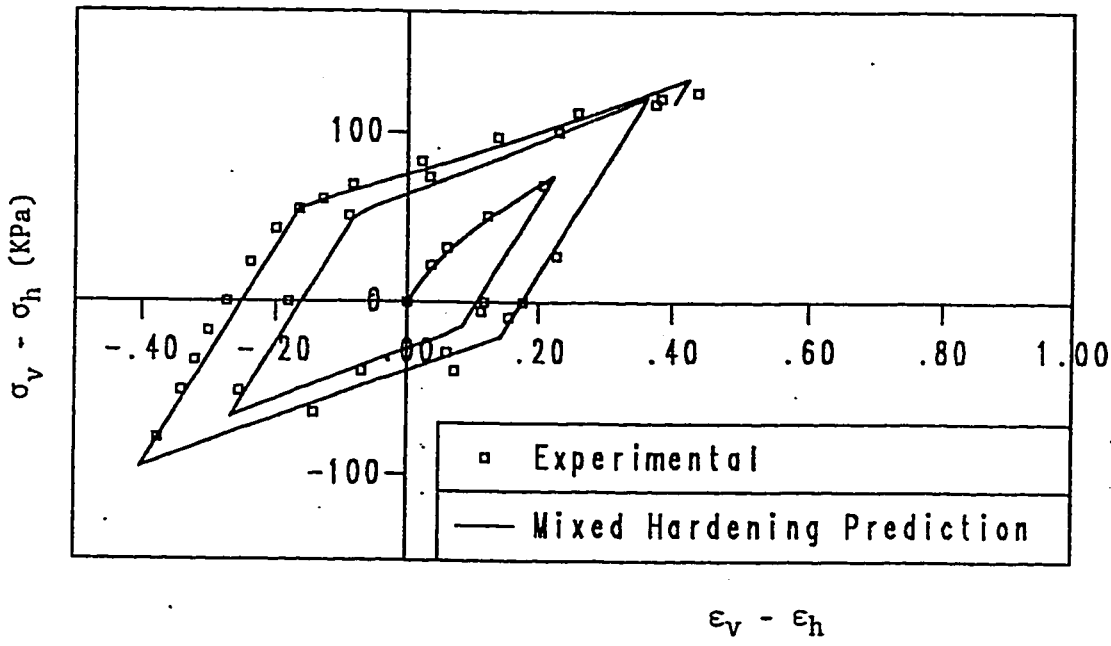

Fig. 5.4 Prediction of 30%, 50% and 70% cyclic loads test (confining pressure = 69 KPa)

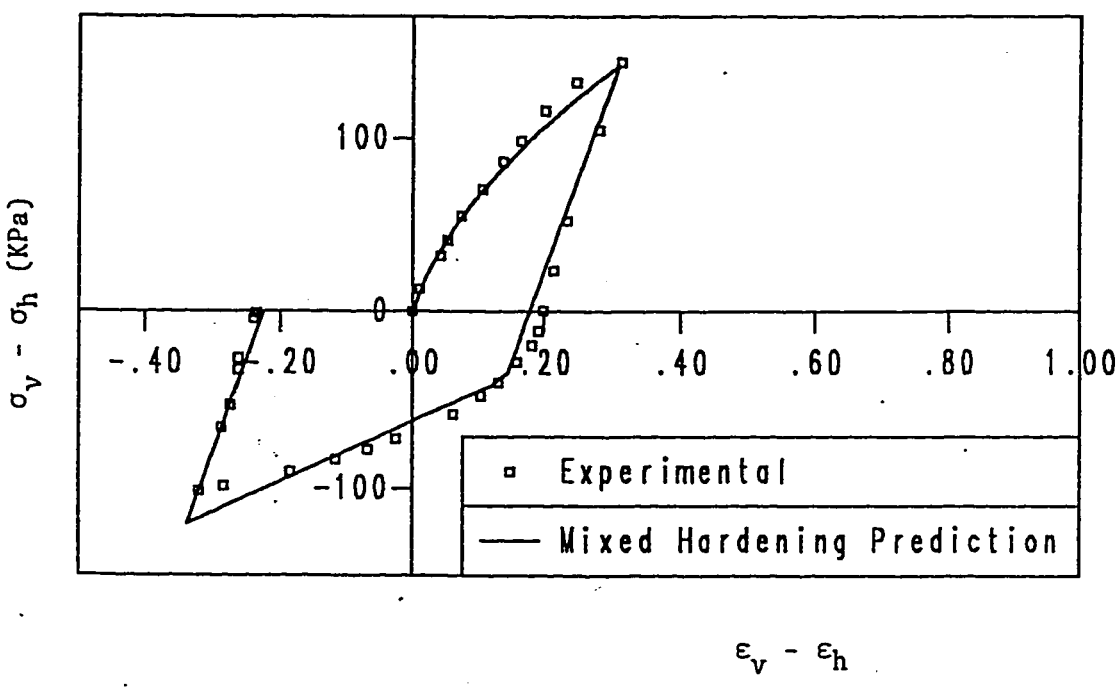

Fig. 5.5 Prediction of the ist cycle of 30% cyclic load test (confining pressure = 139 KPa)

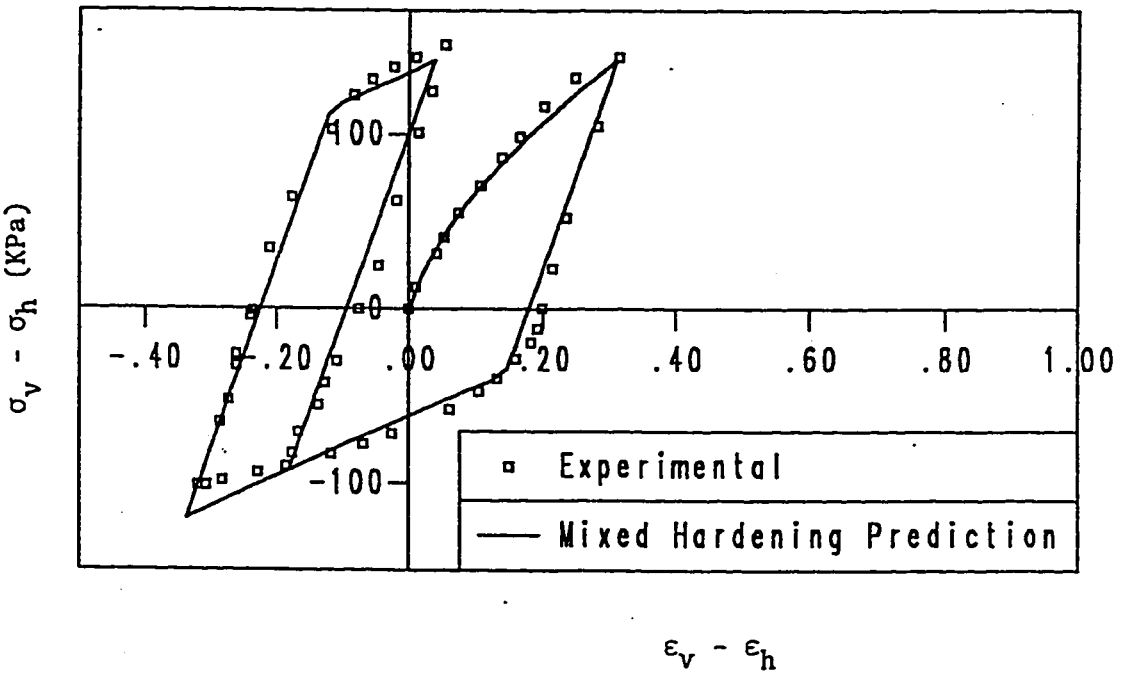

Fig. 5.6 Prediction of two cycles with 30% cyclic load test (confining pressure = 139 KPa)

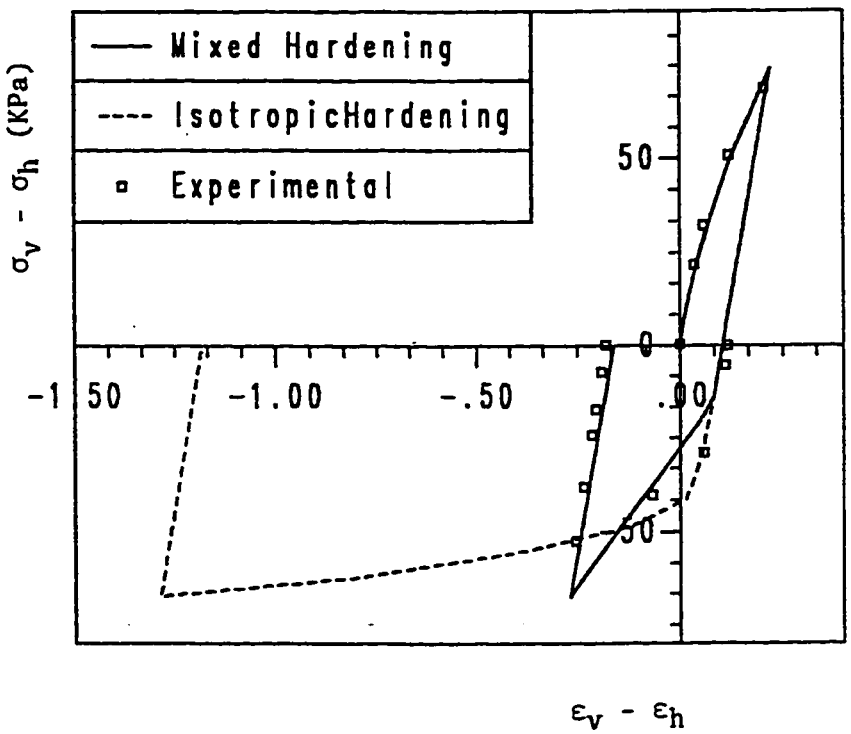

Fig. 5.7 One cycle of loading and unloading in the axial and reverse directions respectively.

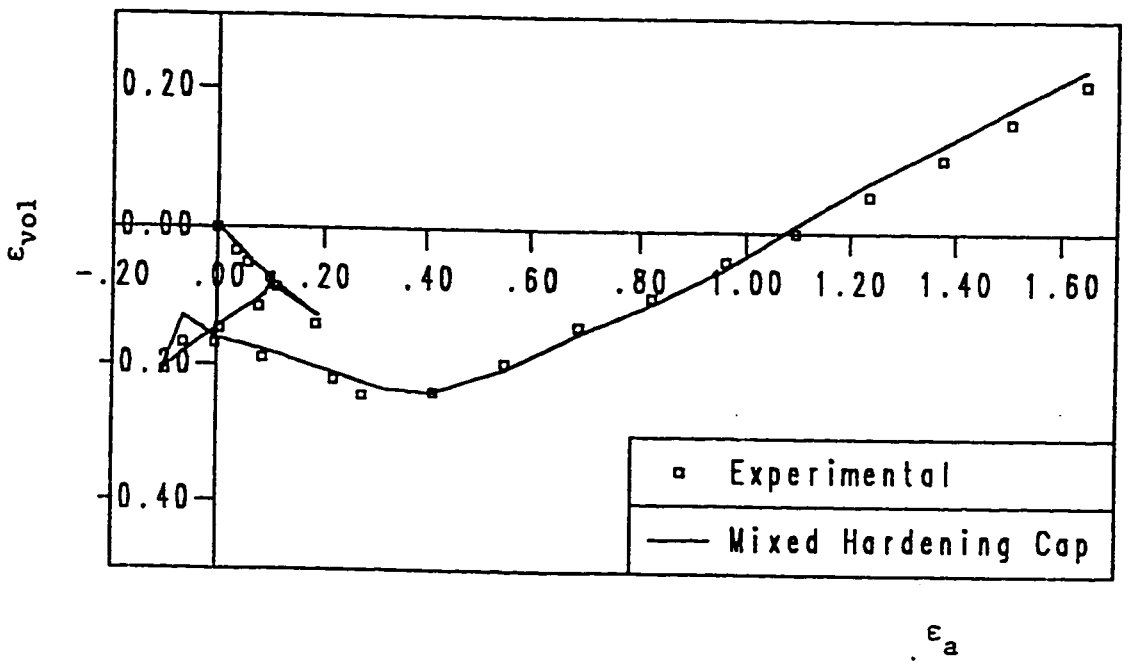

Fig. 5.8 Prediction of the volumetric behavior with two cycles (confining pressure = 69 KPa).

The three invariant dependent combined hardening cap model thus predicts the cyclic stress-strain behavior of Dhahran dune sand under different confining pressures.

5.3 IMPLEMENTATION OF THE CAP MODEL INTO A FINITE ELEMENT CODE

The combined hardening cap model is implemented into a finite element code to solve a problem of rigid strip footing resting on the surface of dry sand. The load-deformation output of the FEM code will be compared with the experimental results. The FEM code, MICROFEM, is originally developed at the university of Colorado, Boulder. Many researchers have contributed in writting this code such as Day, S., E., 1985; Abdul Jauwad, S. N., 1985; Ghamedy, H. N, 1986, Azeemuddin, 1988. This program is modified to include the combined hardening third invariant dependent cap model. Only outline of the FEM algorithm will be discussed here without detailed descriptions. The reader can refer to text books concerned with FEM, such as Desai and Abel (1972), Zienkiewicz(1977),Owen and Hinton (1980) for detailed information.

5.3.1 Program MICROFEM

MICROFEM code is a powerfull program in terms of its arctecture and easyness that enable the user to make use of it in different subjects. The user can easily incorporate his constitutive model in the program.
The main features of the program are :

1. expandability

2. careful accounting of storage use, and

3. portability

MICROFEM makes use of an element and material library strategy which classifies each run of the program on several levels. These classifications include :

1. element type

2. loading type

3. material type

1. Element Type :

Finite element method divides (discritizes) the area under concern into smaller areas called elements. There are many kinds of elements like :

a. 4 node quadrilateral element(Lagrange family).

b. 2 node bar element.

c. 9 node quadrilateral element(Lagrange family).

d. 2,3, or 4 node layered curved beam element(Lagrange family).

e. plate elements.

2. Loading Type :

Several plane conditions are concernd here :

a. plane stress

b. plane strain

c. axisymmetry, and

d. two dimensional Timoshenko beam.

3. Material Type :

Several models exist for different types of materials and response :

a. linear elastic

b. elastic cracking using smeared cracking approach

c. viscoplastic

d. bi-linear softening(softening cracking material).

e. elasto-plastic: softening concrete plasticity model(Day, S. E., 1985)

f. bounding surface plasticity model for soils (Abduljauwad, S. N., 1985)

g. elasto-plastic, ductile and brittle material models: (Ghamdedy, H. N., 1986) which includes:

i. Maximum normal stress

ii. Von-Mises

iii. Tresca

iv. Drucker-Prager with stress and strain cut-offs.

v. Mohr-Coulomb with stress and strain cut-offs.

vi. Independent hardening/softening models.

e. Three-stress invariant dependent cap model (Farouque M. O., Azeemuddin M., 1988).

The non-linear solution techniques incorporate an incremental-iterative solution strategy with a choice from several types of updating stiffness matrix, like :

1. Initial stiffness method
2. Tangential stiffness or Newton-Raphson method
3. Forward-Euler method (updates stiffnes matrix at the start of each increment of load).

Convergence norms are available in two forms :

1. load norm
2. displacement norm.

There are two ways to give data to the MICROFEM. Either by preparing a standard data file and let the program read it, or by an interactive way. The interactive way enables the user to change the load step and number of iterations when necessary (non-linear solutions).

5.3.2 Non Linear Solution Technique

Several techniques are available for solving non-linear problems using finite element method. The method used here is called "incremental-iterative procedure". The applied load is divided into small increments. Inside each increment iterations are performed to satisfy equilibrium. Several strategies are available for the process of iterations. They include Newton-Raphson method and intial stifness method (Fig.'s 5.9 and 5.10).

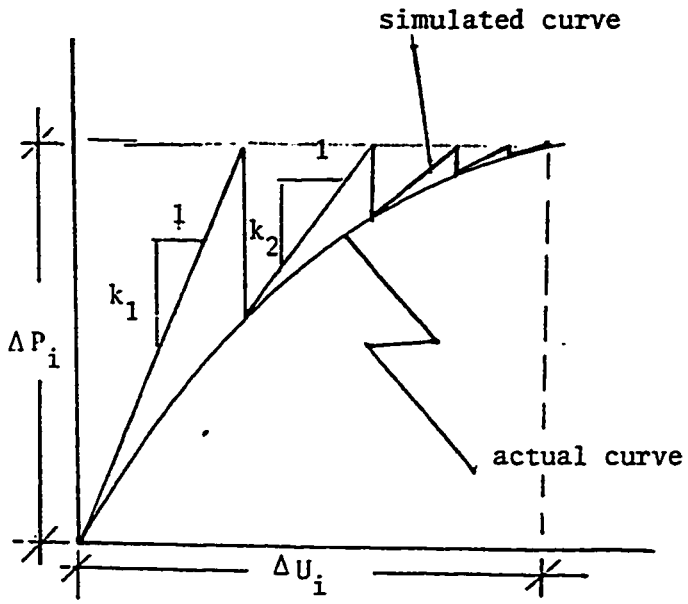

Fig.5.9 Neowton's Raphson's Method

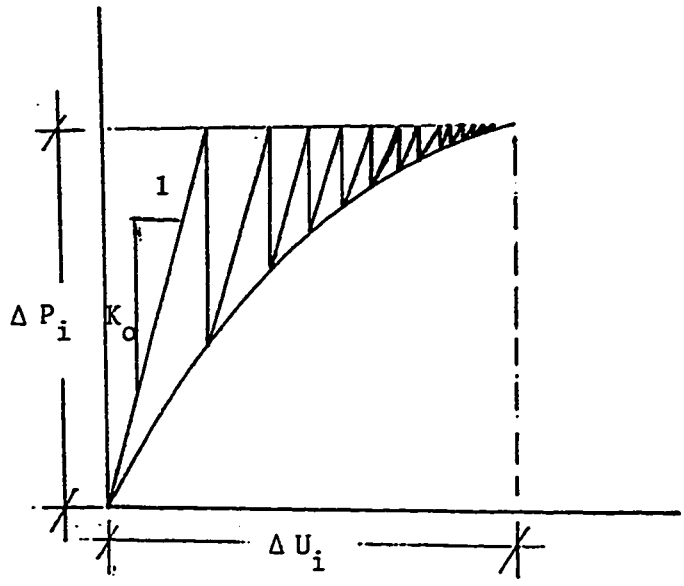

Fig. 5.10 Initial tangential Method

The Newton-Raphson or the tangential stiffness method is most commonly used, because it speeds up convergence. It involves recalculation of the stiffness matrix at the beginnig of every iteration, with the reference point being updated using the residual load (Fig.5.9).

Although the method of Newton-Raphson converges rapidly, it takes long computer time to recalculate the stiffness every iteration. So, a "modified iterative technique" has been propsed which utilizes only the initial stiffness $[K_o]$ (Fig.5.10). Number of iterations here is greater for the same converging tolerance than the Newton-Raphson method, but it saves computer time as it is not necessary to recompute the stiffness for every iteration.

In the present work, the initial stiffness method is used, where the steffness is calculated only at the beginning of every increment and the same is used for subsequent iteration in that increment of load (Fig 5.11).

5.3.3 Numerical Implementation of The Extended Cap Model :

The original three-stress invariant dependent cap model is already incorporated into the MICROFEM code by Azeemuddin, (1988). In this studey, only necessary modifications of the implemented cap model are added to make the program work for combined hardening rule.

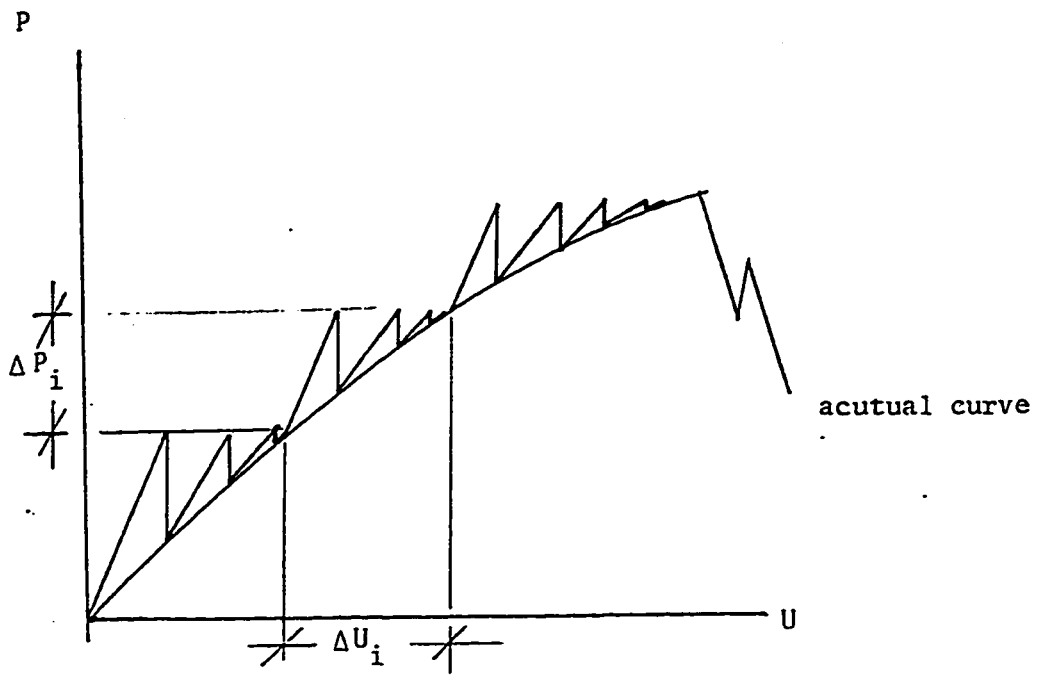

Fig.5.11 Incremental Iterative Technique

Procedure for Implementing the Model into MICROFEM :

When a strain increment is applied, different stress paths may result (Fig.5.11). So, the new state of stress should be checked to know the correct stress path. Then, necessray computations will be performed accordingly. So, a trial state of stress $\{\sigma^t\}$ corresponds to $\{\Delta\varepsilon^{n+1}\}$ is computed using the elasto-plstic matrix $[D_{ep}]$ (or the elastic matrix if the previous state was in the elastic sregion) at the point n.

$$\{\Delta\sigma^t\} = [C^n_{ep}]\{\Delta\varepsilon^{n+1}\} \qquad 5.6$$

the updated trial state of stress is :

$$\{\sigma^t\} = \{\sigma_n\} + \{\Delta\sigma^t\} \qquad 5.7$$

Now, the trial stresses $\{\sigma^t\}$ will be checked against the possibility of crossing either the exsiting failure surface or the yield surface. If none of them takes place, the behavior of the material is purely elastic (Fig.5.12.a). This leads to the case where the hardening parameter (K^n), and the kinematic paremeter, ($\{\alpha\}$) at the point n, do not change over the (n+1)th increment. Consequently, the trial stresses become now the true stresses $\{\sigma^{n+1}\} = \{\sigma^t\}$.

On the other hand, to check for yield surface crossing the following criteria should be satisfied :

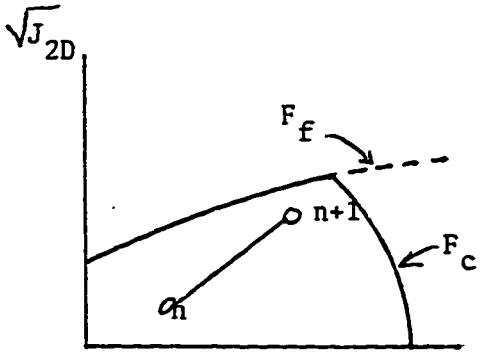

a) Elastic Path

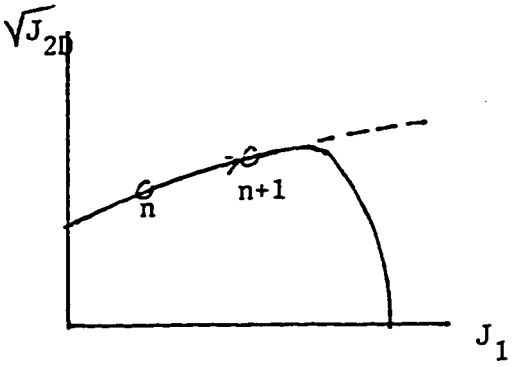

b) Elastic Perfectly plastic path

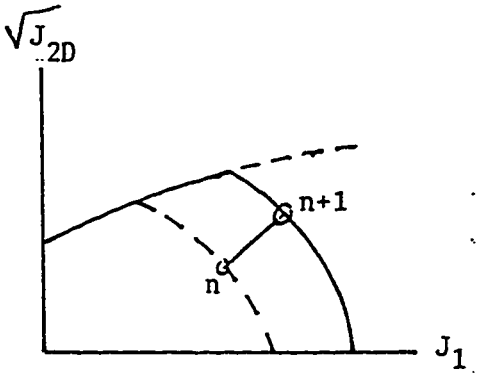

c) elastic work hardening path

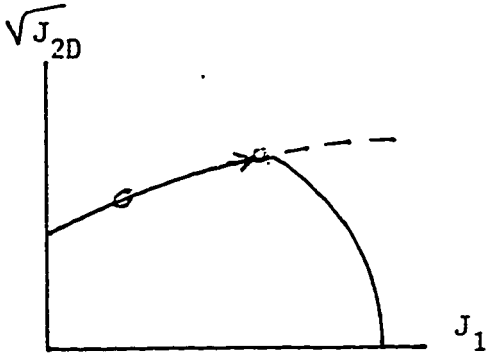

d) Elastic perfectly plastic path with a corner

Fig.5.12 Stress Paths

$$F_c(J_1', \sqrt{J_{2D}'}, K^n) > 0 \qquad 5.8$$

and

$$J_1' > \chi(K^n)$$

or

$$J_1' > I_1(K^n)$$

As a result of crossing the present yield surface a new yield surface is formed and its new place is found by the bisection method (see appendix A) using the following criterion :

$$F_c(J_1', \sqrt{J_{2D}'}, K') < c \qquad 5.9$$

where c is a small offset. Diffrentiation of the yield surface with respect to its components (i.e. $\sigma_{ij}, \varepsilon_v^p$) is performed (see appendix B) to determine the new elasto-plastic matrix, $[C_{e\text{-}p}^{n+1}]$. The process is now continued to check for the other states of stress that violate the yield surface (Fig.5.13).

Sometimes due to the large size of the strain increment $\{\varepsilon^{n+1}\}$ the resulting state of stress violates the failure surface (Fig.'s 5.12.b,d). This is because the assumption that $[C_{e\text{-}p}^n]$ is constant over the (n + 1)th increment, is no longer valid. To avoid such a state the (n + 1)th icrement is subdivided into N equall smaller increments over which $[C_{e\text{-}p}^n]$ can be assumed constant with sufficient accuracy (Faruque, and Desai, 1985), (Owen and Hinto, 1980), and (Siriwarden, and Desai, 1983).

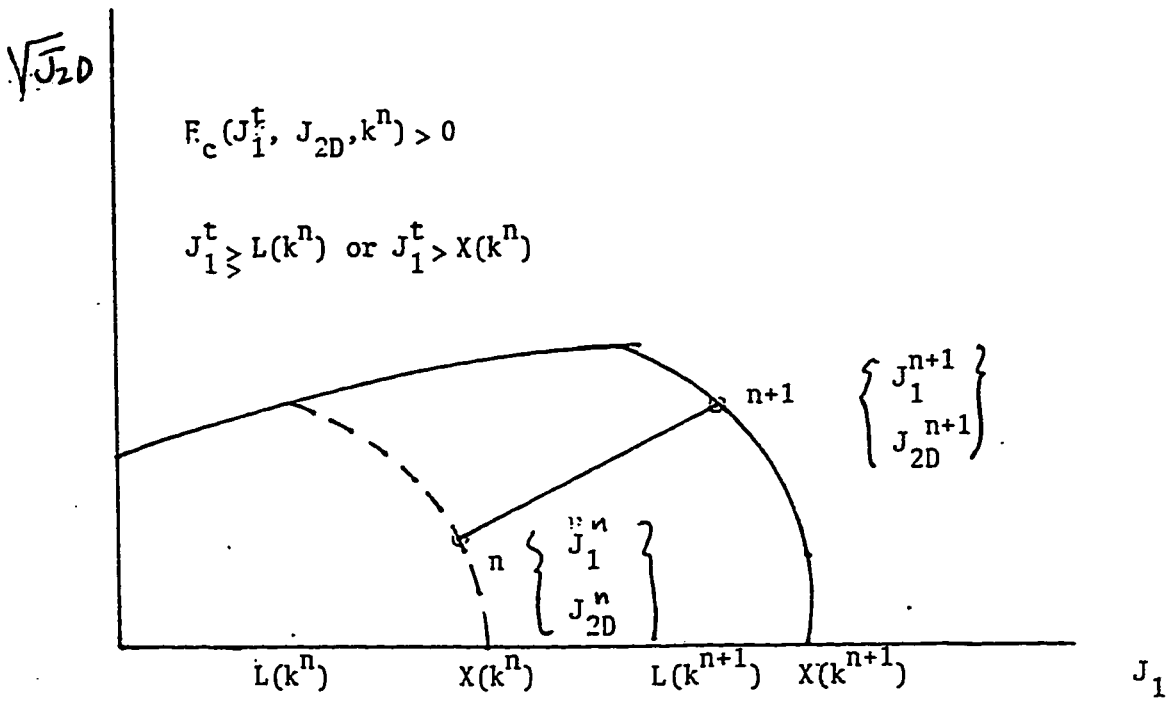

Fig.5.13 Elastic work hardening path

$$\{\Delta\Delta\varepsilon\} = \frac{\{\Delta\varepsilon\}}{N} \qquad 5.10$$

where

$$N = \frac{\varepsilon_{max.}}{0.0005} + 1 \qquad 5.11$$

$$\varepsilon_{max.} = Max(|\Delta\varepsilon_{11}|,|\Delta\varepsilon_{22}|,|\Delta\varepsilon_{33}|,|\Delta\varepsilon_{12}|,|\Delta\varepsilon_{23}|,|\Delta\varepsilon_{31}|) \qquad 5.12$$

Using this criterion $\{\Delta\Delta\varepsilon\}$ will be limited to 0.0005.

At the end of every subincrement stresses are checked to see wheather they violate the failure surface or not according to the following criterion :

$$F_f(J_1^{n+1}, \sqrt{J_{2D}^{n+1}}) = 0 \qquad 5.13$$

Once this Eq. is satsified the state of stresses is on the failure surface. If $J_{1_{n+1}} \geq L(K^n)$ the state of stress lies on the failure surface where the yield surface intersects it (creating a corner) (Fig.5.12.d and Fig.5.14). Here K^n should be updated. Since K^n is a function of ε_{kk}^p , the volumetric plastic strain is updated using the following eqation :

$$\chi = \frac{-1}{D}\ln(1-\frac{\varepsilon_{kk}^p}{w} + Z_0) \qquad 5.14$$

The kinematic parameter α, should be updated also using the following Eq. :

$$\{\alpha^{n+1}\} = \{\alpha^n\} + \{d\alpha\} \qquad 5.15$$

The corresponding $[D_{e\text{-}p}]$ is evaluated after finding the necessary differentiation of F_f with respect to $\{\sigma\}$ and ε_{kk}^p. (see appendix B).

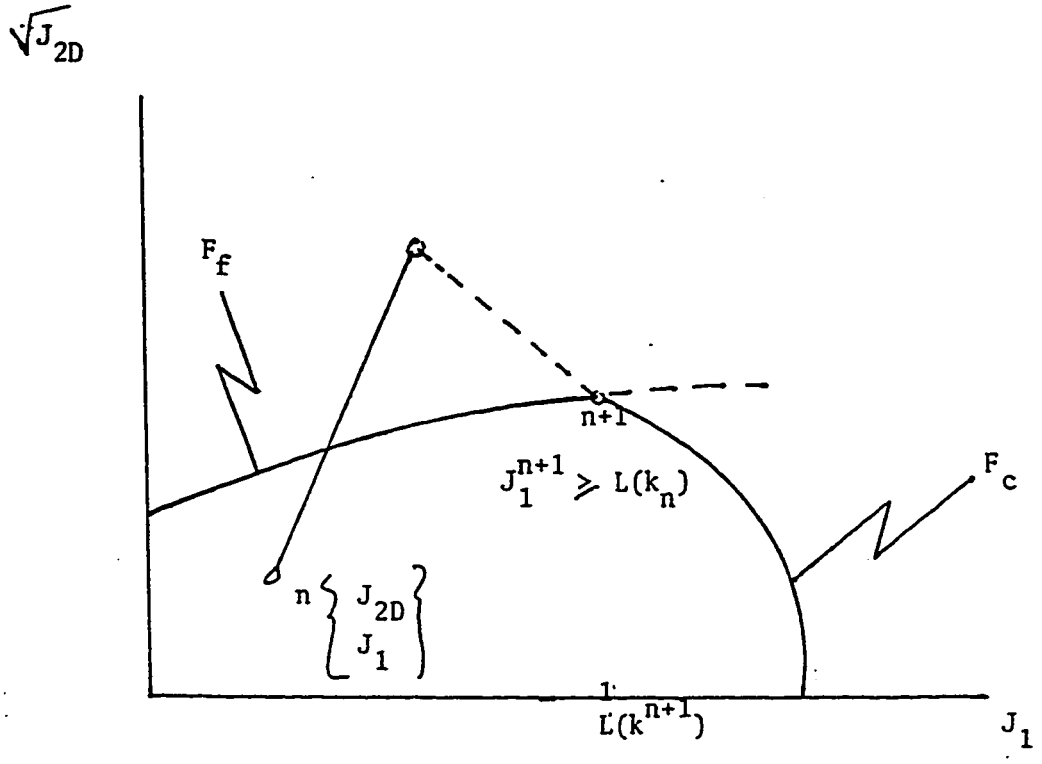

Fig.5.14 Elastic perfectly plastic with a corner

If $J_1^{n+1} < L(K^n)$, the state of stress lies on the failure surface without a corner (Fig.5.11.b and Fig.5.15), and the hardening parameters do not need to be updated.

Program Algorithm :

The major steps of processing MICROFEM will be discussed here Notice that indices that are associated are as follows:

o : initial

i : iterative.

Step 1: Input data defining geometry, element connectivities, boundary conditions and material properties.

Step 2: Evaluate equivalent nodal forces due to gravity loading, pressure loading, etc.

Step 3: Determine shape functions, $[N]$, derivatives, $[B]$, and elastic material matrix $[D_e]$

Step 4: Compute element stiffness matrices and assemble them to obtain the stiffness matrix for the structure.

$$[K] = \int_v [B]^T [D_e][B] dV_e$$

$$[K] = \sum [K]$$

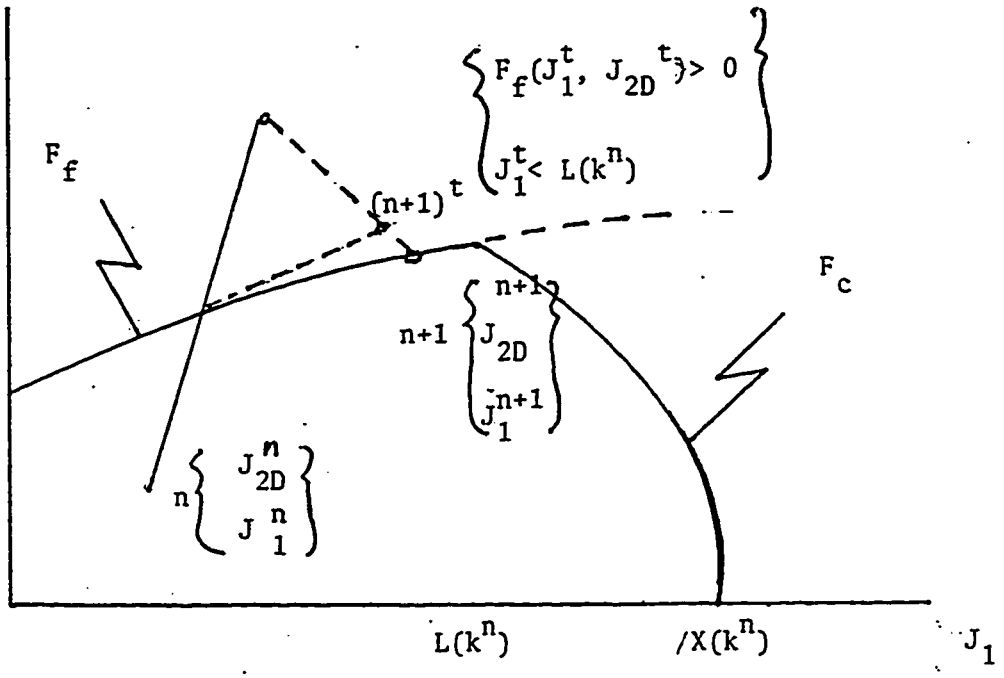

Fig.5.15 Elastic perfectly plastic without a corner

Step 5: Solve the structural equilibrium Eq. for nodal displacement increment corresponding to load step n.

$$\{\Delta U_n\} = [K_n]^{-1}\{\Delta Q_n\}$$

Step 6: Solve for incremental strains

$$\{\Delta \varepsilon_i\} = [B]\{\Delta U_{n,i}\}$$

Step 7: Find stress increment

$$\{\Delta \sigma_i\} = [D_{ep}]\{\Delta \varepsilon_i\}$$

Step 8: Find corresponding incremental load vector balancing the internal stress increment

$$\{Q_{int}\}_i = \int [B]^T \{\Delta \sigma_i\} dV_e$$

Step 9: Subtract to from the residual or iterative load vector

$$\{\Delta Q_R\}_{i+1} = \{\Delta Q_n\} - \{\Delta Q_{int}\}_i$$

Step 10: Check the size of residue against a specified tolerance

$$\textit{If} \quad \frac{\|\{\Delta Q_r\}_{i+1}\|}{\|\{\Delta Q_n\}\|} \leq \quad \textit{tolwrance}, \text{ Go to step (14)}$$

Step 11 Solve for the iterative displacement increment

$$\{\Delta U_{i+1}\} = [K_n]^{-1}\{\Delta Q_R\}_{i+1}$$

Step 12: Add iterative displacements to previous total displacements for the current load step

$$\{\Delta U_{n,i+1}\} = \{\Delta U_{n,i+1}\} + \{\Delta U_{i+1}\}$$

Step 13: Repeat the computations from step (6) to (12) (iteration loop) with i = i + 1, until the residual load vector is sufficiently small.

Step 14: Add displacements, strains, stress, and the kinematic parameter to those at the beginning of the current load increment

$$\{U_n\} = \{U_{n-1}\} + \{\Delta U_n\}$$

$$\{\varepsilon_n\} = \{\varepsilon_{n-1}\} + \{\Delta\varepsilon_n\}$$

$$\{\sigma_n\} = \{\sigma_{n-1}\} + \{\Delta\sigma_n\}$$

$$\{\alpha_n\} = \{\alpha_{n-1}\} + \{\Delta\alpha_n\}$$

Step 15: Recalculate $[D_{ep}]$ using eq 3.59 and calculate new $[K] = [K_{n+1}]$ for the next load step (tangential stiffness format).

Step 16: Repeat steps (5) to (15) (load increment loop) with n = n + 1 until the final load step is applied.

5.3.4 Problem Definition and Geometry

MICROFEM with the combined hardening cap model will be used to solve a problem of a rigid strip footing resting on sand. A comparison between the experimental and theoritical results will be made to evaluate the ability of the model to predict the behavior of soil. This is a plane-strain problem. The soil mass under the footing is descretized using 4-noded quadrilateral elements. Only half of the system will be analyzed due to symmetry (Fig.5.16). So, the number of elements will be 88 elements and 108 nodes. Boundary conditions are determined as follows :

1. left boundaries act as a plane of symmetry, so it is perfectly smooth (movement downward).
2. right boundaries are also smooth (movement downward).
3. bottom boundaries are rough and do not allow relative movements (Fig. 5.16).

Necessary calculations are done to take into account weight of the soil as follows :

vertical stress $= \sigma_v = \sigma_y = \gamma y$

horizontal stress $= \sigma_h = \sigma_x = k_o \sigma_v$

$$\sigma_z = \nu(\sigma_x + \sigma_y)$$

where

γ : unit weight, approximately equal to $16 \frac{KN}{m^3}$.

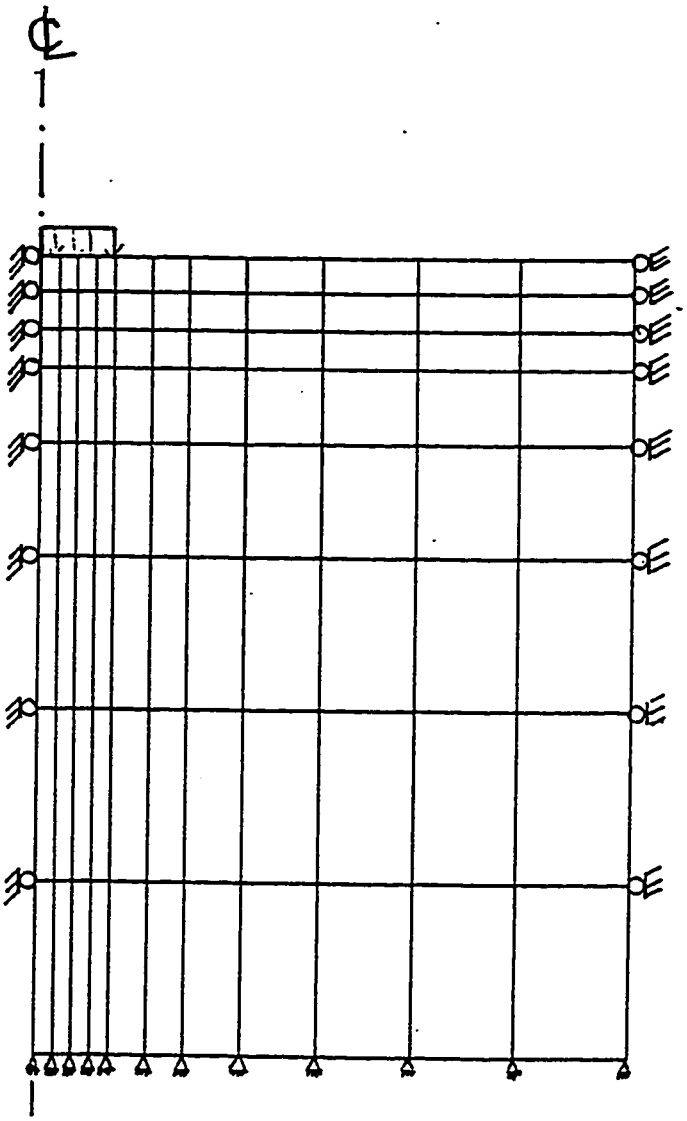

Fig. 5.16 Mesh layout of foundation with 88 elements and 108 nodes.

k_o : coefficient of earth pressure at rest.

v : Poisson's ratio (table 4.1).

5.3.5 Discussion of the MICROFEM Output

The isotropic cap model can not represent the cycles of unloading and reloading when implemented into MICROFEM (Fig.5.17). In other words, it does not represent the elasto-plastic behavior of material upon unloading-reloading sequences. So, extension of the isotropic model into a combined hareding cap model is supposed to give better results, which is found to be right when it is implemented into MICROFEM (Fig.5.18). The combined hardening cap model, when implemented int MICROFEM, can simulate the elasto-plastic behavior of sand under the model footing successfully (Fig.5.18). Comparison between the simulated load-deformation curve and the experimental one shows a good agreement between them. A figure of the deformed mesh (Fig.5.19) shows that the displacement beneath the footing is uniform ,which is typical for rigid footings. Stress distribution beneath the footing is not constant but instead it varies along the bottom of the footing (Fig.5.20).

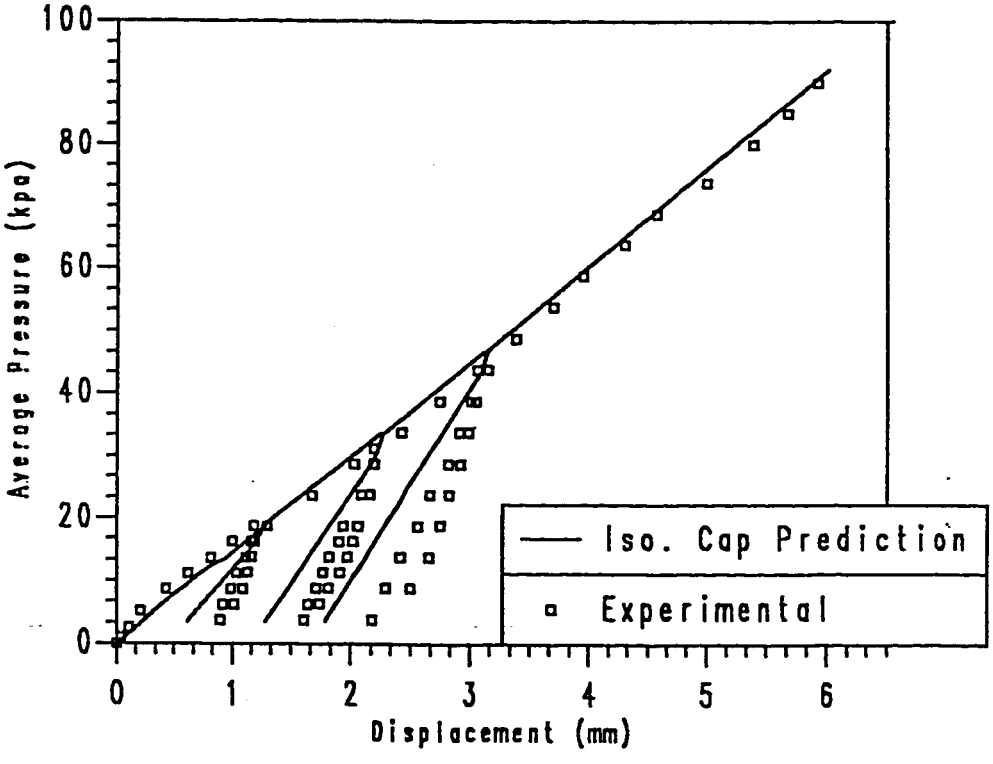

Fig.5.17. Prediction of the Isotropic cap model of the average stress-load covered a comparison with the experimental data.

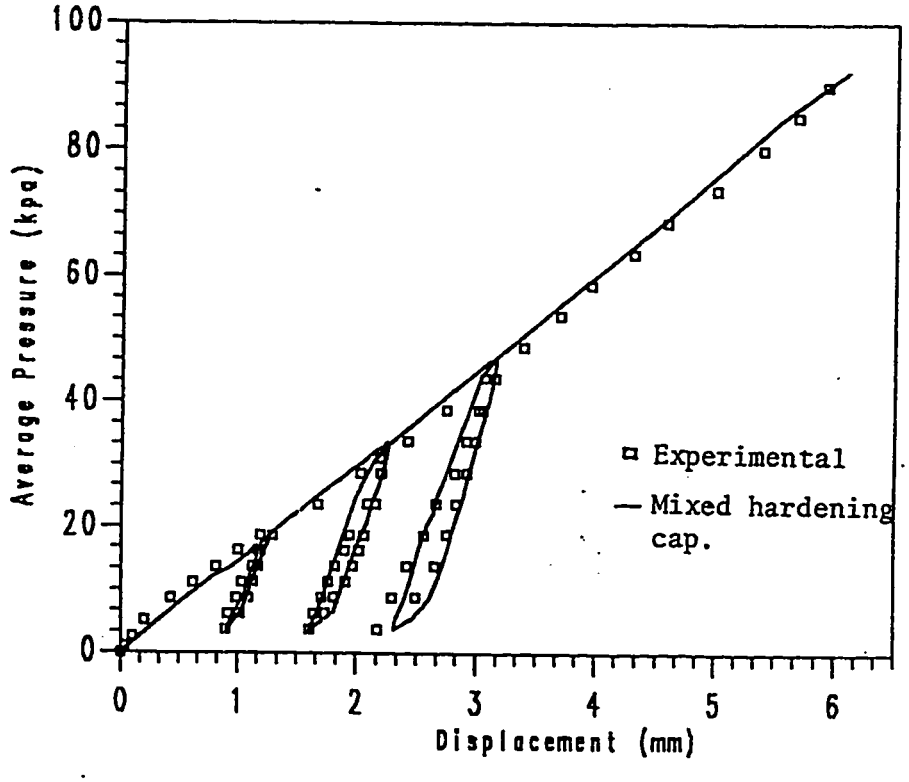

Fig.5.18 Comparison between experiments and cap predicted results.

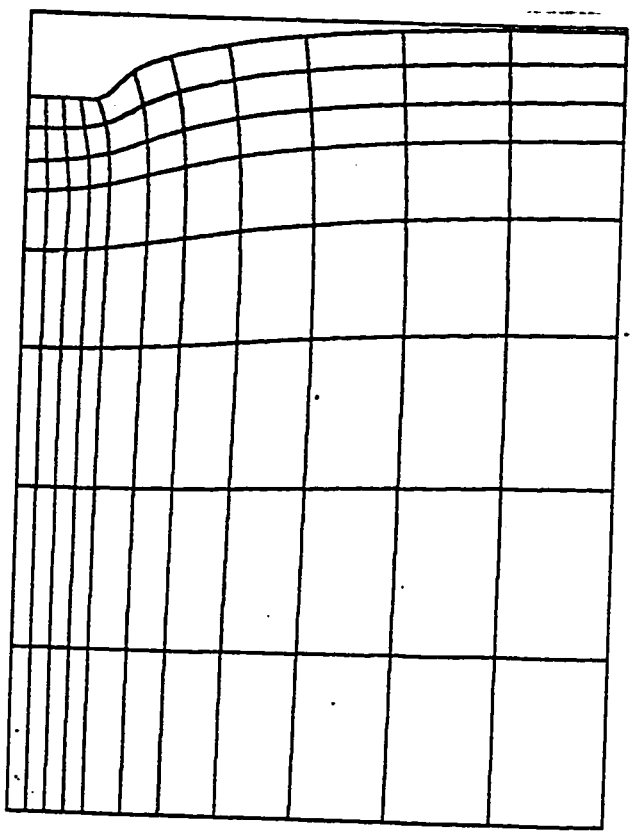

Fig. 5.19 Deformed mesh under footing.

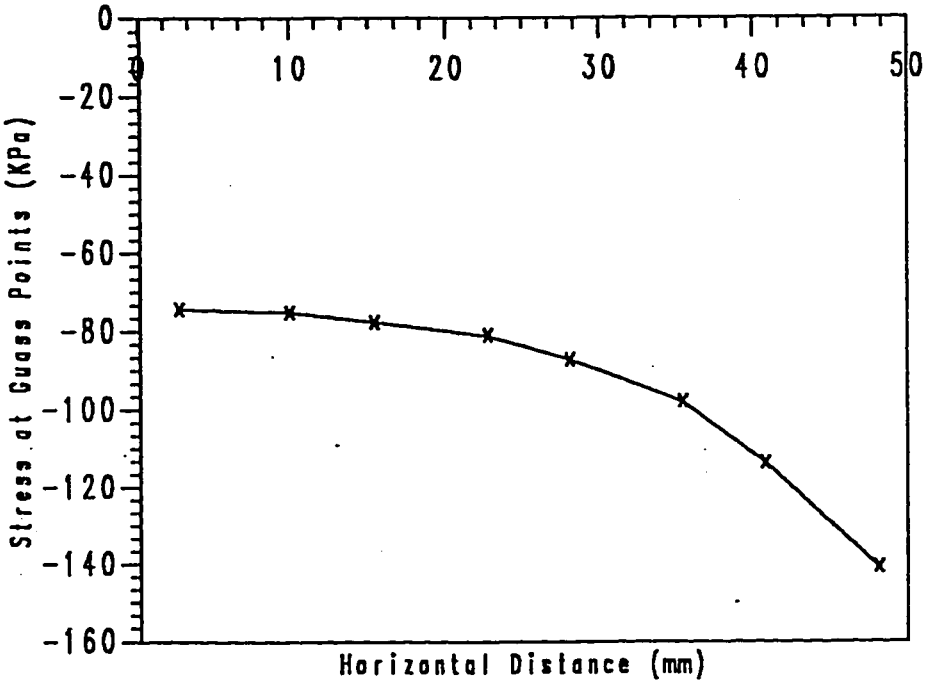

Fig. 5.20 Variation of stress under footing.

CHAPTER 6

CONCLUSION AND RECOMMENDATIONS

6.1 CONCLUSION

From the numerical calculations and the experimental results, the following conclusions can be drawn.

1. The combined hardening three stress invariant cap model is simple to implement in nonlinear finite element analysis and is numerically well-behaved.
2. Good estimate of the kinematic hardening parameter C_α can be obtained from the average slope of the cyclic response at low amplitude load.
3. The combined hardening cap model predicts successfully the cyclic stress-strain response of dune sand.

4. The model predicts very well the load-deformation characteristics of the model strip footing resting on dune sand.

5. Deformation patterns under the model strip footing obtained from the numerical analysis is in a close agreement with the classical pattern.

6.2 RECOMMENDATIONS

The followings are suggestions to further extension of the present study

1. Using a non-linear combined hardening rule may improve the prediction of the cyclic stress-strain response.

2. Developing a 3-D finite element programm to account for general casses rather than plain-strain condition.

3. Comparison of model prediction with the performance of a footing under full scale test.

REFERENCES

Abduljauwad, S.N.(1985), ***Soil-Structure Interaction Analysis and Evaluation of Bounding Surface Plasticity Model***, Ph.D Thesis, University of Colorado, Boulder.

Azeemuddin, M. (1988), ***Constitutive Modelling of Dhahran Dune Sand Using the 3rd Invariant Stress Dependent Isotropic Cap Model***, M.S. Thesis, CE Department, University of King Fahd for Petroleum and Minerals, Dhahran.

Baladi, G.Y., (1977), ***Numerical Implementation of a Transverse-Isotropic Inelastic, Work-Hardening Constitutive Model***, Trans. 4th Int. Conf. Structural Mechanics in Reactor Technology, Vol. M, ***Methods for Structural Analysis***, M6/2, pp. 1-12

Baltov, A., and Sawczuk, A. (1965), ***A Rule for Anisotropic Hardening***, Acta Mech. Vol. 1, No. 2, PP. 81-92.

Bathe, K.J. (1982), ***Finite Element Procedures in Engineering Analysis***, Prentice Hall, New Jersey.

Chen, W.F.(1984), ***Constititve Modelling in Soil Mechanics***, In: C.S. Desai and R.H. Gallagher (Editors), Mechanics of Engineering Materials, John Wiley, London, PP. 91-120.

Chen, W.F. and Baladi, G.Y. (1985), ***Soil Plasticity Theory and***

Implementation, Developments in Geotechnical Engineering, No. 38, Elsevier Science Publishers B.V., Netherlands.

Chen, W.F. and Saleeb, A.F. (1982), ***Constitutive Equations for Engineering Materials***, Vol. 1, Elasticity and Modeling, John Wiley and Sons, New York.

Cook, R.D. (1981), ***Concepts and Application of Finite Element Alanysis***, Second Edition John Eiley and Sons, New York.

Davis, E.H. (1968), ***Theories of Plasticity and the Failure of Soil Masses***, In: I.K.Lee (Editor), Soil Mechanics Selected Topics, Butterworths, London, PP. 341-380.

Day, S.E. (1985), ***A Softening Plasticity Model for Concrete***, M.S. Thesis, CEAE Department, University of Colorado,Boulder.

DeNatale, J.S. (1982), ***Calibration of the Bounding Surface Plasticity Model by Multivariate Optimization***, Ph.D. Thesis, Dept. of Civil Eng'g., Univ. of California, Davis.

Desai, C.S. and Abel, J.F. (1972), ***Introduction to the Finite Element Method***, Van Nostrand Reinhold, New York.

Desai, C.S. and Faruque, M.O. (1984), ***Constitutive Model for (Geological) Materials***, Journal of Eng'g. Mech. Div., ASCE, Vol. 110, No. 9, PP. 1391-1408.

Desai, C.S., Phan, H.V. and Sture, S. (1981), ***Procedure, Selection and Application of Plasticity Models for a Soil,*** Int. J. Numer. Analat. Methods in Geomech., Vol. 5, No. 3, PP. 143-171.

Desai, C.S. and Siriwardane, H.J. (1984), ***Constitutive Laws for Engineering Materials,*** Prentice-Hall, New Jersey.

DiMaggio, F.L. and Sandler, I.S. (1971), ***Material Model for Granular Soils,*** J. Eng. Mech. Div., ASCE, Vol. 97, Em 3, 1971, PP. 935-950.

Drucker, D.C. (1950), ***Some Implications of Work Hardening and Ideal Plasticity,*** Q. Appl. Math., 7(4): 414-418.

Drucker, D.C. (1959), ***A Definition of Stable Inelastic Material,*** J. Appl. Mech., Vol. 26. Drucker, D.C., Gibson, R.E. and Henkel, D.J. (1957), ***Soil Mechanics and Work-Hardening Theories of Plasticity,*** Trans., ASCE, Vol. 122, PP. 338-346.

Drucker, D.C., and Prager, W. (1952), ***Soil Mechanics and Plastic Analysis of Limit Design,*** Quart. Appl. Math., Vol. 10, No. 2.

Faruque, M.O. (1983), ***Development of a Generalized Constitutve Model and Its Implementation in Soil-Structure Interaction,*** Ph.D. Thesis, University of Arizona, Tucson, Arizona.

Faruque, M.O. and Chang, C.J. (1986), ***New Cap Type Model for Fail-***

ure and Yielding of Pressure Sensitve Materials, J. Eng. Mech. Div., ASCE, Vol. 112,PP.1041-1053.

Faruque, M.O. and Desai, C.S. (1985), ***Implementation of a General Constitutive Model for Geological Materials***, Int. J. for Num. and Analytical Methods in Geomechanics, Vol. 9, PP. 415-436.

Faruque, M.O. (1987), ***A third Invariant Dependent Cap Model for Geologic Materials***, Japanese Society of Soil Mechanics and Foundation Engingeering, Vol. 27, No. 2, PP. 12-20.

Ghamedy, H.N. (1986), ***Nonlinear Finite Element Analysis of Inelastic Structures With Applications to Reiforced Concrete***, Ph.D. Thesis, Dept. of Civil, Environmental and Architerctural Eng'g., Uinv. of Colorado, Boulder.

Hill, R. (1950), ***The Mathematical Theory of Plasticity***, Oxford Univ. Press, Oxford, U.K.

Lad, P.V. (1977), ***Elasto-Plastic Stress Strain Theory for Cohesionless Soil With Curved Yield Surfaces***, Int. J. Solids Struct., 13: 1014-1035.

Lade, P.V. and Duncan, J.M. (1975), ***Elasto-Plastic Stress Strain Theory for Cohesionless Soil***, J. Geotech. Eng. Div., ASCE, Vol. 101, PP.1037-1053.

Lade, P.V. and Musante (1977), ***Failure Conditions in Sand and Remoulded Clay***, Proc. 9th International Conf. on Soil Mech. and Foundation Eng'g., Tokyo, Vol. 1, PP. 181-186.

Matsuoka, H. (1976), ***On the Significance of the Spatial Mobilized Plane , Soils and Foundations***, Vol. 16, No. 1, PP. 91-100.

Mroz, S. (1963), ***Non-Associated Flow Laws in Plasticity***, J. De Mecanique, Vol. 2, No. 1, PP. 21-41.

Mroz, Z. (1976), ***On the Description of Anisotropic Work-Hardening***, J. Mech. and Physics of Solids, Vol. 15, PP. 163-175.

Mroz, Z. (1972), ***A Description of Work-Hardening of Metals with Application to Variable Loading***, Proc. Int. Symp. Found. Plasticity (Editors:Sawczuk, A.), Noordhoff International Publishing Company.

Mroz, Z., Norris, V.A. and Zienkiewicz, O.C. (1978), ***An Anisotropic Hardening Model For Soils and its Application to Cyclic Loading***, Int. J. Num. Analyt. Methods in Geomech., Vol. 2, PP. 203-221.

Mroz, Z., Norris, V.A. and Zienkiewicz, O.C. (1978), ***Application of An Anisotropic Hardening Model in the Alnalysis of Elasto-Plastic Deformation of Soils***, Geotechnique, Vol. 29, No. 1, PP. 1-34.

Ottosen, N.S. (1977), ***A Failure Criterion for Concrete***, Journal of Engineering Mechanics Division, ASCE, Vol. 103, No. EM4, August 1977, PP. 527-535.

Owen, D.R.J. and Hinton, E. (1980), ***Finite Element in Plasticity, Theory and Practice***, Pineridge Press Limited, Swansea, U.K.

Podgorsk J. (1985), ***General Failure Criterion for Isotropic Mdeia***, J. Eng. Mech. Div., ASCE, Vol. 111, PP. 188-201.

Prager, W. (1955), ***The Theory of Plasticity: A Survey of Recent Advancements (James Clayton Lecture)***, Proc. Inst. Mech. Eng., Vol. 169, PP.41-57.

Prager, W. (1956), ***A New Method of Analyzing Stresses and Strains in Work Hardening Plastic Solids***, J. Appl. Mech., Vol. 78, PP. 493-496.

Prevost, J.H. (1977), ***Mathematical Modelling of Monotonic and Cyclic Undrained Clay***, Int. J. Num. Analyt. Methods in Geomech., Vol. 1, PP. 196-216.

Prevost, J.H. (1979), ***Mathematical Modelling of Soil-Stress-Strain-Strength Behavior***, Proc. 3rd Int. Conf. Num. Methods in Geomech., Aachen, Ed. W. Wittke, Balkema Press, Vol. 1, PP. 347-361.

Roscoe, K.H., and Burland, J.B. (1968), ***On the Generalized Stess-Strain Behavior of Wet Calys***, Engineering Plasticity, Heyman, J., and Leckie, F.A., Cambridge Univ. Press.

Roscoe, K.H., Schofield, A.N. and Worth, C.P. (1958), ***On the Yielding of Soils***, Geotechnique, Vol. 8, No. 1.

Sandler, I.S. and Baron, M.L. (1979), ***Recent Development in the Constitutive Modelling of Geological Materials***, Proc. Int. Conf. Num. Meth. Geomech., Vol. 1, PP. 363-376.

Sandler, I.S., DiMaggio, F.L. and Baladi, G.Y. (1976), ***Generalized Cap Model for Geological Materials***, J. Geotechnical Div., ASCE, Vol. 102, GT7,PP. 683-699.

Sandler, I.S., and Rubin, D. (1979), ***An Algorithm and a Modular Subroutine for the Cap Model***, Int. J. Num. Analyt. Methods in Geomech., Vol. 3, 1979.

Schofield, A., and Worth, C.P. (1968), ***Critical State Soil Mechanics***, McGraw-Hill, London.

Siriwardane, H.J.and Desai, C.S. (1983), ***Computatoinal Procedures for Non-Linear Three-Dimensional Analysis with Some Advanced Constitutive Laws***, Int. J. Numer. Analat. Methods in Geomech., 7, 143-171.

Smith, I.M. (1982), ***Programming the Finite Element Method with Application to Geomechanics***, John Wiley and Sons, Chichester.

Steinar, Nordal (1983), ***Elasto-Plastic Behavior of Soils Analized by the Finite Element Method***, Ph.D. Thesis, Norwegian Institute of Technology, University of Trondheim.

Sture, S., Desai, C.S. and Janardhanam, R. (1979), ***Development of a Constitutive Law for an Artificial Soil***, Proc. 3^{rd} Int. Conf. on Num. Meth. in Geomech., Aachen.

Willam, K.J. and Warnke, E.P. (1974), ***Constitutive Models for Triaxial Behavior of Concrete***, Int. Assoc. Bridge Struct. Eng. Sem. Concr. Struct. Subjected to Triaxial Stresses, Bergamo, Italy, Int. Assoc. Bridge Struc. Eng. Proc., Vol. 19, PP. 1-30.

Yamada, Y., Yishimura, N. and Sakurai, T. (1968), ***Plastic Stress-Strain Matrix and its Application for the Solution of Elastic-Plastic Problems by the Finite Element Method***, Int. J. Mechanical Sciences, Vol. 10, No. 5.

Zaman, M.M., Desai, C.S. and Faruque, M.O., ***An Algorithm for Determining parameters for Cap Model from Raw Laboratroy Test Data***, Proc. 4^{th} Int. Conf. Numer. Methods in Geomech., Edmonton, Canda, 1982.

Zienkiewiez, O.C. (1977), ***The Finite Element Method***, Third Edition, McGraw-Hill, London, U.K.

Zienkiewicz, O.C., Valliappan, S. and King, I.p. (1969), ***Elasto-Plastic Solutions of Engineering Problems, Initial Stress Finite Element Approac***, Int. J. Numerical Methods in Engineering, Vol. 1, PP. 75-100.

APPENDIX-A

LINEARLY ELASTIC STRESS-STRAIN RELATIONSHIPS

LINEARLY ELASTIC STRESS-STRAIN RELATIONSHIPS

(i) A general three-dimensional state :

$$\{d\sigma\} = \{d\sigma_{11}, d\sigma_{22}\, d\sigma_{33}, d\sigma_{12}, d\sigma_{23}, d\sigma_{13}\}^T \qquad (\Lambda.01)$$

$$\{d\varepsilon\} = \{d\varepsilon_{11}, d\varepsilon_{22}, d\varepsilon_{33}, d\gamma_{12}, d\gamma_{23}, d\gamma_{13}\}^T \qquad (\Lambda.02)$$

$$\{d\sigma\} = [D]\,\{d\varepsilon\} \qquad (\Lambda.03)$$

$$\{d\varepsilon\} = [D]^{-1}\,\{d\sigma\} \qquad (\Lambda.04)$$

$$[D] = \frac{E}{(1+\nu)(1-2\nu)} \begin{bmatrix} (1-\nu) & \nu & \nu & 0 & 0 & 0 \\ & (1-\nu) & \nu & 0 & 0 & 0 \\ & & (1-\nu) & 0 & 0 & 0 \\ & & & \frac{1}{2}(1-2\nu) & 0 & 0 \\ & SYM. & & & \frac{1}{2}(1-2\nu) & 0 \\ & & & & & \frac{1}{2}(1-2\nu) \end{bmatrix}$$

$$(\Lambda.05)$$

$$[D] = \begin{bmatrix} K+\frac{4}{3}G & K-\frac{2}{3}G & K-\frac{2}{3}G & 0 & 0 & 0 \\ & K+\frac{4}{3}G & K-\frac{2}{3}G & 0 & 0 & 0 \\ & & K+\frac{4}{3}G & 0 & 0 & 0 \\ & & & G & 0 & 0 \\ & SYM. & & & G & 0 \\ & & & & & G \end{bmatrix}$$

(A.06)

$$[D]^{-1} = \frac{1}{E}\begin{bmatrix} 1 & -\nu & -\nu & 0 & 0 & 0 \\ & 1 & -\nu & 0 & 0 & 0 \\ & & 1 & 0 & 0 & 0 \\ & & & 2(1+\nu) & 0 & 0 \\ & SYM. & & & 2(1+\nu) & 0 \\ & & & & & 2(1+\nu) \end{bmatrix}$$

(A.07)

$$[D]^{-1} = \begin{bmatrix} \frac{1}{9K}+\frac{1}{3G} & \frac{2}{9K}-\frac{1}{6G} & \frac{2}{9K}-\frac{1}{6G} & 0 & 0 & 0 \\ & \frac{1}{9K}+\frac{1}{3G} & \frac{2}{9K}-\frac{1}{6G} & 0 & 0 & 0 \\ & & \frac{1}{9K}+\frac{1}{3G} & 0 & 0 & 0 \\ & & & \frac{1}{G} & 0 & 0 \\ & SYM. & & & \frac{1}{G} & 0 \\ & & & & & \frac{1}{G} \end{bmatrix} \qquad (\Lambda.08)$$

(ii) **Plane Stress :**

Requirements : $d\sigma_{33} = d\sigma_{13} = d\sigma_{23} = 0$ (Λ.09)

Consequently : $d\gamma_{13} = d\gamma_{23} = 0$ (Λ.10)

$$\{d\sigma\} = \{d\sigma_{11}, d\sigma_{22}, d\sigma_{12}\}^T \qquad (\Lambda.11)$$

$$\{d\varepsilon\} = \{d\varepsilon_{11}, d\varepsilon_{22}, d\gamma_{12}\}^T \qquad (\Lambda.12)$$

$$\{d\sigma\} = [D]\{d\varepsilon\} \qquad (\Lambda.13)$$

$$\{d\varepsilon\} = [D]^{-1}\{d\sigma\} \qquad (\Lambda.14)$$

$$[D] = \frac{E}{1-\nu^2}\begin{bmatrix} 1 & \nu & 0 \\ & 1 & 0 \\ SYM. & & \frac{1}{2}(1-2\nu) \end{bmatrix} \qquad (\Lambda.15)$$

$$[D] = \begin{bmatrix} \frac{12K+4G}{3K+4G}G & \frac{-6K+4G}{3K+4G}G & 0 \\ & \frac{12K+4G}{3K+4G}G & 0 \\ SYM. & & G \end{bmatrix} \qquad (\Lambda.16)$$

$$[D]^{-1} = \frac{1}{E}\begin{bmatrix} 1 & -\nu & 0 \\ & 1 & 0 \\ SYM. & & 2(1+\nu) \end{bmatrix} \qquad (\Lambda.17)$$

$$[D]^{-1} = \begin{bmatrix} \frac{1}{9K}+\frac{1}{3G} & \frac{2}{9K}-\frac{1}{6G} & 0 \\ & \frac{1}{9K}+\frac{1}{3G} & 0 \\ SYM. & & \frac{1}{G} \end{bmatrix} \qquad (\Lambda.18)$$

In addition :

$$d\varepsilon_{33} = -\frac{\nu}{E}(d\sigma_{11} + d\sigma_{22}) = (\frac{2}{9K}-\frac{1}{6G})(d\sigma_{11} + d\sigma_{22}) \qquad (\Lambda.19)$$

$$= \frac{\nu}{(1-\nu)}(d\varepsilon_{11} + d\varepsilon_{22}) = (\frac{-3K+2G}{3K+4G})(d\varepsilon_{11} + d\varepsilon_{33}) \qquad (A.20)$$

(iii) **Plane Strain :**

Requirements : $d\varepsilon_{33} = d\gamma_{13} = d\gamma_{23} = 0$ (A.21)

Consequently : $d\sigma_{13} = d\gamma_{23} = 0$ (A.22)

$$\{d\sigma\} = \{d\sigma_{11}, d\sigma_{22}, d\sigma_{12}\}^T \qquad (A.23)$$

$$\{d\varepsilon\} = \{d\varepsilon_{11}, d\varepsilon_{22}, d\gamma_{12}\}^T \qquad (A.24)$$

$$\{d\sigma\} = [D]\{d\varepsilon\} \qquad (A.25)$$

$$\{d\varepsilon\} = [D]^{-1}\{d\sigma\} \qquad (A.26)$$

$$[D] = \frac{E}{(1+\nu)(1-2\nu)}\begin{bmatrix} (1-\nu) & \nu & 0 \\ & (1-\nu) & 0 \\ SYM. & & \frac{1}{2}(1-2\nu) \end{bmatrix} \qquad (A.27)$$

$$[D] = \frac{E}{(1+\nu)(1-2\nu)}\begin{bmatrix} K+\frac{4}{3}G & K-\frac{2}{3}G & 0 \\ & K+\frac{4}{3}G & 0 \\ SYM. & & G \end{bmatrix} \qquad (A.28)$$

$$[D]^{-1} = \frac{1}{E}\begin{bmatrix} 1-\nu^2 & -\nu(1+\nu) & 0 \\ & 1-\nu^2 & 0 \\ SYM. & & 2(1+\nu) \end{bmatrix} \qquad (\Lambda.29)$$

$$[D]^{-1} = \begin{bmatrix} \frac{3K+4G}{12K+4G}\frac{1}{G} & \frac{-3K+2G}{12K+4G}\frac{1}{G} & 0 \\ & \frac{3K+4G}{12K+4G}\frac{1}{G} & 0 \\ SYM. & & \frac{1}{G} \end{bmatrix} \qquad (\Lambda.30)$$

In addition :

$$d\sigma_{33} = \frac{E}{(1+\nu)(1-2\nu)}(d\varepsilon_{11} + d\varepsilon_{22}) = (K-\frac{2}{3}G)(d\varepsilon_{11} + d\varepsilon_{22}) \quad (\Lambda.31)$$

$$= \nu(d\sigma_{11} + d\sigma_{22}) = (\frac{3K-2G}{6K+2G})(d\sigma_{11} + d\sigma_{22}) \qquad (\Lambda.32)$$

APPENDIX-B

DERIVATION OF CONSTITUTIVE RELATIONS FOR THE MODEL

Derivation of Constitutive Relations for the Model

The equations of the fixed yield surface, F_f (Failure Surface), and the moving yield surface, F_c (Hardening Cap), for the three-invariant dependent cap model were given in Chapter 3 as Eq.3.6 to Eq.3.7. In order to evaluate the complete elasto-plastic matrix, $[C^{e\text{-}p}]$, given by Eq.3.33, the gradient tensor $\frac{\partial F}{\partial \sigma_{ij}}$ and the hardening term A_h^{**} have to obtained. Here the function F refers to either F_f or F_c, depending upon which surface is violated.

Using chain rule of differentiation, $\frac{\partial F}{\partial \sigma_{ij}}$ can be written as

$$\frac{\partial F_f}{\partial \sigma_{ij}} = \frac{\partial F_f}{\partial J_1}\frac{\partial J_1}{\partial \sigma_{ij}} + \frac{\partial F_f}{\partial J_{2D}}\frac{\partial J_{2D}}{\partial \sigma_{ij}} + \frac{\partial F_f}{\partial J_{3D}}\frac{\partial J_{3D}}{\partial \sigma_{ij}} \tag{B.01}$$

$$\frac{\partial F}{\partial \sigma_{ij}} = \frac{\partial F_f}{\partial J_1}\delta_{ij} + \frac{\partial F_f}{\partial J_{2D}}S_{ij}\frac{\partial F_f}{\partial J_{3D}}(S_{ik}S_{kj} - \frac{2}{3}J_{2D}\delta_{ij}) \tag{B.02}$$

Using the expression for F_f given by Eq.3.6

$$F_f = g(0,J_1)[\frac{1}{\sqrt{2}}(S_{ij}-\alpha_{ij})] - A - MJ_1 + C\exp(-\beta J_1) = 0 \tag{B.03}$$

where the partial derivative of the function g, is obtained as

$$\frac{\partial g}{\partial J_1} = \frac{\partial g}{\partial A_t}\frac{\partial A_t}{\partial J_1} \tag{B.04}$$

where

$$\frac{\partial g}{\partial J_1} = -\frac{2}{3\sqrt{3}}\sin[\frac{1}{3}\cos^{-1}(-A_t\cos 30)]\cos 3\frac{0}{\sqrt{(1-A_t^2\cos^2 30)}} \tag{B.05}$$

and

$$\frac{\partial A_t}{\partial J_1} = -\frac{\gamma}{P^a}A_0 e^{-\frac{\gamma J_1}{P_a}} \tag{B.06}$$

similarly,

$$\frac{\partial F_f}{\partial J_{2D}} = -\frac{1}{2\sqrt{J_{2D}}}g(0,J_1) \tag{B.07}$$

and

$$\frac{\partial F_f}{\partial J_{3D}} = \sqrt{J_{2D}}\frac{\partial g(0,J_1)}{\partial J_{3D}} \tag{B.08}$$

$$\sqrt{J_{2D}}\frac{\partial g(0,J_1)}{\partial 0}\frac{\partial 0_f}{\partial J_{3D}} \tag{B.09}$$

where

$$\frac{\partial g(0,J_1)}{\partial 0} = \frac{2}{\sqrt{3}}A_t\sin[\cos^{-1}(-A_t\cos 30)]\sin 3\frac{0}{\sqrt{(1-A_t^2\cos^2 30)}} \tag{B.10}$$

and

$$\frac{\partial \theta}{\partial J_{3D}} = -\frac{\sqrt{3}}{2sin3\theta}\frac{1}{J_{2D}^{3/2}} \tag{B.11}$$

Similarly, using the expression for F_c given by Eq.3.7

$$\frac{\partial F_c}{\partial J_1} = \frac{2(J_1 - L)}{R^2} \tag{B.12}$$

$$\frac{\partial F_c}{\partial J_{2D}} = g^2(0,L) \tag{B.13}$$

$$\frac{\partial F_c}{\partial J_{3D}} = \frac{\partial F_c}{\partial \theta}\frac{\partial \theta}{\partial J_{3D}} \tag{B.14}$$

where

$$\frac{\partial F_c}{\partial \theta} = 2g(0,L)\frac{\partial g(0,L)}{\partial \theta}J_{2D} \tag{B.15}$$

where $\frac{\partial g(0,L)}{\partial \theta}$ is the same as $\frac{\partial g(0,J_1)}{\partial \theta}$ given in Eq. B.10 and $\frac{\partial \theta}{\partial J_{3D}}$ is given by Eq. B.11.

The hardening term also has to be evaluated. In the present model, hardening was assumed to be a function of the plastic volumetric strain, ε_v^p. Thus,

$$\frac{\partial F_c}{\partial \varepsilon_v^p} = -\frac{1}{R^2}[2(X - L)(\frac{\partial X}{\partial \varepsilon_v^p} - \frac{\partial L}{\partial \varepsilon_v^p}) + 2(J_1 - L)\frac{\partial L}{\partial \varepsilon_v^p}] \tag{B.16}$$

where

$$\frac{\partial X}{\partial \varepsilon_v^p} = \frac{1}{D(W - \varepsilon_v^p)} \tag{B.17}$$

and

$$\frac{\partial L}{\partial \varepsilon_v^p} = \frac{\frac{\partial X}{\partial \varepsilon_v^p}}{1 + AR + RBCe^{-BL}} \tag{B.18}$$

Due to the effect of kinematic hardening, $\frac{\partial F}{\partial \alpha_{ij}}$ should be evaluated. But as seen in the formulation of the elasto-plastic matrix $[C^{e\text{-}p}]$, in chapter 3, $\frac{\partial F}{\partial \alpha_{ij}}$ was replaced by $-\frac{\partial F}{\partial \sigma_{ij}}$ according to the following proof:

$$\begin{aligned}\frac{\partial F}{\partial \sigma_{ij}} &= \frac{\partial F}{\partial \sigma_{pq}-\alpha_{pq}} \frac{\partial \sigma_{pq}-\alpha_{pq}}{\partial \sigma_{ij}} \\ &= \frac{\partial F}{\partial \sigma_{pq}-\alpha_{pq}} \delta_{ip}\delta_{jq} \\ &= \frac{\partial F}{\partial \sigma_{ij}-\alpha_{ij}}\end{aligned} \tag{B.19}$$

$$\begin{aligned}\frac{\partial F}{\partial \alpha_{ij}} &= \frac{\partial F}{\partial \sigma_{pq}-\alpha_{pq}} \frac{\partial \sigma_{pq}-\alpha_{pq}}{\partial \alpha_{ij}} \\ &= \frac{\partial F}{\partial \sigma_{pq}-\alpha_{pq}} -\delta_{ip}\delta_{jq} \\ &= -\frac{\partial F}{\partial \sigma_{ij}-\alpha_{ij}}\end{aligned} \tag{B.20}$$

From B.19 and B.20 it is clear that

$$\frac{\partial F}{\partial \alpha_{ij}} = -\frac{\partial F}{\partial \sigma_{ij}} \tag{B.21}$$

APPENDIX-C

COMPUTER PROGRAM

```
C       THIS IS A MODULAR SUBROUTINE FOR A NEW CAP TYPE
C       CONSTITUTIVE MODEL THAT USES THE COMBINED HARDENING RULE.
C       BOTH FAILURE ENVELOPE AND YIELD CAP ARE DEPENDENT
C       UPON THE THIRD STRESS INVARIANT  J3D
C
      IMPLICIT REAL*8 (A-H,O-Z)
C     IMPLICIT REAL*4 (A-H,O-Z)
C
      DIMENSION SIG(6),STN(6),DSIG(6),CEL(6,6),ALFA(6),DALFA(6)
      DIMENSION SG1(300),SN1(300),SN2(300),SN3(300),STNP(6)
      DIMENSION CIL(6,6),EPIJ(6),DSTNE(6),DSTNP(6),S(6)
      DIMENSION CEP(6,6)
      COMMON /PARA1/ BM,SM,AA,UU,BB,CM,GG,RR,DD,WW,PA
      COMMON SN
      OPEN (UNIT=56,FILE='STSH',STATUS='UNKNOWN',ACCESS='SEQUENTIAL')
      OPEN (UNIT=57,FILE='STSV',STATUS='UNKNOWN',ACCESS='SEQUENTIAL')
      OPEN (UNIT=58,FILE='STDV',STATUS='UNKNOWN',ACCESS='SEQUENTIAL')
      OPEN (UNIT=59,FILE='STS3',STATUS='UNKNOWN',ACCESS='SEQUENTIAL')
C     OPEN(UNIT=1,NAME='VAX$VPLOT:CHARGEN.DAT',TYPE='OLD',
C    ;READONLY)
C
C     OPEN(UNIT=8)
      READ(5,*)JSIG3,N,CALFA
C     WRITE(9,665)JSIG3.N,CALFA
```

```
C665  FORMAT(4X,2I4,3X,F13.4)
      READ(5,*)SMALL,NOPT
C     WRITE(9,666)SMALL,NOPT
C666  FORMAT(4X,F13.10,I7)
      READ(5,*)BM,SM,AA,UU,BB,CM,GG,RR,DD,WW,PA
C     WRITE(9,11)BM,SM,AA,UU,BB,CM,GG,RR,DD,WW,PA
C11   FORMAT(4F20.9// 4F20.9// 3F40.9)
      IFLAG=0
      DO 10 I=1,6
      SIG(I)=0.0
      STN(I)=0.0
      STNP(I)=0.0
10    ALFA(I)=0.
      ZETAV=SMALL
C     WRITE(9,667)ZETAV
 667  FORMAT(4X,'ZETAV=',F20.9)
      CALL ELASTM(BM,SM,CEL)
      READ(5,*)NSINC
      WRITE(56,8)NSINC
8     FORMAT('1',I4,1X,'2')
      WRITE(56,9)NSINC
9     FORMAT(I3)
      WRITE(57,81)NSINC
81    FORMAT('0',I4,1X,'1')
```

```
      NNC=0
C ************************************
C                        A
C   APPLYING STRESS INCREMENTS    2
C                        A
C ************************************
      DO 100 INC=1,NSINC
          READ(5,*)NSUB,(DSIG(I),I=1,6)
C ***
      CALL SUMMAT(CALFA,DALFA,ALFA,SIG,DSIG,STN,NSUB,CEL,IFLAG,ZETAV,STN
     ;P,CIL,DSTNE,DSTNP,S,CEP,INC)
      IF (SIG(1) .EQ. SIG(2) .AND.SIG(2).EQ. SIG(3) )THEN
      STN(1)=0.
      STN(2)=0.
      STN(3)=0.
      STN(4)=0.
      STN(5)=0.
      STN(6)=0.
      ENDIF
C   ..*..*..*..*..*..*..*..*..*..*..*..*..*..*..*..*..*..*..*..*..*
C   WRITE(9,1000)INC
C   WRITE(9,5000)((CEP(I,J),J=1,6),I=1,6)
C5000 FORMAT(6F13.6)
C   ..*..*..*..*..*..*..*..*..*..*..*..*..*..*..*..*..*..*..*..*..*
```

```
      EPSV=-(2*STN(3)+STN(1))*100
      DEVS=SIG(1)-SIG(3)
      DEVR=STN(1)-STN(3)
      WRITE(56,*) (STN(1)*100),DEVS
      WRITE(57,*) (STN(1)*100),EPSV
      WRITE(58,*) (DEVR*100),DEVS
      WRITE(59,*) (STN(3)*100),DEVS
C
C     WRITE(9,1500)ALFA(1)
C     WRITE(9,2000)
C     DO 20 I=1,6
C20   WRITE(9,3000)SIG(I),STN(I)
C
C20   WRITE(6,4000)STN(1),SIG(1),STN(3),SIG(3)
C
      DIFF=SIG(1)-SIG(3)
      ARE = DABS(DIFF)
C     IF ((DABS(DIFF)) .LE. 0.1E-05) BSTN=STN(1)
C     WRITE(6,*) 'ARE=',ARE
      IF (ARE .LE. 0.1E-05) BSTN=STN(1)
      IF(DABS(DIFF).LE.0.1E-05) GO TO 43
      NNC=NNC+1
      TERM=(SIG(1)-SIG(2))**2+(SIG(2)-SIG(3))**2+(SIG(3)-SIG(1))**2
      SG1(NNC)=DSQRT(TERM)/3.
```

```
      SN1(NNC)=(STN(1)-BSTN)*100.
      SN2(NNC)=(STN(2)-BSTN)*100.
      SN3(NNC)=(STN(3)-BSTN)*100.
43      CONTINUE
C    IF(SN1(NNC).GT.15.) GO TO 150
100     CONTINUE
C150    NPT=NNC
        STOP
1000   FORMAT(///20X,'INCREMENT NO. =',I4/)
C1500   FORMAT(///20X,'   ALFA    =',E15.4/)
2000   FORMAT(/16X,' STRESS ',3X,' STRAIN '/)
3000   FORMAT(12X,2E15.4)
4000   FORMAT(10X,4(E14.4))
C5000  FORMAT(12X,2E15.4)
      END
C
C
      SUBROUTINE SUMMAT(CALFA,DALFA,ALFA,SIG,DSIG,STN,NSUB,CEL,IFLAG,ZET
     ;AV,STNP,CIL,DSTNE,DSTNP,S,CEP,INC)
C
      IMPLICIT REAL*8 (A-H,O-Z)
C
      DIMENSION SIG(6),DSIG(6),STN(6),CEL(6,6),TSIG(6),CEP(6,6),
     ;DSUB(6),DSTN(6),CC(6,6),DSN(6),ALFA(6),DALFA(6),DSTNE(6),
```

```
     ;DSTNP(6),STNP(6),CIL(6,6),EPIJ(6),S(6)
C
      COMMON /PARA1/ BM,SM,AA,UU,BB,CM,GG,RR,DD,WW,PA
C
      DO 10 I=1,6
10     TSIG(I)=SIG(I)+DSIG(I)
      CALL YCIIECK(ALFA,TSIG,F,ZETAV,S)
C     WRITE(9,*) 'F=',F
      IF(F.LE.0.)GO TO 200
      IF(IFLAG.NE.0)GO TO 20
      CALL ELASTM(BM,SM,CEP)
      CALL MATINV(6,CEP)
      IFLAG=1
20     CONTINUE
      DO 30 I=1,6
30     DSUB(I)=DSIG(I)/FLOAT(NSUB)
C
C    ..*..*..*..*..*..*..*..*..*..*..*..*..*..*..*..*..*..*..*..*
C    .                                .     .     .
C    *              SUBINCREMENTATION                *
C    .                                              .
C    ..*..*..*..*..*..*..*..*..*..*..*..*..*..*..*..*..*..*..*..*
C.
C LOOP NO..
```

```
C       .
C       .
C       V
        DO 150 ISUB = 1,NSUB
         DO 50 I = 1,6
          SUM = 0.0
            DO 40 K = 1,6
40       SUM = SUM + CEP(I,K)*DSUB(K)
50       DSTN(I) = SUM
        DO 60 I = 1,6
        SIG(I) = SIG(I) + DSUB(I)
60     STN(I) = STN(I) + DSTN(I)
        CHEK = STN(1)*100.
        IF(CHEK.GT. 25.) GO TO 300
        CALL YCHECK(ALFA,SIG,F,ZETAV,S)
        IF(F.LE.0.0)GO TO 150
          CALL ELASTM (BM,SM,CIL)
          CALL MATINV(6,CIL)
          CALL DIVIAT(DSUB,CIL,DSTN,STNP,EPIJ,DSTNP,DSTNE)
          CALL ALPHA (CALFA,ALFA,EPIJ)
C
        CALL CPLAST(ALFA,SIG,DSTN,CEL,CEP,ZETAV,CALFA,DSTNP)
        CALL MATINV(6,CEP)
150       CONTINUE
```

```
C
C   ..*..*..*..*..*..*..*..*..*..*..*..*..*..*..*..*..*..*..*..*..*
C   .                                                       .
C   *          END OF   SUBINCREMENTATION                   *
C   .                                                       .
C   ..*..*..*..*..*..*..*..*..*..*..*..*..*..*..*..*..*..*..*..*..*
C
        GO TO 300
200     IFLAG=0
        CALL ELASTM(BM,SM,CC)
        CALL MATINV(6,CC)
C       IF (INC.EQ.20.OR.INC.EQ.21.OR.INC.EQ.22.OR.INC.EQ.23
C     * .OR.INC.EQ.40.OR.INC.EQ.41.OR.INC.EQ.42.OR.INC.EQ.43
C     * .OR.INC.EQ.72.OR.INC.EQ.73.OR.INC.EQ.74.OR.INC.EQ.75
C     * ) WRITE(58,312)INC
C312    FORMAT(///20X,'INCREMENT NO. =',I4/)
        DO 220 I=1,6
        SUM=0.0
        DO 210 K=1,6
210     SUM=SUM+CC(I,K)*DSIG(K)
          DSN(I)=SUM
C       IF (INC.EQ.20.OR.INC.EQ.21.OR.INC.EQ.22.OR.INC.EQ.23
C     * .OR.INC.EQ.40.OR.INC.EQ.41.OR.INC.EQ.42.OR.INC.EQ.43
C     * .OR.INC.EQ.72.OR.INC.EQ.73.OR.INC.EQ.74.OR.INC.EQ.75
```

```
C   * )THEN
C       WRITE(58,301)DSN(I),(CC(I,J),J = 1,6),DSIG(I)
C     ENDIF
220  CONTINUE
C301  FORMAT(F10.5,6F10.7,F10.5)
      DO 230 I = 1,6
      STN(I) = STN(I) + DSN(I)
230   SIG(I) = TSIG(I)
300   CONTINUE
      RETURN
      END
C
C
C
      SUBROUTINE CELAST(YNG,YNU,C)
C
      IMPLICIT REAL*8 (A-H,O-Z)
C
      DIMENSION C(6,6)
      CNST = YNG*(1.-YNU)/((1. + YNU)*(1.-2.*YNU))
      DO 10 I = 1,6
      DO 10 J = 1,6
10    C(I,J) = 0.0
      DO 20 I = 1,3
```

```
      C(I,I)=1.
20    C(I+3,I+3)=(1.-2.*YNU)/(2.*(1.-YNU))
      C(1,2)=YNU/(1.-YNU)
      C(1,3)=C(1,2)
      C(2,1)=C(1,2)
      C(2,3)=C(1,2)
      C(3,1)=C(1,2)
      C(3,2)=C(1,2)
      DO 30 I=1,6
      DO 30 J=1,6
30    C(I,J)=C(I,J)*CNST
      RETURN
      END
C     ****************************************************************
C
      SUBROUTINE YCHECK(ALFA,SIG,F,ZETAV,S)
C
      IMPLICIT REAL*8 (A-H,O-Z)
C
      DIMENSION SIG(6),S(6),ALFA(6)
      COMMON /PARA1/BM,SM,AA,UU,BB,CM,GG,RR,DD,WW,PA
      DATA EPSLON,EPSN /.1E-00,.1E-03/
C.
      XJ1=SIG(1)+SIG(2)+SIG(3)-(ALFA(1)+ALFA(2)+ALFA(3))
```

```
      CALL DEVIAT(SIG,S,ALFA)
      XJ2D=(S(1)**2+S(2)**2+S(3)**2+2.*(S(4)**2+S(5)**2+S(6)**2))/2.
      XJ3D=(S(1)**3+S(2)**3+S(3)**3+6.*S(4)*S(5)*S(6)+3.*(S(1)*
     ;S(4)**2+S(1)*S(6)**2+S(2)*S(4)**2+S(2)*S(5)**2+S(3)*S(5)**2
     ;+S(3)*S(6)**2))/3.
      XXJ=-DLOG(1.-ZETAV/WW)/DD
      CALL XLDET(XXJ,XLJ)
      A=DEXP(-GG*XLJ/PA)
      TM1=((XXJ-XLJ)**2-(XJ1-XLJ)**2)/(RR**2)
      IF(XJ2D.LE.EPSN) GO TO 10
      CTH=3.*SQRT(3.)*XJ3D/(2.*XJ2D**(1.5))
C     ****************************************************************
C
C
C     ****************************************************************
      IF (CTH .GT. 1.) CTH = 1.0
      IF (CTH .LT. -1.0) CTH = -1.0
      GT=(2./SQRT(3.))*(DCOS((DACOS(-A*CTH))/3.))
      F=GT*GT*XJ2D-TM1
      GO TO 20
10    F=-TM1
20    CONTINUE
      RETURN
      END
```

```
C
C   C**********************************************************************
C
      SUBROUTINE CPLAST(ALFA,SIG,DSTN,CEL,CEP,ZETAV,CALFA,DSTNP)
C
      IMPLICIT REAL*8 (A-H,O-Z)
C
      DIMENSION SIG(6),S(6),T(6),DELF(6),CF(6),CFC(6,6),CEL(6,6),
     ;CEP(6,6),DSTN(6),CSTN(6),DEFT(6),ALFA(6),CFL(6),DELF1(6),DSTNP(6)
C
      COMMON /PARA1/ BM,SM,AA,UU,BB,CM,GG,RR,DD,WW,PA
      DATA EPSLON,EPSN /.1E-00,.1E-03/
C
C
      CALL DEVIAT(SIG,S,ALFA)
      T(1)=S(1)**2+S(4)**2+S(6)**2
      T(2)=S(2)**2+S(4)**2+S(5)**2
      T(3)=S(3)**2+S(5)**2+S(6)**2
      T(4)=S(1)*S(4)+S(2)*S(4)+S(5)*S(6)
      T(5)=S(2)*S(5)+S(3)*S(5)+S(4)*S(6)
      T(6)=S(1)*S(6)+S(3)*S(6)+S(4)*S(5)
      XJ1=SIG(1)+SIG(2)+SIG(3)-(ALFA(1)+ALFA(2)+ALFA(3))
C.    XJ1=SIG(1)+SIG(2)+SIG(3)
      XJ2D=(S(1)**2+S(2)**2+S(3)**2+2.*(S(4)**2+S(5)**2+S(6)**2))/2.
```

```
      XJ3D=(S(1)**3+S(2)**3+S(3)**3+6.*S(4)*S(5)*S(6)+3.*(S(1)*S(4)
     ;**2+S(1)*S(6)**2+S(2)*S(4)**2+S(2)*S(5)**2+S(3)*S(6)**2+
     ;S(3)*S(5)**2))/3.
      XXJ=-DLOG(1.-ZETAV/WW)/DD
      CALL XLDET(XXJ,XLJ)
      A=DEXP(-GG*XLJ/PA)
      IF(XJ2D.LE.EPSN) GO TO 2
C
      CTH=3.*SQRT(3.)*XJ3D/(2.*XJ2D**(1.5))
      IF (CTH .GT. 1.) CTH = 1.0
      IF (CTH .LT. -1.0) CTH = -1.0
      STH=DSIN(DACOS(CTH))
      IF (STH .GT. 1.0) STH = 1.0
      IF (STH .LT. -1.0) STH = -1.0
      G1=(2./SQRT(3.))*(DCOS((DACOS(-A*CTH))/3.))
      TM1=2.*A*DSIN(DACOS(-A*CTH)/3.)/(DSQRT(3.*(1.-A*A*CTH*CTH)))
      DGJ1=0.0
      DFJ1=2.*G1*DGJ1*XJ2D+2.*(XJ1-XLJ)/(RR*RR)
      DFJ2D=G1**2
      DGT=TM1*STH
      DFTH=2.*G1*DGT*XJ2D
      GO TO 3
2.    DFJ1=2.*(XJ1-XLJ)/(RR*RR)
      DO 1 I=1,3
```

```
      DELF(I)=DFJ1
1     DELF(I+3)=0.0
      GO TO 4
3     CONTINUE
C
      IF (DFTH.EQ.0) GO TO 8
C
      DO 10 I=1,3
      DELF(I)=DFJ1+DFJ2D*S(I)+DFTH*(-SQRT(3.)*3*
     +XJ2D**(-1.5)/(2.*STH))*(T(I)-2.*XJ2D/3.-1.5*(XJ3D/
     +XJ2D)*S(I))
C
10    DELF(I+3)=DFJ2D*S(I+3)+DFTH*(-SQRT
     +(3.)*XJ2D**(-1.5)/(2.*STH))*(T(I+3)-1.5*(XJ3D/XJ2D)
     +*S(I+3))
      GO TO 9
C
8     DO 5 J = 1,3
      DELF(J)=DFJ1+DFJ2D*S(J)
5     DELF(J+3)=DFJ2D*S(J+3)
C
C
9     CONTINUE
4     CONTINUE
```

```
      DXVP = 1./(DD*(WW-ZETAV))
      DLVP = DXVP/(1. + UU*RR + RR*BB*CM*DEXP(-BB*XLJ))
      DFVP = -(2.*(XXJ-XLJ)*(DXVP-DLVP) + 2.*(XJ1-XLJ)*DLVP)/(RR*RR)
      TERVOL = 3.*DFJ1
      DO 40 I = 1,6
      SUM = 0.0
      DO 30 K = 1,6
30    SUM = SUM + CEL(I,K)*DELF(K)
40    CF(I) = SUM
      DO 50 I = 1,6
      DO 50 J = 1,6
50    CFC(I,J) = CF(I)*CF(J)
      SUM = 0.0
      DO 60 I = 1,6
60    SUM = SUM + DELF(I)*CF(I)
      SUM1 = SUM
      DO 65 I = 1,3
         CFL(I) = CALFA*(DELF(I)-(DELF(1) + DELF(2) + DELF(3))/3.)
65    CFL(I + 3) = CALFA*DELF(I + 3)
      SUM2 = 0.0
      DO 66 I = 1,6
66    SUM2 = SUM2 + DELF(I)*CFL(I)
C.
      CONST = (SUM1 + SUM2-DFVP*TERVOL)
```

```
      DO 70 I=1,6
      DO 70 J=1,6
70      CFC(I,J)=CFC(I,J)/CONST
      DO 80 I=1,6
      DO 80 J=1,6
80     CEP(I,J)=CEL(I,J)-CFC(I,J)
C    C**********************************************************************
C     DO 389 NB=1,6
C389   WRITE(6,493)(CEP(NB,MB),MB=1,6)
C493   FORMAT(/,5X,6(E12.6))
C    C**********************************************************************
      DO 100 I=1,6
      SUM=0.0
      DO 90 K=1,6
90     SUM=SUM+CEL(I,K)*DSTN(K)
100    CSTN(I)=SUM
      SUM=0.0
      DO 110 I=1,6
110   SUM=SUM+DELF(I)*CSTN(I)
            XLAM=SUM/CONST
C    IF(XLAM.LT.0.)WRITE(6,*)XLAM
      DZETAV=XLAM*TERVOL
      IF(DZETAV.LT.0.)DZETAV=0.0
      ZETAV=ZETAV+DZETAV
```

```
      RETURN
      END
C
C     ****************************************************************
C
      SUBROUTINE DEVIAT(TSIG,DVS,ALFA)
C
C     SUBROUTINE DEVIAT(TSIG,DVS)
C
      IMPLICIT REAL*8 (A-H,O-Z)
C
      DIMENSION TSIG(6),DVS(6),ALFA(6)
C     DIMENSION TSIG(6),DVS(6)
C
      XJ=(TSIG(1)+TSIG(2)+TSIG(3))/3.
      DVS(1)=TSIG(1)-XJ-ALFA(1)
      DVS(2)=TSIG(2)-XJ-ALFA(2)
      DVS(3)=TSIG(3)-XJ-ALFA(3)
      DO 10 I=4,6
10    DVS(I)=TSIG(I)-ALFA(I)
      RETURN
      END
C.
C
```

```
      SUBROUTINE DIVIAT(DSUB,CIL,DSTN,STNP,EPIJ,DSTNP,DSTNE)
      IMPLICIT REAL*8 (A-H,O-Z)
      DIMENSION DSUB(6),CIL(6,6),DSTNP(6),DSTN(6)
      DIMENSION DSTNE(6),EPIJ(6),STNP(6)
C
C     ****************************************
C
C     COMPUTING INCREMENTAL PLASTIC STRAIN
C
C     ****************************************
C
       DO 80 I = 1,6
          SUM = 0.
        DO 70 K = 1,6
70      SUM = SUM + CIL(I,K)*DSUB(K)
            DSTNE(I) = SUM
            DSTNP(I) = DSTN(I)-DSTNE(I)
80     STNP(I) = STNP(I) + DSTNP(I)
C     ************************************************
C
C     COMPUTING INCREMENTAL PLASTIC DEVIATORIC STRAIN
C
C.    ************************************************
C
```

```
C
      XJ=(DSTNP(1)+DSTNP(2)+DSTNP(3))/3.
      DO 10 I=1,3
        EPIJ(I)=DSTNP(I)-XJ
        EPIJ(I+3)=DSTNP(I+3)
10    CONTINUE
      RETURN
      END
C
C     ****************************************
C
      SUBROUTINE ALPHA (CALFA,ALFA,EPIJ)
C     SUBROUTINE ALPHA (CALFA,ALFA,EPIJ,SIG)
C
C     ****************************************
C
      IMPLICIT REAL*8 (A-H,O-Z)
C
      DIMENSION ALFA(6),DALFA(6),EPIJ(6)
C     DIMENSION SIG(6),ALFA(6),DALFA(6),EPIJ(6)
C
C     CALL FALPHA(ALFA,SIG,EF)
      DO 80 I=1,6
          DALFA(I)=CALFA*EPIJ(I)
```

```
      ALFA(I)=ALFA(I)+DALFA(I)
80    CONTINUE
      RETURN
      END
C
C
C
      SUBROUTINE MATINV(N,A)
C
      IMPLICIT REAL*8 (A-H,O-Z)
C
      DIMENSION A(N,N),B(10,10)
C
      FN=N
      SUM=0.
      DO 4 I=1,N
      DO 2 J=1,N
2       B(I,J)=0.
      SUM=SUM+DABS(A(I,I))
4     B(I,I)=1.
      AVA=SUM/FN
      RER=.1E-15*AVA
      DO 40 I=1,N
      IF(DABS(A(I,I))-RER)6,6,20
```

```
6       IF(I-N)10,7,10
7       WRITE(3,100)
C     CALL EXIT
C     EXIT
        RETURN
C     GO TO 255
10      DO 12 II=I,N
        IF(DABS(A(II,I))-RER)12,12,14
12      CONTINUE
        GO TO 7
14      DO 16 JJ=1,N
        A(I,JJ)=A(I,JJ)+A(II,JJ)
16      B(I,JJ)=B(I,JJ)+B(II,JJ)
20      R=1./A(I,I)
        DO 22 J=1,N
        A(I,J)=R*A(I,J)
22      B(I,J)=R*B(I,J)
C     WRITE(6,*)N
        DO 37 II=1,N
        IF(II-I)32,37,32
32      C=-A(II,I)
        DO 35 J=1,N
        A(II,J)=A(II,J)+C*A(I,J)
        B(II,J)=B(II,J)+C*B(I,J)
```

```
35    CONTINUE
37    CONTINUE
40    CONTINUE
      DO 42 I=1,N
      DO 42 J=1,N
42    A(I,J)=B(I,J)
C255  CONTINUE
      RETURN
100   FORMAT('0      *****   MATRIX IS SINGULAR   *****')
      END
C
C
C
      SUBROUTINE XLDET(XX,XLJ)
C
      IMPLICIT REAL*8 (A-H,O-Z)
C
      COMMON /PARA1/ BM,SM,AA,UU,BB,CM,GG,RR,DD,WW,PA
      DATA TOL/.0001/
C
      XL=0.0
         FL=-XX+RR*(AA-CM)
        XR=XX
10      XM=(XL+XR)/2.
```

```
      FM=XM-XX+RR*(AA+UU*XM-CM*DEXP(-BB*XM))
      IF(DABS(FM).LE.TOL) GO TO 20
      PD=FL*FM
C     WRITE(6,*)PD
      IF(PD.LT.0.) GO TO 15
      XL=XM
      GO TO 10
15    XR=XM
      GO TO 10
20    XLJ=XM
      RETURN
      END
C
C
C
      SUBROUTINE ELASTM(BM,SM,C)
C
      IMPLICIT REAL*8 (A-H,O-Z)
C
      DIMENSION C(6,6)
C     WRITE(9,999) BM,SM,AA,UU,BB,CM,GG,RR,DD,WW,PA
C999  FORMAT(3F7.1,2F7.5,F7.1,F7.5,F7.1,2F7.5,F7.1)
C.
      DO 10 I=1,6
```

```
      DO 10 J=1,6
10    C(I,J)=0.0
      DO 20 I=1,3
      DO 20 J=1,3
20    C(I,J)=BM-2.*SM/3.
      DO 30 I=1,6
30    C(I,I)=C(I,I)+2.*SM
      RETURN
      END
```